INVESTIGATIONS OF THE AERODYNAMIC INTERACTIONS BETWEEN WIND TUNNEL MODELS AND THEIR SUPPORT SYSTEMS AT THE GALCIT TEN FOOT WIND TUNNEL

Thesis by

Josiah E. Smith

In Partial Fulfillment of the Requirements

For the Degree of

Aeronautical Engineer

California Institute of Technology

Pasadena, California

1948

Acknowledgments

The author wishes to express his appreciation to Mr. Louis Schmidt, Mr. Edwin Pounder, and other members of the GALCIT Ten Foot Wind Tunnel staff for their great assistance in the preparation of the data, sketches, and figures. Grateful acknowledgment is also made to Dr. Clark B. Millikan and Mr. Richard W. Bell for their helpful suggestions.

Abstract

This work is divided into two parts. Part I describes the GALCIT image system tare procedure as it is used at the present time, the techniques of operation, and the assumptions used. The tare procedure is an experimental method for obtaining the aerodynamic interference forces and moments produced on a wind tunnel model by the supporting structure which holds it fixed in the windstream. The present technique has been in use at GALCIT for over five years, during which time many small inconsistencies kept recurring, indicating the need for refinement of the procedures. Part II is a report on the first phase of the investigations planned for the attack on these problems.

In Part II are given the measurements of the interactions on a simple, rectangular wing, and of the air loads on the suspension system without a model present. An attempt is made to give a physical picture of the rather elaborate flow patterns around the windshields, and of what happens to the aerodynamic characteristics of a wing when it is immersed in such a flow field. Some of the inadequacies of the present techniques are isolated and their magnitudes determined. A first try is made at measuring the tares for a yawed wing, with encouraging results. The need for further experimental work is clearly indicated, as well as for a theoretical study of the flow patterns in the tunnel throat.

PART I

REPORT ON

THE GALCIT PROCEDURE, AS OF JUNE 1943,

FOR THE EXPERIMENTAL DETERMINATION OF THE AERODYNAMIC INTERFERENCES

OF THE MODEL SUSPENSION SYSTEM OF THE 10 FOOT WIND TUNNEL

No. of pages 26

Date June 1, 1948

TABLE OF CONTENTS

SUMMARY

The GALCIT model support interference determination procedure is described. An example set of tare test data is presented in sufficient detail to enable anyone familiar with wind tunnel testing to use the technique.

The procedure requires the use of an image system of support struts and windshields which is mounted as the reflection below the model of the permanent support system above the model. When the model is inverted the geometrical relation of the image system to the model is the same as the geometrical relation of the permanent support system to the model mounted in normal rig. It is assumed that the effects of the image system on the inverted model are equal to the effects of the permanent support system on the model in normal rig. Then the effects of the image system are the interference tares.

Also included in the procedure are the corrections for clear-tunnel windstream inclination and curvature.

The method is used only for models at zero yaw angle.

It is estimated that this procedure gives tare values accurate to within 5% to 10% of the correct values.

INDEX OF FIGURES

TABLE 1

NOTATION

α_g (geometrical) = Angle of attack of wing chord line relative to tunnel axis. (Angle of attack is positive when airplane nose is raised, trailing edge lowered.)

α_τ = Angle of attack tare

C_L = Lift coefficient = $\frac{\text{measured lift force}}{qS}$ (C_L is positive when it tends to lift the airplane)

C_{D_p}' = Parasite drag coefficient uncorrected for drag tare

= $\frac{\text{measured drag force}}{qS} - \frac{C_L^2}{\pi AR} + \Delta C_D$ (Drag is positive when it acts in the direction of the relative wind)

C_{D_τ} = Drag tare coefficient = $\frac{\text{drag tare force}}{qS}$

ΔC_D = Wind tunnel wall interference correction to the observed drag

= Constant x C_L^2

C_{m_u} = Pitching moment coefficient = $\frac{\text{measured pitching moment}}{qSc}$

(C_m is positive when it tends to raise the airplane nose)

C_{m_τ} = Pitching moment tare coefficient = $\frac{\text{pitching moment tare}}{qSc}$

Lift and drag forces act through the model trunnions

Pitching moment is measured about the model trunnion axis acting in the vertical plane containing the lift and drag force vectors

For the above coefficients use:

S = Projected wing area

c = Mean aerodynamic chord

TABLE 1 (Cont'd)

AR = Wing aspect ratio = $\frac{b^2}{S}$

b = Wing span

q = Dynamic pressure averaged over model span for tunnel with normal support struts and windshields

= $\frac{1}{2} \rho V^2$

V = Windstream velocity averaged over model span

ρ = Mass density of air

I_s = Windshield and bayonet image system installed below the model in the tunnel and acting as the image of the main support windshields and bayonets.

Model (Inv.) = Model mounted with suction side up in tunnel

Model (Normal) = Model mounted with pressure side up in the tunnel so that the main support struts enter the pressure side of the wing

REPORT ON

THE GALCIT PROCEDURE, AS OF JUNE 1943,

FOR THE EXPERIMENTAL DETERMINATION OF THE AERODYNAMIC INTERFERENCE OF THE MODEL SUSPENSION SYSTEM OF THE 10 FOOT WIND TUNNEL

A. Introduction

This report describes the experimental procedure for determining the aerodynamic interference effects of the model suspension system as developed at GALCIT by June 1943. The original version of this report, which was included in GALCIT Report 402, was written by the author as a part of his research work, and has been revised into the present form for inclusion in the thesis manuscript. All aerodynamic interference, or tare, effects have been measured (at GALCIT) according to this procedure since June 1943, even though the results have been frequently inconsistent. In general, these inconsistencies have been small, being of the order of 5% to 10% of the correct values.

Section B of this report contains a discussion of the basic principles underlying the tare procedure. Section C contains a discussion of the effects of unsymmetrical clear tunnel flow. In Section D a typical tare test is described. In Section E the problem of when to make tare tests is briefly discussed. It should be noted that the procedures described herein apply only to the GALCIT Ten Foot Wind Tunnel and will not necessarily be proper for other tunnels.

Before proceeding to the discussion of the tares it is necessary to briefly describe the GALCIT test setup* and some of the terminology.

Models are suspended from three struts which enter the tunnel

---

* See Figure I-1, Page I-23

through the top wall. Each strut is enclosed in a windshield, except for the lower 8 inches of the struts. Airflow between each strut and its windshield is prevented by means of thin rubber diaphragm seals. The two main wing struts are adjustable in the spanwise direction, and the tail or aft strut is adjustable fore and aft. The attachment points of the struts to the model are called the trunnion points. The trunnion fittings are sunk into the wing at the trunnion points and the trunnion well is filled with sponge rubber which prevents airflow through the wing and also fills out the wing contour around the trunnion. The lower part of each strut is detachable and is called a bayonet. It is the bayonet portion of the strut which is exposed to the wind stream. Two types of bayonets are used for the wing struts, one having a very thin streamline cross-section and the other an elliptical cross-section. The tail strut bayonet has a circular cross-section. All bayonets are roughened to prevent laminar separation on them. The most important details to keep in mind are: 1) the exposed length of each strut is a constant dimension regardless of the type of model or of the attitude of the model in the tunnel; 2) the spanwise location of the main wing struts (and their windshields) generally is fixed for a given wing, but will vary for different models; 3) the fore and aft location of the tail strut and its windshield is fixed for a given wing by the sting length, and for a given fuselage by the tail length; and 4) for a given model operated only in pitch the main struts and windshields remain fixed, while the tail strut and windshield undergo considerable **vertical** motion and some fore and aft motion as the model is pitched.

All normal tests are made with the model upside down so that the support struts enter the lower or pressure surface of the wing and fuselage. In this manner the suspension system interferences are reduced to the minimum.

When the model is upside-down it is said to be in the "normal" attitude; when the model is rightside-up it is said to be in the "inverted" attitude. Since the model can only be supported by the three suspension struts which are fixed above the model in the upper half of the tunnel, it is necessary to mount the "image" of the suspension system in the lower half of the tunnel below the model. This image system consists of three windshields and three bayonets which are exact replicas of the main suspension system bayonets and windshields. In effect the image system is the vertical reflection of the main system into the lower side of the trunnion plane. When the tares are to be determined, the model is inverted and two runs are made-- with and without the image system in place. Then the tare is equal to the difference between the forces and moments for the two runs, and is assumed to be equal to the interference tare of the main suspension system for the model mounted in the normal attitude. Notice that the image system with model inverted has the same relationship to the model as the main suspension system has with the model in the normal attitude.

No attempt was ever made prior to March 1947, to measure tares for the model in yaw. Some preliminary yaw tests are reported in Part II of this manuscript.

B. Basic Principles of GALCIT Tare Procedure

The GALCIT tare procedure is based entirely on the supposition that all aerodynamic interferences on the model caused by the model suspension system are constant and additive (within the desired accuracy limits) if measured at the same model lift coefficient, provided the model configuration and the tunnel free stream velocity are not changed. This means that, within the desired accuracy limits, we assume the interferences due to the installation of an exact image of the main suspension system are equal to and independent

of the interferences caused by the installation of the main suspension system; i.e., the tare obtained with an image system is equal to the true tare of the main system. For this supposition to be true it is necessary to meet the following condition: all portions of the model at which the air flow is modified by the image and main suspension systems must have the air forces acting on these portions follow a linear law (within the desired accuracy limits) with respect to the changes in either direction or magnitude of the air flow which are caused by the interference of the image system or the main suspension system, either separately or combined. There are additional limitations which are concerned with any lack of axial symmetry in the clear tunnel flow when neither of the windshield systems nor a model is in the tunnel; but for the present, symmetrical flow will be assumed, i.e., the clear tunnel flow everywhere has constant velocity parallel to the tunnel axis.

If the fundamental tare procedure supposition is correct, then the tare correction simply amounts to taking the difference between the forces and moments for the run (model inverted) with image system in and the run (model inverted) with image system out, and subtracting it from the forces and moments for the run (model normal) with image system out to give the final corrected data. Note that both the difference and the subtraction operations are carried out at the same lift coefficient. From the basic condition stated in the first paragraph we conclude that there are no direct restrictions on the magnitude or sign of the interference velocities and forces. The latter may have any possible variation provided they remain constant and additive when measured at the same model lift coefficient. Up to the present time there have been no theoretical calculations made in this field and therefore we are forced to rely on experimental correlation data for justification of the accuracy of the procedure.

It is clear that the precision of the tare values will be equal to the

precision of the total measured quantities and of the final corrected coefficients-- this is true because the same measuring system is used throughout. Similarly, the accuracy of the tare values (i.e., the accuracy of measurement) is essentially equivalent to the accuracy of the final corrected coefficients. This means that the numerical data can be measured with the desired accuracy and precision and that the only question to be answered is: do the measurements and calculations made in the GALCIT tare procedure give the true tare values? It is believed by the author that there is only one reliable method which will answer this question. The method is: measure tares on a given model for as large a variation as possible in the number, type, and location of the struts in the tunnel while the model is held in a fixed location, and then compare the final corrected coefficients for each strut orientation. If the final results agree, it seems evident, with such a wide variation in the interferences on the model, that the tare procedure must be correct. This checking method can be considerably improved if the model is symmetrical about the vertical and horizontal planes containing the wing root chord. In this case it is necessary that, at zero lift coefficient, $\alpha = 0$, $C_m = 0$, and the drag be a minimum; provided, of course, that the tunnel flow has axial symmetry. Some tests have been made using this method and the results were all favorable. The chief difficulties which have been encountered have been in the attempts to correct for the decidely unsymmetrical clear tunnel flow pattern in the GALCIT tunnel.

At the GALCIT tunnel it has been found experimentally that 85% to 90% of the tares are caused by aerodynamic interference with the wing and horizontal tail surfaces -- this is evidence which lends support to the use of the model lift coefficient as the independent variable throughout the tare procedure. Because of this dependence of the tares on the wing and tail lift

coefficients it is reasonable to assume that the requirements of the original supposition can be met if the flow (including all interferences) around the wing and tail follows the first order wing theory. Thus it seems quite possible that the tares are additive for normal size models and moderate angles of attack. As the model lift coefficient increases through and above the value of 1.0, the first order wing theory breaks down and, similarily, it is probable that the tares are no longer additive. Fortunately, however, the model drag increases so rapidly near $C_L = 1.0$ and above, that the drag tare soon becomes negligible in comparison with the corrected model drag. On the other hand, the angle of attack and pitching moment tares are normally constant up to the wing stall so that it is sufficient to extrapolate them to any desired lift coefficient.

From consideration of the preceding discussion and from the experience gained in the GALCIT tunnel in hundreds of tare runs, we can now set down a number of practical rules to follow during a tare investigation:

1) The model suspension struts and their windshields should be as thin as possible. The area-blocking by the windshields should not be larger than 3% to 6% (4.5% at GALCIT).

2) The tips of the main wing windshields should be not less than one half and not more than three-halfs of the local wing chord above the wing. The tail windshield should have somewhat more exposed bayonet length than the main windshields.

3) All three windshields should be kept as far from each other as is practicable. The main windshields must be kept away from the fuselage, nacelles, or other protuberances on the wing. The tail windshield should be as far aft as possible and still be six to ten inches ahead of the model tail-surfaces.

4) The trunnion wells must be filled to prevent airflow through them, and the filler material must be flush with the normal wing contours for all model attitudes.

5) The air gap between each strut and its windshield must be sealed off from the tunnel wind stream. This should be done without allowing appreciable forces to be transmitted through the seals to the struts.

6) The image system windshields and bayonets should be exact replicas of the main suspension system. Particular attention should be given to all parts of the image system on which the air forces add directly into the tares.

7) Do not use the elliptical bayonets on small chord wings (less than 10 inches), or near protuberances on the wing, or when the trunnions are forward of the 30% point of the local wing chord, or when the trunnions are forward of the transition point.

8) All experimental data should be plotted immediately after they are taken so that all "scatter points" can be checked before starting the next run. All abrupt changes in the slope and curvature must be checked carefully, and, if they look abnormal, the operator must make sure that they are not caused by interferences from the image or suspension systems.

9) When testing low drag, laminar flow airfoils or wings with similar profiles there will usually be sharp breaks in the lift, drag, and pitching moment curves even for normal attitude tests. In this case all the tare data should show the breaks to occur at the same lift coefficient. If such is not true then the assumption of additive interferences is no longer valid. At the GALCIT this effect is not large and the tare curves are faired into smooth continuous lines.

10) Pressure measurements in the vicinity of any of the three windshields will be in error by the amount of the interference velocity field. If an accuracy of better than 2% or 3% of q is desired, it will probably be necessary

to make corrections to the pressure data unless the measurement points are at least 15 inches from the nearest windshield.

C. Effects of Unsymmetrical, Clear-Tunnel Flow on Tare Procedure

The entire discussion of Part B was based on the assumption of parallel and uniform clear-tunnel flow throughout the tunnel throat. That this is not true for the GALCIT tunnel has been proven in many ways. In fact the deviations from symmetrical flow are so important that a considerable portion of the time spent in developing the present GALCIT tare procedure has been used up in the attempt to determine the characteristics of the clear-tunnel flow. There are three reasons for this: 1) even though the tares may be correct, the final results are not correct since the free flight condition of parallel and uniform flow is not fulfilled, 2) most of the possible unsymmetries will cause errors in the tares, and 3) the great usefulness of symmetrical models in verifying the correctness of the tare procedure is largely nullified.

The most important unsymmetries in the GALCIT tunnel flow are: inclination of the flow in the vertical or pitch direction, spanwise variation in the magnitude of this inclination, curvature in the flow, a differential inclination between the wing and tail positions, and vertical velocity-gradients. Still other unsymmetries have been found which, so far as is known, have negligible effects. The probable origins of the unsymmetries are: a poorly loaded wind tunnel fan, a small contraction ratio, a short settling chamber ahead of the throat, and a large cut-out* in the top of the throat which is only partially corrected for by a deflector upstream of the cutout. This cutout or "conning tower" must be open whenever the model is yawed, in order to allow space for the movement of the three windshields.

---

*See Figure I-1, Page I-23

For most tests the conning tower is left open even though the model is not yawed. It should be understood that the unsymmetries which have been mentioned are not large deviations and that their effects are small, except for the vertical inclination. All of these effects except that of the vertical velocity-gradient can be accounted for by a simple extension of the tare procedure outlined in Section B.

This extension brings up to date the development of the tare procedure, which now consists of the following tests:

Run 1: model inverted,

Run 2: " " plus image system,

Run 3: " normal " " " ,

Run 4: " " ,

for each run measure lift, drag, and pitching moment versus angle of attack.

All details of the calculation procedure are given in Section D. These will include a discussion of the methods for correcting for the dissymmetries in the clear-tunnel flow.

D. Typical Tare Determination Test

In the standard GALCIT tare investigation four runs are made, from the results of which the tare values are completely determined. One of the runs is also the base run to which the tares are applied to give the final corrected coefficients. The base run may be either model inverted or model normal depending on the attitude at which the model is rigged for the rest of the test. Whenever it is possible, the model should be tested in normal rig because the interferences are smaller in that case. For the example given here we will assume that the model is to be tested in normal rig. No restriction is applied because of the model configuration since the tare

procedure (at present) does not vary with the model arrangement. However, it is of great importance to realize that a given tare test applies only to the model configuration and the tunnel velocity used in the tare test. How far it is possible to go in assuming the tares are universal is discussed in Section E.

In practice the tare procedure must be adjusted to conform with the manner in which the tunnel velocity calibration was obtained. At the GALCIT the velocity (or dynamic pressure) calibration is made with the three main suspension struts and windshields mounted in the tunnel. A more correct method would be to use the calibration for clear-tunnel conditions. However, the present method makes the tare calculations simpler and does not appreciably impair the correctness or accuracy of the results. For each run in the tare series it is necessary to read lift, drag and pitching moment by one degree increments in angle of attack over the pitch range of from two degrees below zero lift to the wing stall. All of the data should be plotted, and the curves drawn in completely.

The data for the typical tare plots are presented on Fig. I-2, I-3, and I-4; they represent the actual results obtained on a conventional model tested in the GALCIT tunnel in March 1943. On Fig. I-2 is plotted the uncorrected lift coefficient (C_L) vs. angle of attack (α_g) for each of the four runs. The slope ($dC_L/d\alpha_g$) of each curve is measured for the straight portion of the curve going through zero lift. For this plot the normal dynamic pressure (q_o) is used in calculating C_L, with the result that the two runs with image system in have a higher lift curve slope than do the two runs with image system out. This increase in the lift curve slope is taken to be equivalent to the effective increase in the velocity due to the blocking effect of the image system. Therefore, all data for the runs with image system in are

reduced with the effective q obtained from Plot I, so that they may be directly compared with the image-system-out runs. For the tare results to be considered reliable the curves of Plot I should have the following characteristics: 1) all four curves should have very closely the same shape, 2) the two runs with the image system out should have the same lift curve slope and nearly the same maximum lift coefficient, 3) the two runs with the image system in should have the same lift curve slope and nearly the same maximum lift coefficient, and 4) the effective increase in q due to the image system should be 2% to 5% of the nominal value, q_o. An examination of Fig. I-2 shows that most of these characteristics are present below $C_L = 0.9$, and that above $C_L = 0.9$ the agreement is quite poor. This indicates that the tares will not be reliable above $C_L = 0.9$. Therefore it is considered to be better to extrapolate the tares beyond $C_L = 0.9$ according to the experience gained from previous tests.

On Fig. I-3 are presented the lift, drag, and pitching moment curves (vs. C_L) for all four runs of the tare series. Notice that the two runs with image-system-in have now been corrected for the blocking effect of the image system. We will consider first the two runs with model normal and inverted and image-system-in -- this is the so-called "symmetrical tunnel" setup. We find: 1) the pitching moment curves are parallel and spread apart, 2) the α_g curves are parallel and spread apart, and 3) the drag curves are spread apart (in rotation only) about the zero lift point. Now items 2 and 3 can be accounted for by straight inclination in the clear tunnel flow, but item 1 must be explained by an effective curvature in the clear tunnel flow for model without a tail (camber change), or by a differential inclination between the wing and the tail positions for model with a tail. Actually both of these effects are present in the GALCIT tunnel. Since the ultimate aim of the wind tunnel test is to obtain data for free flight conditions, it is necessary to correct the data for these dissymmetries in the clear-tunnel flow.

The correction just amounts to averaging the data for the two runs in question, and then using the "average curve" as the true curve for model with image-system-in. Such a curve is plotted only for the pitching moments. (See Fig. I-3). The differences between the drag curves are plotted as $\delta C_{D_p'}$ vs. C_L and a straight line drawn through the points. Then the inclination effect on drag is taken as one half of the ordinates of this straight line. One half of the difference between the α_g curves is taken as the combined inclination and curvature effect on angle of attack. The basic theory substantiating these corrections for inclination and curvature in the wind stream is well known and will not be discussed here.

After obtaining these "average" curves for the symmetrical tunnel setup, the final tare values are taken directly from the curves as shown on Fig. I-3. The pitching moment tare, C_{m_τ}, and the drag tare, C_{D_τ}, are plotted on Fig. I-4. The angle of attack tare, α_τ, is assumed to be constant and equal to the value measured at zero lift coefficient.

For the tares to be considered reliable (by present standards) it is necessary to meet the following conditions: 1) all four pitching moment curves should be closely parallel; 2) all four α_g curves should be parallel; 3) the two curves for model normal should be symmetrically spaced (from the "average curve") with respect to the two curves for model inverted for both pitching moment and angle of attack; 4) all four runs should show nearly the same maximum lift coefficient and stall pattern; 5) the two runs with image-system-in should have the same drag at $C_L = 0$; 6) the $\delta C_{D_p'}$ values should conform closely to a straight line when plotted against C_L; 7) the two runs with image-system-out should have nearly the same drag at $C_L = 0$; 8) the pitching moment tare should be nearly constant with a value between 0 and +0.0400; 9) the angle of attack tare should have a value between -0.1° and

and -1.0°; 10) the clear tunnel inclination obtained from the drag curves should lie between 0.1° and 0.8° downwash in the tunnel; 11) the value of C_{D_τ} at $C_L = 0$ may vary between 0.0020 and 0.0100, and the slope (dC_{D_τ}/dC_L) should be of the order of -0.01; 12) sharp breaks in the curves for any of the three quantities, C_{m_u}, α_g, C'_{D_p}, should occur at very nearly the same lift coefficient for all four runs.

Examination of Fig. I-3 will show that all conditions except item (6) have been satisfactorily met for lift coefficients below 0.8. On going above $C_L = 0.8$ the indicated tares must be considered increasingly unreliable, and extrapolated values should be used --- this has been done for the final-tare plots on Fig. I-4. The fact that Runs 100 and 103 do not have the same drag value at $C_L = 0$ is sufficient cause to repeat the entire tare test unless it can be justified by extenuating circumstances such as: changes in the model configuration or surface finish for Run 103 which would not affect the tares but would change the model drag for the final run; differences in the wind-shield interference effects for model normal and inverted --- these can usually be expected for large fuselages or nacelles. For the model in question both of these effects were definitely present and therefore the tare results were approved and used.

In practice the greatest difficulty encountered in the use of the GALCIT tare procedure is in fulfilling the absolute requirement that the model surface condition and all movable surfaces remain fixed throughout the first three runs of the tare series. Since the fourth run is used as a check insofar as the tare determination is concerned, it is not necessary (although desirable) to maintain the model conditions fixed for run four, unless the tares for model inverted are also required. Notice that for model-inverted-tares the last three runs are used in the tare determination, the

results of which are applied to the first run. In general it is best to keep the model condition fixed for all four runs of the tare series.

E. When Are Tare Tests Required?

For most models it is possible to estimate the tares within the following limits:

$$\Delta C_{D_\tau} \backsim \pm 0.0015$$

$$\Delta \alpha_\tau \backsim \pm 0.2^\circ$$

$$\Delta C_{m_\tau} \backsim \pm 0.0080$$

Thus, if the results are not required to have a precision better than the error in the estimated tares, it is not necessary to run tare tests. In some cases the estimates can be made even more closely. Similarly, it frequently happens that the absolute magnitude of the results is not required, in which case tares are usually not required and need not be measured.

The tare values (in coefficient form) will vary with tunnel velocity, suspension strut location, type of bayonet, and model configuration. The variation of the tares with tunnel velocity is small but not negligible. In the region of 30 to 35 lb/ft^2 dynamic pressure there will frequently be a critical point (probably transition on the bayonets) and the tares will change rapidly with small changes in velocity. Except for this critical region the tares may be assumed constant for variations of 5 to 10 lb/ft^2 velocity head.

Suspension strut spacing has a large effect on the tare values, and additional tests must be run for changes in the spacing of more than three inches. If either of the two main wing struts is near the fuselage, nacelles, or a wing protuberance, new tares may be necessary for even a one inch change in spacing. As the bayonets are directly exposed to the windstream they contribute a large portion of the interference drag but have very little effect on the pitching moment or on the angle of attack tares. The most

reliable procedure to follow is to determine the basic tares (making all four runs) with the streamline bayonets and then change to the elliptical bayonets in a fifth run which will give the additional tare due to the larger bayonets. A similar procedure is required when changing from the normal "power-off" tail strut bayonet to the large, hollow, "power-on" bayonet.

It is necessary to make separate tare determination tests for each of the following model configurations:

1) wing alone
2) wing plus fuselage
3) wing plus nacelles
4) wing plus nacelles plus fuselage
5) wing plus fuselage plus tail
6) wing plus fuselage plus tail plus nacelles

Deflecting the flaps will have a large effect, but normally only the C_{m_τ} variation is of any importance. Large external radiators will change the tares considerably. And, finally, if the bayonets are in the model propeller slipstream the drag tare will become very large and will change rapidly with the propeller torque.

It should be apparent that a complete wind tunnel investigation on a particular model will involve a considerable number of tare tests if the most accurate results are desired. Unfortunately a tare determination is lengthy and expensive if it is run properly, which results in a strong tendency to estimate tares more often than is desirable.

F. Conclusions

The GALCIT Tare Procedure, as developed by June 1943, has been described. An example set of tare plots has been worked up in sufficient detail to enable anyone familiar with wind tunnel testing to use the technique.

Experience gained at GALCIT has shown this procedure to give results accurate to within 5% to 10% of the true values. Experience has also shown that tare tests are very difficult to run when interspersed among routine model tests, and still obtain reliable results. The tare runs should always be made consecutively, and only by experienced members of the operating crew. The balance data are reduced and plotted during each run, and numerous check points are taken. Above all, every care must be used to keep the model in the same physical condition throughout the series. This is not easy to do if the model is built of wood.

This tare procedure has never been thoroughly checked. The estimates of its reliability are based on comparative data from tests run on the same models in other wind tunnels, from comparative tests run on the GALCIT "Wire Suspension System" and on the present strut system, and from predictions derived from aerodynamic theory and two-dimensional test data. It is expected that future research on interference effects, such as is described in Part II of this thesis, will refine the test procedures considerably and may even allow the tares to be calculated with reasonable accuracy.

PART II

REPORT ON

SOME MEASUREMENTS OF THE

INTERFERENCES BETWEEN WIND TUNNEL MODELS

AND THEIR SUPPORT SYSTEMS

No. of pages 170

Date June 1, 1948

TABLE OF CONTENTS - PART II

TABLE OF CONTENTS - PART II (Cont'd)

SUMMARY - PART II

A detailed report is given of an extensive investigation into the reliability of the GALCIT Image System Tare Procedure. Testing techniques and operating conditions are described. Some past experiences with tare tests are mentioned and difficulties which have arisen are pointed out. A serious attempt is made to present a clear picture of the complex flow patterns in the tunnel with both windshields and model present. Several different, but simple, flow patterns are considered and the tare procedure is outlined for each one. Then these are combined into a modified tare procedure which is proposed for future tare tests. The limitations of this modified system are discussed at length. The great importance of having uniform flow in the clear tunnel is emphasized.

Experiments are reported which satisfactorily account for all air loads on the suspension system without a model present. The large conning tower in the throat ceiling is shown to markedly change the normal blocking effect of the windshields. Many data are described which help to define the flow patterns. Tare test results are given for a straight, rectangular wing at yaw angles of 0°, 19°, and 27°. Comparison with theory as well as other experimental results indicate that the tare procedures are not yet satisfactory. Nevertheless, some of the difficulties have been isolated and measured and it is believed that definite progress has been made in the understanding of these interference problems.

INDEX OF RUNS

Date	Run	Model Configuration	ψ	α_g	Remarks
1947					
3-3	1	P	—	—	Windshield holes sealed
"	2	PF_M^S	—	—	$t_M^S = 0$, $\psi = 0°$, 5°, 15°, 25°; Pitot slipped. See note on data sheet Run 2.
"	3	$PF_M^S A_S$	—	—	$t_M^S = 0$, $\psi = 0°$, 15°, 25°; Pitot in same position as for Run 2
"	4	$F_M^S A_S B_M^S b_M^S$	—	—	$t_M^S = 0$, $\psi = 0°$, 15°, 25°, 27° 20°, 5°, 10°
3-4	5	$F_M^S B_M^S b_M^S$	—	—	" , "
"	6	$PF_M^S A_S B_M^S b_M^S$	—	—	$t_M^S = 31"$, $\psi = 0°, \pm 5°, \pm 10°, \pm 15°, \pm 20°, \pm 25°, \pm 27°$
"	9	"	—	—	$t_M^S = 58"$, "
"	10	$PF_M^{SN} A_{SN} B_M^S b_M^S$	—	—	$t_M^{SN} = 31"$, "
3-5	14	$PF_M^{SN} E_M A_{SNT}$	0	—	" , $l_M = 23.68"$, $\alpha_g = 0°, \pm 10°, \pm 20°$; No tail strut; Tail windshield sealed at tip by mistake, repeated correctly in Run 15
"	15	"	"	—	$t_M^{SN} = 31"$, $l_M = 23.68"$, $\alpha_g = 0°$. Repeat Run 14
"	16	"	"	—	$t_M^{SN} = 31"$, $l_M = 15"$, $\alpha_g = 0°, \pm 10°, \pm 20°$; no tail strut
"	17	"	—	0	$t_M^{SN} = 31"$, $l_M = 11.75"$, $\psi = 0°, \pm 10°, \pm 20°, \pm 27°$ (NO TAIL STRUT)
"	18	"	—	"	" , $l_M = 40"$, $\psi = 0°, \pm 2°, \pm 4°, \pm 6°, \pm 8°$ (NO TAIL STRUT)
"	19	$PF_M^{SN} E_M A_{SN}$	0	"	" , $l_M = 40"$, 20", 15", 11.75"; tail strut tied to boom
"	20	$PF_M^{SN} E_M A_{SN} B_M^{ST} b_M^{ST}$	"	"	$t_M^{SN} = 31"$, $l_M = 40"$, 20", 15", 11.75"; tail strut tied to boom

Date	Run	Model Configuration	ψ	α_g	Remarks
3-5	21	$PF_M^{SN} E_M \delta_{SNT} B_M^{ST} b_M^{ST}$	0	0	t_M^{SN} = 31", ℓ_M = 40", 20", 15", 11.75"; tail strut tied to boom
"	22	$PF_M^{SN} E_M \delta_{SNT} B_M^{S} b_M^{S}$	"	"	t_M^{SN} = 31", ℓ_M = 40", 20", 15", 11.75"; tail sturt tied to boom
"	23	"	"	"	$t_M^{SN} = \ell_M$ = 35.42"; tail strut out
"	25	$PF_M^{SN} F_I^{S} E_M \delta_{SNT}$	"	"	" ; " ; checked pressure in F_{MI}^{S} & found F_I^{S} pressure 1 q more neg. than F_M^{S}. Plug 1-3/4" below tip of F_I^{S} brought press. together within 2 cm H_2O. Press. in tip were measured at base of hole downstream
3-6	26	" $B_M^{S} b_M^{S}$	"	"	$t_M^{SN} = \ell_M$ = 35.42"; t_I^{S} = 34.43", 35.42", 36.43"; Tail strut out; F_I^{S} plugged 1-3/4" below tip
"	28	" "	"	"	$t_M^{SN} = t_I^{S} = \ell_M$ = 35.42"; Tail strut out; F_I^{S} plugged 1-3/4" below tip; Move F_I^{S} up 3" and down 3" from std. position
"	29	" "	—	"	$t_M^{SN} = t_I^{S} = \ell_M$ = 35.42"; $\psi = 0^{\circ}, \pm 3^{\circ}, \pm 10^{\circ}$; Tail strut out, plug in F_I^{S};
"	30	$PF_M^{SN} F_I^{S} E_M \delta_{SNT} B_{MI}^{S} b_{MI}^{S}$	"	"	$t_M^{SN} = t_I^{S} = \ell_M$ = 35.42"; Tail strut out; 3/16" vent hole in lower part of F_I^{S} ; With F_I^{S} at std. position set brass plug (1/8" clearance in F_I^{S} tip) at 1-3/4", 1-1/4", 2-1/4", 2-3/4", 3-3/4" from tip, also plug out; Keeping brass plug at 1-3/4" from tip move F_I^{S} up 1/4", 1/2" and down 1/4", 1/2"

INDEX OF RUNS (Cont'd)

Date	Run	Model Configuration	ψ	α_g	Remarks
3-6	33	$PF_M^{SN} F_I^S E_M \mathcal{A}_{SNT} B_M^S b_M^S + B_I^S$ secured in F_I^S but clear of main bay; i.e., it projects into ball on B_M^S	0	0	$t_M^{SN} = t_I^S = \ell_M = 35.42"$; Tail strut out; F_I^S sealed at 1-3/4" below tip. 3/16" vent hole in F_I^S
"	34	$PF_{MI}^{SN} E_M \mathcal{A}_{SNT}$	"	"	$t_{MI}^{SN} = 35.42"$; Tail strut out; $\ell_M = 40", 20", 15"$; In all following runs (& Run 34) F_I^{SN} has 3/16" vent hole near base & vented to atmos. press., also tips are plugged at 1-3/4" below tip. If B_I^{SN} are in, seal at same point with dental dam seal.
"	36	" hole and deflector in center floor plates for image tail strut	"	"	$t_{MI}^{SN} = 35.42" = \ell_M$; Hole in floor for image tail windshield spacings of $\ell_I = 40", 19"$; Tail strut out
"	38	$PF_{MI}^{SN} E_{MI} \mathcal{A}_{SNT}$	"	"	$t_{MI}^{SN} = \ell_{MI} = 35.42"$; Tail strut in, here & all following runs. Checked press. in E_I & found within 1/2 cm H_2O of press. in main windshield E_M. Had to seal all holes in E_I to do this. Note E_I does not need strut seal, probably because volume geometry is different than for F_M windshield.
"	40	$PF_{MI}^{SN} E_{MI} \mathcal{A}_{SNT} B_M^T b_M^T$	"	—	$t_{MI}^{SN} = \ell_{MI} = 35.42"$, $\alpha_g = 0°, 2°$;
"	40A	$PF_{MI}^{SN} E_{MI} \mathcal{A}_{SNT}$	"	—	" , $\alpha_g = 0°, \pm 2°, \pm 4°, \pm 6°$ } E_I set at $\alpha_g = 0°$
"	42	$PF_{MI}^{SN} E_{MI} \mathcal{A}_{SNT} B_{MI}^T b_{MI}^T$	"	"	" ,
3-7	44	$W_A T_S F_M^{SN} E_M \mathcal{A}_{SNT} B_M^{SNT}$	"	—	$t_M^{SN} = 35.42"$, ± Stall by 1°'s. Trunnion on chord line. Took many readings to determine repeatability and scatterlevel. $\ell_M = 35.60"$

INDEX OF RUNS (Cont'd)

Date	Run	Model Configuration	ψ	α_g	Remarks
3-7	45	$W_A T_s F_M^{SN} E_M \Delta_{SNT} B_M^{SNT}$	0	–	t_M^{SN} = 35.42". Trunnions 1/4" above chord towards B surface
3-8	49	"	"	–	t_M^{SN} = 58"
3-10	51	$W_A T_s F_{MI}^{SN} E_{MI} \Delta_{SNT} B_{MI}^{SNT}$	"	–	" . Main image struts have rubber diaphragm seal and ground indication. Until otherwise noted.
3-10	54	"	"	–	t_M^{SN} = 35.42", Trunnions 1/4" offset
"	45A	$W_A T_s F_M^{SN} E_M \Delta_{SNT} B_M^{SNT}$	"	–	" , " , ck. Run 45
3-11	55	$W_A T_s F_{MI}^{SN} E_{MI} \Delta_{SNT} B_{MI}^{SNT}$	"	–	" , Trunnions on chord line
"	56	$W_A' T_s F_{MI}^{SN} E_{MI} \Delta_{SNT} B_{MI}^{SNT}$	"	–	t_{MI}^{SN} = 35.42", " " " "
3-12	86	$W_A' T_s F_{MI}^{SN} E_{MI} \Delta_{SNT} B_{MI}^{SNT}$	-27°	–	" , " " " " "
"	68	$W_A' T_s F_M^{SN} E_M \Delta_{SNT} B_M^{SNT}$	"	–	t_M^{SN} = 35.42", " " " " "
"	66	"	-19°	–	" , " " " " "
3-13	89	$W_A' T_s F_{MI}^{SN} E_{MI} \Delta_{SNT} B_{MI}^{SNT}$	"	–	t_{MI}^{SN} = 35.42", " " " "
"	80	"	"	–	t_{MI}^{SN} = 58",
"	94	" $- B_I^{SNT}$	"	–	"
"	74	$W_A' T_s F_M^{SN} E_M \Delta_{SNT} B_M^{SNT}$	"	–	t_M^{SN} = 58"
3-14	95	"	-27°		"
"	96	"	+19°		"
"	97	" + D	0		"

INDEX OF RUNS (Cont'd)

Date	Run	Model Configuration	ψ	α_g	Remarks
3-22	101	$W_A^i T_s F_M^{SN} E_M \delta_{SNT} B_M^{SNT}$	0	—	t_M^{SN} = 58" Trouble with main drive. Stopped and reworked balances
3-24	101ck	"	"	—	t_M^{SN} = 58"
"	101A	"	"	—	" , Ck. Run 101
3-24 3-25	97A	" + D	"	—	" , Ck. Run 97
3-25	98	" + D	-19°	—	"
"	99	" + D	+19°	—	"
"	100	" + D	-27°	—	"
"	101A ck	"	0	—	" , Checked Run 101A at α_g = 0°
"	60	$W_A^i T_s F_{MI}^{SN} E_{MI} \delta_{SNT} B_{MI}^{SNT}$	"	—	"
3-26	51A	$W_A T_s F_{MI}^{SN} E_{MI} \delta_{SNT} B_{MI}^{SNT}$	"	—	" , Ck. Run 51
"	49A	$W_A T_s F_M^{SN} E_M \delta_{SNT} B_M^{SNT}$	"	—	" , Ck. Run 49
"	101B	$W_A^i T_s F_M^{SN} E_M \delta_{SNT} B_M^{SNT}$	"	—	" , Ck. Run 101A
"	102	" + Tape off bottom trunnion plates at 58"	"	—	" , Taking tape off leaves bay. slot open in cover plate. Trunnion well sealed. See data sheet
"	103	" + Tape off and rubber seals removed at 58"	"	—	" , This leaves trunnion wells on bottom open but can't get flow thru wing to other side
"	104	"	"	—	" , Ck. Run 101B as base run

INDEX OF RUNS (Cont'd)

Date	Run	Model Configuration	ψ	α_g	Remarks
3-26	105	$W_A^i T_S F_M^{SN} E_M \delta_{SNT} B_M^{SNT}$ + Lower trunnion wells open at 58"	0	—	t_M^{SN} = 58", Wells completely open but no flow thru; wing cover plates off.
3-27	106	" + Lower trunnion wells open at 58" and top trunnion seals out	"	—	" , Same as Run 105 except rubber seals out of upper trunnions, thus get airflow thru trunnion; air gap very small
"	107	" + Lower & upper trunnion plates out at 58"	"	—	" , No seals, no cover plates at 58". Air passage 1/8 $in.^2$
"	108	" + Upper cover plates off and seal out, lower cover plates on and seal out and slot open	"	—	" , Air passage thru wing still open
3-27	109	$W_A^i T_S F_M^{SN} E_M \delta_{SNT} B_M^{SNT}$ + Upper cover plates & seals out. Lower cover plates on and slot taped	"	—	" , No airflow thru wing
"	110	" + No trunnion seal	"	—	" , Same as Run 109 with upper cover plates on
"	111	" + No trunnion seal & no tape on lower cover plate	"	—	" , Cover plates all on, no rubber seal, no tape on cover plate gap. Air passage is open

INDEX OF RUNS (Cont'd)

Date	Run	Model Configuration	ψ	α_g	Remarks
3-27	112	$W_A^L T_S F_M^{SN} E_M \phi_{SNT} B_M^{SNT}$	0	—	t_M^{SN} = 58", Ck. Base run
"	112A	"	"	—	" , Ck. Run 112
"	113	" + Main strut seals out but tail strut seals in	"	—	" ,
"	114	" + 35.42" trunnion wide open	"	—	" , 1" Diam. holes open at 35.42" trunnion
"	115	" + F_I^N	"	—	" , t_I^N = 58", Image wind. sealed at std. location
"	116	" + "	"	—	" , t_I^N = 35.42", Image wind. sealed at std. location
"	117	" + "	"	—	" , t_I^N = 0, Image wind. sealed at std. location
"	118	" + "	"	—	" , " , Image wind. sealed, F_I^N lowered to 14-1/8" below trunnion ℄
"	119	" + "	"	—	" , " , Image wind. sealed, F_I^N raised to 4-1/4" below trunnion ℄
3-28	120	" + F_I^S	"	—	" , t_I^S = 0
"	121	" + F_I^N	"	—	" , t_I^N = 35.42", Ck Run 116
"	122	" + F_I^S	"	—	" , t_I^S = -35.42", t_I^S is on north side
"	123	" + F_I^S F_I^N	"	—	" , t_I^{SN} = -35.42, " " " " " t_I^N is on south side

INDEX OF RUNS (Cont'd)

Date	Run	Model Configuration	ψ	α_g	Remarks
3-28	124	$W_A^L T_s F_M^{SN} E_M \delta_{SNT} B_M^{SNT} + F_I^S F_I^N$	"	—	t_M^{SN} = 58", t_I^{SN} = 35.42"
"	125	" $+ F_I^S$	"	—	" , t_I^S = 35.42"
"	126	" $+ F_I^N$	"	—	" , t_I^N = -35.42"
"	127	" $+ F_I^{SN}$	"	—	" , t_I^{SN} = -35.42", Ck. Run 123
"	128	" + "	"	—	" , t_I^{SN} = 35.42", Ck. Run 124
3-31	128A	" + "	"	—	" , " , " " "
"	129	" + "	"	—	" , t_I^{SN} = -35.42", Ck. Run 123
"	130	" + " + 12" flaps streamers 5' up stream of wing	"	0	" , " , Checked swirl visually & by roll moment on wing. Bowen tweaked 4th corner vanes until roll was negligible. This means should not compare tares before & after Run 130
"	131	" + "	"	—	t_M^{SN} = 58", t_I^{SN} = -35.42",
"	132	" + "	"	—	" , t_I^{SN} = 35.42"
"	133	$W_A T_s F_M^{SN} E_M \delta_{SNT} B_M^{SNT} + F_I^{SN}$	"	—	" , "
"	134	" + "	"	—	" , t_I^{SN} = -35.42"
"	135	" + " + F_I^N rotated 2°, T.E. inb'd 1/2"	"	—	" , " , Lift on F_I^N is southward

INDEX OF RUNS (Cont'd)

Date	Run	Model Configuration	ψ	α_g	Remarks
4-1	136	$W_A^i T_s F_M^{SN} E_M \delta_{SNT} B_M^{SNT} + F_I^{SN}$	0	—	t_M^{SN} = 58", t_I^{SN} = -35.42", Ck. Run 131, Found swirl way out again
"	137	"	"	0	" , 4th corner vanes tweaked by S/ to reduce swirl. Believe in future should try to line up T.E. with axis to give best & most stable distribution
"	138	$W_A^i T_s F_M^{SN} E_M \delta_{SNT} B_M^{SNT}$	"	—	" , Ck. Run 137 & found roll still O.K.
		Shut down and completely overhauled balances. Sharpened knife edges on Drag & Lift balances. See S/ comments on bal. conditions. Reconverged & recalibrated rigging and balances. Believe should now get much less scatter. Reworked F_I^N to proper thickness. But nose radius now too large			
4-18	139	$W_A^i T_s F_M^{SN} E_M \delta_{SNT} B_M^{SNT}$	0	—	t_M^{SN} = 58"
4-18 4-19	140	$W_A T_s F_M^{SN} E_M \delta_{SNT} B_M^{SNT}$	"	—	"
4-19	139A	$W_A^i T_s F_M^{SN} E_M \delta_{SNT} B_M^{SNT}$	"	—	" , Ck. Run 139
4-19 4-21	140A	$W_A T_s F_M^{SN} E_M \delta_{SNT} B_M^{SNT}$	"	—	" , Ck. Run 140
4-21	141	"	"	—	t_M^{SN} = 35.42"
4-21 4-22	142	$W_A^i T_s F_M^{SN} E_M \delta_{SNT} B_M^{SNT}$	"	—	"
4-22	141A	$W_A T_s F_M^{SN} E_M \delta_{SNT} B_M^{SNT}$	"	—	" , Ck. Run 141
"	142A	$W_A^i T_s F_M^{SN} E_M \delta_{SNT} B_M^{SNT}$	"	—	" , Ck. Run 142
4-23	143	$W_A^i T_s F_{MI}^{SN} E_{MI} \delta_{SNT} B_{MI}^{SNT}$	"	—	t_{MI}^{SN} = 58"
"	144	$W_A T_s F_{MI}^{SN} E_{MI} \delta_{SNT} B_{MI}^{SNT}$	"	—	"

Date	Run	Model Configuration	ψ	α_g	Remarks
5-12	145	$W_A^L T_S F_M^{SN} E_M \delta_{SNT} B_M^{SNT}$ + No wax on wing at all	0	-5°	t_{MI}^{SN} = 58", Set model at α_g = -5° & don't move during run. Heat wing very slowly (90 min.) to 160°F, to 200°F, cool to 30°F. After each temp. change start tunnel & watch drift of forces with time. Found too hard to get quick readings because of q fluctuations.
5-23	146	"	"	—	t_{MI}^{SN} = 35.42"
"	147	"	"	—	t_M^{SN} = 58"
"	148	"	27°	—	"
"	149	"	-27°	—	"
"	150	"	-19	—	"
"	151	"	19	—	"
5-26	152	$F_M^{SN} E_M$ + Noted	—	0	" ; Data on effect of strut seals and bayonets . See Data sheet
1948 1-27	153	$PF_M^{SN} \delta_{SN}$ + Ceiling fairings in Deflector out	0	—	t_M^{SN} = 35.42"; Data N.G., fairing blew out
"	153A	" + "	"	—	"
"	154	$PF_M^{SN} F_I^S \delta_{SN}$ + "	"	—	" , t_I^S = 35.42"
1-28	155	$PF_M^{SN} F_I^{SN} \delta_{SN}$ + "	"	—	" , t_I^{SN} = 35.42"
"	156	$PF_M^{SN} F_I^N \delta_{SN}$ + "	"	—	" , t_I^N = 35.42"
1-29	157	$PF_M^N F_I^N \delta_N$ + "	"	—	$t_M^N = t_I^N$ = 35.42"

Note: All runs are listed in chronological order

INDEX OF FIGURES

INDEX OF FIGURES (Cont'd)

INDEX OF FIGURES (Cont'd)

INDEX OF FIGURES (Cont'd)

INDEX OF PHOTOS

Photo No.	
1.	Pitot-static tube mounted at centerline of throat. View looking across tunnel.
2.	Main wing windshield mounted on yaw axis above pitot-static tube. View looking downstream.
3.	Main wing windshield mounted on yaw axis above pitot-static tube. View looking across tunnel.
4.	View looking across tunnel showing main wing windshield and bayonet with ball tip.
5.	View looking downstream at pitot-static tube on tunnel center line and main wing windshield and strut at the 35.42" trunnion spacing.
6.	Downstream view of all three main windshields and south image wing windshield with bayonets.
7.	Upstream view of steel wing mounted on suspension system and image system in place.
8.	Side view showing wing and all six windshields and bayonets.
9.	View looking upstream showing wing tare setup at $\Psi = 27^{\circ}$.
10.	Side view showing wing tare setup at $\Psi = 27^{\circ}$.
11.	Closeup view showing junction of main wing bayonet and wing.
12.	Closeup view showing sting attached to wing.
13.	Closeup view showing cover plates for both trunnion spacings.

TABLE 1

Definition of Angular Measurements

α_g = Angle of attack of wing chord line relative to the horizontal plane through the wing trunnions and measured in the vertical plane of symmetry of the model

Angle of attack is positive when the wing nose is raised, trailing edge lowered

α_τ = Tare angle of attack

= Effective windstream inclination with respect to the horizontal plane

α_u = $\alpha_g - \alpha_\tau$

α = α_u corrected for wind tunnel wall interference

= $\alpha_u + \Delta\alpha$

ψ = Angle of yaw of model plane of symmetry relative to wind tunnel axis. Angle is positive when right-hand wing moves back.

Definition of Coefficients

C_{L_g} = Uncorrected lift coefficient = $\frac{\text{measured lift force}}{qS}$

(C_{L_g} is positive when it tends to lift the wing)

C_{L_τ} = Lift tare

C_L = $C_{L_g} - C_{L_\tau}$

C_{D_g} = Uncorrected drag coefficient = $\frac{\text{measured drag force}}{qS}$

(C_{D_g} is positive when it acts in the direction of the relative wind). C_{D_g} acts along the wind tunnel axis.

C_{D_τ} = Drag tare

C_{D_u} = $C_{D_g} - C_{D_\tau}$

C_D = $C_{D_u} + \Delta C_D$ (where ΔC_D is the wall interference correction)

C_{D_P} = Parasite drag coefficient

= $C_D - \frac{C_L^2}{\pi AR}(1 + \delta_R)$

TABLE 1 (Cont'd)

C_{c_g} = Uncorrected crosswind force coefficient

= $\frac{\text{measured crosswind force}}{qS}$ (C_c is positive when it acts to the right)

C_{c_τ} = Crosswind force tare

C_c = $C_{c_g} - C_{c_\tau}$ (Wall interference assumed to be zero)

C_{ℓ_g} = Uncorrected rolling moment coefficient

= $\frac{\text{measured rolling moment}}{qSb}$ (C_{ℓ_g} is positive when it tends to lower the right wing)

C_{ℓ_τ} = Rolling moment tare

C_ℓ = $C_{\ell_g} - C_{\ell_\tau}$ (Wall interference assumed to be zero)

C_{m_g} = Uncorrected pitching moment coefficient

= $\frac{\text{measured pitching moment}}{qSc}$ (C_{m_g} is positive when it tends to raise the nose of the wing)

C_{m_τ} = Pitching moment tare

C_{m_u} = $C_{m_g} - C_{m_\tau}$

C_m = $C_{m_u} + \Delta C_m$ (where ΔC_m is the wall interference correction)

C_{n_g} = Uncorrected yawing moment

= $\frac{\text{measured yawing moment}}{qSb}$ (C_{n_g} is positive when it tends to move the right wing back)

C_{n_τ} = Yawing moment tare

C_n = $C_{n_g} - C_{n_\tau}$ (Wall interference assumed to be zero)

All moments are referred to the wing trunnion location, which for this wing is at the 1/4 chord point. As defined above, all coefficients are referenced to wind axis. Whenever the wing is yawed the six components are referenced to stability axes. Stability axes are described as

TABLE 1 (Cont'd)

orthogonal axes having, at zero yaw, the same directions and algebraic signs as the wind axes, but differing from the latter in that they rotate with the wing in yaw (but not in pitch), while the wind axes remain fixed with respect to the relative wind. The subscript (s) is used, as in the defining equations below, to indicate force or moment coefficients which are referred to stability axes.

$$C_{L_s} = C_L$$

$$C_{D_s} = C_D \cos\psi - C_c \sin\psi$$

$$C_{c_s} = C_c \cos\psi + C_D \sin\psi$$

$$C_{m_s} = C_m \cos\psi - \frac{b}{c} C_\ell \sin\psi$$

$$C_{\ell_s} = C_\ell \cos\psi + \frac{c}{b} C_m \sin\psi$$

$$C_{n_s} = C_n$$

R = Reynolds Number = $\frac{\rho c V}{\mu}$

h = Pressure difference between the 12½' and 20' piezometer rings = 8.684 gm/cm^2 for this test

$(H-p)_o$ = (Total pressure - static pressure) at center of throat on yaw axis with three main windshields installed, deflector in, and conning tower out.

= $K q^*$ = 24.68 gm/cm^2

K = Compressibility correction to impact pressure

= 1.0085

q^* = $\frac{1}{2} \rho V^2$ at center of throat on yaw axis

$q^*A.F.$ = 50 lb/ft^2 = average q over model span

A.F. = Averaging factor = 0.994

$H - p$ = Pitot-static tube pressure difference

$\frac{H - p}{(H - p)_o}$ = q/q^* (Neglecting compressibility corrections)

H = Total or stagnation pressure (assumed to be constant everywhere in the throat)

TABLE 1 (Cont'd)

p = Static pressure reading of pitot-static tube

$\frac{H - T_M}{(H - p)_o}$ = Main wing windshield tip pressure coefficient, where T_M is the tip pressure

$\frac{H - A}{(H - p)_o}$ = Atmospheric pressure coefficient, where A is the atmospheric pressure

$\frac{H - G_m}{(H - p)_o}$ = Main wing windshield base pressure coefficient, where G_m is the base pressure

$\frac{H - T_t^M}{(H - p)_o}$ = Main tail windshield tip pressure coefficient, where T_t^M is the tip pressure

$\frac{H - G_t}{(H - p)_o}$ = Main tail windshield base pressure coefficient, where G_t is the base pressure

$\frac{H - T_I}{(H - p)_o}$ = Image wing windshield tip pressure coefficient, where T_I is the tip pressure

$\frac{H - T_t^I}{(H - p)_o}$ = Image tail windshield tip pressure coefficient, where T_t^I is the tip pressure

C_{s_p} = Strut-to-windshield seal pressure coefficient

$$= \frac{\text{Pressure difference across seal}}{(H - p)_o} \times \frac{\text{Total wing lift coefficient}}{\text{Local wing lift coefficient}}$$

$$= \frac{\Delta p}{(H - p)_o} \times \frac{C_L}{C_\ell}$$, where C_ℓ here is the local wing lift coefficient

For the foregoing coefficients use:

S = Wing area = 8.274 ft^2

c = Wing chord = 14 in.

b = Wing span (including tips) = 7.140 ft

AR = Wing aspect ratio = $\frac{b^2}{S}$ = 6.161

V = Windstream velocity

ρ = Mass density of air (effective free air density)

TABLE 1 (Cont'd)

μ = Absolute viscosity of air

= 3.726×10^{-7} $\frac{\text{lb. weight x sec.}}{\text{ft}^2}$

Wall Interference Corrections

ΔC_D = Drag correction = $0.01390\ C_L^2$ ($\Psi = 0^\circ$)

$\Delta \alpha$ = Angle of attack correction

= $0.893\ C_L$ ($\Psi = 0^\circ$)

ΔC_m = Pitching moment correction = $0.002\ C_L$ ($\Psi = 0^\circ$)

Induction Effects for Finite Span Rectangular Wing

C_{D_i} = Induced drag = $\frac{1 + \delta_R}{\pi\ AR}\ C_L^2$ (where $\delta_R = 0.053$)

= $0.0544\ C_L^2$

α_i = Induced angle of attack

= $\frac{1 + \tau_R}{\pi\ AR}\ C_L$ (where $\tau_R = 0.18$)

= $3.493\ C_L$, in degrees

C_{D_o} = C_{D_p} = Parasite drag = $C_D - C_{D_i}$

α_o = $\alpha - \alpha_i$ = Angle of attack for infinite AR

TABLE 2

P	=	GALCIT standard Prandtl pitot-static tube mounted on tuhnel centerline at yaw axis
W_A^i	=	GALCIT steel, calibration wing and sting; profile NACA 0012, span 7 ft., chord 14 in.; rectangular planform, no twist or dihedral. The wing surfaces are stamped A and B, with the notation W_A indicating that the A side is the "pressure" surface (corresponds to lower wing surface on an airplane). The superscript (i) means that W_A is inverted in the tunnel, i.e., the A side faces the bottom of the throat.
T_S	=	Small, cylindrical tips on wing, making the overall span equal to 7.14 ft.
D	=	Dummy sting (wooden) mounted 8 in from the wing centerline on left hand wing
$F_{M,I}^{S,N}$	=	Wing strut windshields. M is main or upper windshields. I is image or lower windshield. S is south, and N is north. Note that when looking upstream you are facing to the east.
$E_{M,I}$	=	Tail strut windshields. M,I have same meaning as is given above.
$\mathcal{A}^{S,N,T}$	=	Strut-to-windshield seal for F_M^S, F_M^N, and E_M respectively. When image wing windshields are installed the seals are assumed to be in place unless otherwise noted. No seal is used in the image tail windshield in these tests.
$B_{M,I}^{S,N,T}$	=	Bayonets; with subscripts and superscripts meaning same as above.
$b_{M,I}^{S,N,T}$	=	Rubber ball mounted on bayonet tip. Other notation same as above
$t_{M,I}^{S,N}$	=	Spacing between wing windshields. Other notation same as above.
$\ell_{M,I}$	=	Distance from trunnion axis to tail strut, measured perpendicular to trunnion axis when $\alpha_g = 0^o$. Other notation same as above. $\ell_{MI} = 35.60$ in. for W_A and sting.

All tests were made with the throat ceiling fairings out (conning tower open) and the ceiling deflector in. (See Discussion).

REPORT ON
SOME MEASUREMENTS OF THE
INTERFERENCES BETWEEN WIND TUNNEL MODELS
AND THEIR SUPPORT SYSTEMS

A. Introduction

This Report describes the results of an extensive series of tests made on and with the GALCIT Ten Foot Wind Tunnel Model Suspension System to determinewhat factors importantly effect the aerodynamic interferences between the Suspension System and the models suspended from it. Many of the tests were purely exploratory in nature, some were made to determine the magnitudes of known effects, and still others consisted of standard tare investigation runs similar to those described in Part I of this Thesis. Since the scope of this entire investigation of tare effects is considerably greater than could be reasonably contained in one Thesis, it was decided to present at this time the results obtained to date. It is expected that the work will be carried on intermittently until satisfactory procedures are obtained.

The complexity of the problem depends, of course, on the desired accuracy of the final results. The procedure now in use at GALCIT (See Part I) is estimated to give results accurate to within 5% - 10% of the true value. This error is much too large to meet the requirements of commercial tests- - 1% is the desired result, unless the tares can be reduced in magnitude. The general magnitude and characteristics of the interferences tares are discussed in Part I for polar runs at zero yaw angle.

The tests included herein were made during the periods of 3-3-47 to 3-14-47, 3-24-47 to 4-1-47, 4-18-47 to 4-23-47, 5-12-47 to 5-13-47, and 5-23-47 to 5-26-47, with the tunnel in operation 15 hours a day. A total of 117 runs were completed. The suspension system and balances were thorough-

ly overhauled before the tests were started, and the velocity calibration was rechecked. Even with these preliminary precautions it was soon found that an unusual amount of scatter in the balance readings existed, particularlywith the wing mounted on the struts. These difficulties were largely removed by sharpening the balance knife edges and pallets, recalibrating the balances, and realigning the suspension system. All data of doubtful accuracy have been omitted. The original data are available in the GALCIT files under the heading of Report 521. An extensive Bibliography on wind tunnel model-support interferences is included on pp. II - *90* to *93*

B. Description of Model and Test Setup

All experiments were made in the closed working section of the GALCIT Ten Foot Wind Tunnel using the normal operating procedures and the standard tunnel configuration. Sketches and photographs included at the end of this report show the general arrangement of the tunnel and suspension system (See also Fig I - 1). The tunnel is vented to atmospheric pressure at the downstream end of the throat or working section, thus causing the static pressure level in the throat to be nearly at the atmospheric value. Particular attention should be given to the so-called "conning tower" in the top of the throat. This oddly shaped break in the otherwise circular section is required only when tests are made with model yaw angle variable; but it has now become standard GALCIT practice to make all conventional tests in both pitch and yaw with the conning tower open even though the symmetry of the tunnel wall is thereby destroyed. A sheet metal deflector is placed just ahead of the conning tower on the ceiling to jump the airflow across the gap. The deflector was adjusted, when originally installed, to make the velocity at the trunnion center line nearly equal to that obtained at the same point when the throat has a circular cross-section, i.e., when the conning tower is covered. The tower is always sealed to prevent airflow through the walls.

The model used for these tests was the GALCIT steel calibration-wing, which has a rectangular planform and an NACA 0012 profile (Fig. II - 1). Both the wing and its sting are symmetrical about the wing chord plane and the vertical plane through the root chord. No wax fairing was used at any time on the model since it was more important to retain fixed surface conditions than to smooth up the wing to give the minimum drag. Except for cover plate screw heads, the joints at the edge of the cover plates, and a rather bad flatting of the leading edge in spots, the wing surface was in good condition.

Because of the all-metal construction it is quite certain that the aerodynamic characteristics of the wing and sting did not vary during the entire test and that they will still be the same during future tests, a condition which is rarely attained in the conventional tests made at GALCIT. Details of the trunnion cutouts, cover plates, etc., are discussed elsewhere in the report. All tests were made with small wing tip fairings in place. Wing strut trunnion spacings of 35.42" and 58" were used, both located on the chord line at 25% of the wing chord aft of the leading edge. It is reasonably certain that model deflections under load were small and their effects negligible.

The three model support struts reach down from the suspension system cross-tube through holes in the conning tower and through their respective wind-shields to hold the model in a horizontal position at the center of the tunnel. The two wing struts are free to move only in yaw - - they do not counter-rotate. The tail strut is used to pitch the model about the wing trunnions and also moves in yaw. The model point of rotation in yaw and/or pitch is at the inter-section of the tunnel center line and the wing trunnion axis. All three struts are covered for 85% of their length by streamline sheet metal fairings which have a Navy Strut #1 profile of 33% maximum thickness (See Fig. II - 5, 6). These fairings or windshields are attached to the flat, horizontal turntable and struts. The final sealing-up (from the windstream) of these gaps is ac-complished at the tips of the windshields where thin, sheet rubber seals are inserted. All three windshields "counter-rotate" in yaw so that their chord planes are always parallel to the tunnel axis. The tail strut windshield also follows the motion of the tail strut in pitch, the arrangement being such that the portion of the tail strut exposed to the windstream always remains the same length. The latter condition is also true for the wing struts. The wind-

shields make no physical contact with any part of the metrical system except through the sheet rubber seals, a low voltage ground-indicator system being employed to ensure the continuous maintenance of this clearance.

The image system is a set of three windshields and bayonets duplicating the main system in all aspects except for structural details. It is mounted below the model as the reflection or mirror image of the main system. There is no cutout in the lower half of the tunnel which duplicates the conning tower - - the circular contour is retained even when the image system is installed. (See photos at end of report.) The standard setup does not allow the image system to be yawed. For the yaw tare tests described in this report it was necessary to build up special mounting platforms for the image fairings - - still retaining the circular tunnel contour in the lower half of the tunnel and the open conning tower in the upper half. To allow for the small fore and aft motion of the image tail windshield an open hole through the tunnel wall is left in the floor with the windshield projecting through it and a small sheet metal deflector is placed on the floor just ahead of this hole to jump the airflow across the gap. The gap length is 1 1/2 to 2 times the chord of the tail windshield, and the gap width is about twice the windshield thickness. There are no open gaps around the image wing-windshields.

C. Operating Conditions

All tests were made with a constant pressure difference between the two piezometer rings - - this means that the stagnation pressure (referenced to the ring pressure difference) was invariable for any model and windshield configuration, thus providing a fixed reference point for pressure readings. The effects, on the constancy of this reference pressure, of atmospheric pressure and Energy Ratio variations from run to run were negligible. The piezometer ring pressure difference was 17.78 lbs/ft^2, for which the average dynamic pressure in the throat was approximately 50 lbs/ft^2 and the Mach Number was approximately 0.185. Air density ratio, ρ/ρ_o , was about 0.92. The average Reynolds Number (based on wing chord) was 1.0×10^6. Air temperatures in the throat varied from 23° C to 35° C. Tunnel fan rpm, which varies with the power requirements on the D.C. driving motor, ranged from 720 to 760.

The turbulence level in the windstream has been measured in the past by several methods: (1) the critical Reynolds number of a 15 cm sphere is about 325,000; (2) hot wire anemometer tests show,

$$\frac{\sqrt{\overline{u'^2}}}{U} = 0.0075 \text{ (parallel to the wind direction),}$$

and $\frac{\sqrt{\overline{v'^2}}}{U} = \frac{\sqrt{\overline{w'^2}}}{U} = 0.0100$ (perpendicular to the wind direction); and (3), it has been observed that only about one half the depth of the drag bucket for low-drag airfoils is obtained under normal operating conditions. The scale of the turbulence has been estimated to be of the order of one inch.

Under these operating conditions it is believed that the transition line on the wing was well forward of the 20% chord line, especially as the wing leading edge was rather rough. Also, the transition position probably was

quite stable. The Mach Number was low enough to avoid important compressibility effects. The dynamic pressure was high enough to avoid any difficulties with the bayonet tares, which have been found to have a critical region around, $q = 33$ lbs/ft^2.

Greater scatter than is usual for GALCIT tests occurs in much of the data for Runs 44 to 138. This was caused by the poor condition of the balances at the start of the test. The balance troubles were finally eliminated after Run 138. Those runs in which the scatter completely masked the small differences being looked for are not included in this report. The most important runs were repeated. The scatter level is still not satisfactory and additional revisions are in process. The general accuracy level of all the data is about $\frac{1}{2}\%$. Numerous check points were taken during all Runs.

The size of the equipment, the large number of simultaneous readings, and operation of expensive equipment for 15 hour working days necessitated that most of the observations be made by the regular tunnel-operating crews. Most of the data reduction and plotting was done by the regular tunnel-computing crew.

D. Data Reduction Methods

All force and moment data are reduced to the standard American system of absolute units, as defined in Table 1. Wall interference corrections are applied only to the drag data (C_{D_P} vs. C_L); the correction was based on the theoretical spanwise lift distribution for a rectangular wing. (Fig. II - 34).

All pressure data are reduced to coefficient form by dividing the readings by, $(H - p)_o = 50.546$ lbs/ft^2. This figure is equal to the impact pressure at the center of the tunnel with the three main struts and windshields installed, the conning tower open, and the piezometer ring setting given in Section C. No compressibility correction was applied to these pressure coefficients as it would be only about 1%. However, the force and moment coefficients are corrected for compressibility effects, and, unless otherwise indicated, the dynamic pressure is assumed to be 50 lbs/ft^2. Static tares were eliminated by the normal GALCIT methods so that only aerodynamic effects are presented.

During the test it was found that some scatter in the final coefficients was caused by not carrying enough significant figures in the calculations. This was corrected by carrying out all calculations to one more decimal point than is customary for GALCIT tests.

E. Some Results from other GALCIT Tare Tests

The standard GALCIT Tare Procedure is described in Part I of this thesis and the results of a complete tare test on a conventional airplane are presented in Figures I-2, I-3, and I-4. These data were consistent and in fair agreement with the rules of thumb used in the procedure.

In Figures II-7, II-8, and II-9 are presented some results from earlier tests run in March 1942, from which one can easily understand the possible troubles which can originate from critical interferences. A bad break occurred in the lift curve just below $C_L = 0.9$ with model inverted and a similar break occurred in the drag curve. It was found that this effect, which had not been noticed previously on wings of other profiles (this wing used a Davis airfoil), was a combination of bad flow behind the elliptical bayonet, of open trunnion wells, and of the great sensitivity of the Davis airfoil to adverse flow interferences forward of the 25% chord line. A cure was effected by streamlining the bayonet and sealing the trunnion wells. These modifications are shown in Figure II-7. Also, the extent of the bad flow is indicated by the very large effect of the 4" by 1" roughness strip which was mounted on the upper wing surface in front of each bayonet. In Figure II-8 is shown the effect of Reynolds Number on the lift curve break. Increasing Reynolds Number made the situation worse. Perhaps the most inexplicable result was that, with model normal and image bayonets installed on the suction side of the wing, the break in the lift and drag curves did not occur. In Figure II-9 are shown the drag tare results before and after the trunnion and bayonet modifications were made.

Such "triggering"effects make it mandatory that great care be used when conducting tare investigations, or any wind tunnel test, to make certain such

conditions do not exist. All results must be critically examined for any unusual phenomena by a person who is quite familiar with the tare technique.

The results described above should be compared with Figures II-36 to II - 38 involving similar modifications made on the 0012 wing of the current tests. It is readily seen that this wing is very much less sensitive to airflow interferences than is the Davis wing.

One other important factor, which was found in January 1942, was the need for seals between the struts and the windshields which would prevent airflow along the strut inside the windshield. Tests showed that the drag vs. lift curves undergo a considerable "rotation" about $C_L = 0$ when the seals are removed, thus causing an apparent inclination of the windstream. See also Figure II-44 in this report.

F. Description of the General Flow Patterns

To complete the picture of the testing conditions it is desirable to describe the general flow pattern in the throat under the various configurations encountered. The data available were taken several years ago and are not necessarily correct today, but they will serve our purpose here.

In figure II-10 is shown the static pressure or dynamic head variation along the tunnel axis for four conditions. All curves have been corrected to correspond with the operating procedure of this test of holding the stagnation pressure constant at the value determined by q^* A.F. = 50 lbs/ft^2 at the trunnion ℄ for Throat Condition 3. Condition 1 is the pressure gradient for clear tunnel with completely circular cross-section. Condition 2 is the gradient for clear tunnel with the conning tower open and the deflector installed. The deflector imparts enough curvature to the flow to cause a 2% increase in dynamic pressure at the trunnion ℄ even though the throat area is sharply increased. There is a one to two inch increase in boundary layer thickness on the throat ceiling downstream of the open conning tower, which is sufficient to account for the 2% higher q at the end of the working section for Condition 2. Condition 3 shows the effects of adding the three main struts and windshields with the conning tower open. The area blocking of the two wing windshields is about 4 ½% of the throat area while the q increase is (from Figure II-10) only 2½%. Note that the tips of these wing windshields are about 19 inches from the tunnel axis. The large increase at the tail position is, of course, primarily the effect of the local high velocity field from the tail strut windshield. The dashed curve for Condition 4 was estimated from the results of Condition 3, by assuming the image windshields

have the same effect as do the main windshields.**

From consideration of Figure II-10, of the streamline patterns around each of the 3 to 6 windshields, and of the effect of the deflector on the ceiling we see that the overall flow pattern is quite complicated and that the gradients and the changes in the gradients are large and sudden. Somewhat similar q variations may be expected elsewhere in the throat. Coupled with these effects must be large deviations in the angle between the direction of the streamlines and the tunnel axis. (Note that 0.1° is considered to be a large angularity because of the rotation of the wing lift vector.)

To these windshield, deflector, and conning tower effects there must be added the irregularities in the free stream coming into the throat. These include such phenomena as single and double vortex swirl, and stagnation pressure variations. The latter are quite small and may be neglected. Characteristics of the swirl flow in the GALCIT tunnel are not well known, but the primary effect on the model is a variation in downwash and sidewash along the span. The method of control of swirl at GALCIT has been to adjust the trailing edge flaps on the corner vanes until there is no appreciable rolling moment on the steel wing at $\alpha_g = \psi = 0^{\circ}$. The reliability of this procedure has never been satisfactorily established, even though the use of large windshields makes it doubly important that cross-flow be reduced to zero to prevent the development of windshield "lift" and the resulting unsymmetrical velocity fields around the windshields. For some symmetrical swirl patterns the tare procedure tends to eliminate the effects - - at least at zero yaw angle.

- - - - - - - - -

** This assumption is seriously incorrect for the conditions given. See discussion of experimental results.

G. Interference Effects of Several Simple Flow Patterns

In this section we will consider some of the flow patterns which surround the model and discuss possible methods of determining their effects on the model.

Case 1. In Fig. II-11 is shown a wing immersed in the augmented dynamic pressure caused by the wing windshields. It is assumed that the flow direction is not changed by the addition of the windshields. The non-uniform q increase over the wing span will change the load distribution on the wing, the effective aspect ratio, the effective Mach Number, and the Reynolds Number; it may also change the transition location and the stall pattern. But if $2\delta q$ is everywhere small and the model and bayonets are not near a critical Reynolds Number condition it may be assumed that the effects of the q increase are linear and additive. Thus the image windshields will have the same effects on the model as do the main windshields, and the interference tare of the latter will be equal to the difference between model-inverted with images and model-inverted without images. Still further, if the lift, drag, and pitching moment values with images in can all be brought back to the corresponding values at the same geometric angle of attack with images out by a constant factor, A, it may be assumed that, within the desired accuracy limits, an average value for δq may be used and the interference effect would be simply a uniform change in velocity (i.e., $\delta L = AC_L \delta q$, $\delta D = AC_D \delta q$, $\delta M = AC_m \delta q$). When performing the calculations note that corrections to C_D and C_m which are proportional to C_L may be applied before the tare correction is made to C_L; but corrections which are proportional to C_L^2 should not be made until after the lift tares have been applied unless $C_L^2 \beta \frac{\delta q}{q}$ is negligible (where $\Delta C_D = \beta C_L^2$).

Suppose, instead of the simple result stated above, we assume:

$\delta L = AC_L \delta q + B$, $\delta D = AC_D \delta q + C$, and $\delta M = AC_m \delta q + E$; where $B \frac{\delta q}{q}$, $C \frac{\delta q}{q}$, and $E \frac{\delta q}{q}$ are negligible quantities. Then the interference effect is a uniform change in velocity plus an additive constant. Again, note that corrections to C_D and C_m which are proportional to C_L should not be applied before the tare correction is made to C_L unless γB is negligible, where $\Delta C_m = \gamma C_L$, etc. Similarly one should not apply a correction proportional to C_L^2 before lift tares unless $(\beta C_L^2 \frac{\delta q}{q} + 2B\beta C_L)$ is negligible.

So far in Case I we have considered only the tares on the wing. We will now take up the determination of the bayonet tares. There will be an increase in q on the main bayonets when image windshields are added which will cause an increase in drag, an increase in buoyancy lift of the bayonet, an increase in the pressure lift across the strut seal inside the windshield, and an increase in the interaction lift, drag, and pitching moment between wing and bayonet. These effects are all small and may be assumed to be proportional to the local q rise at the bayonet positions. Inserting the image bayonets will have the effect of doubling the direct bayonet forces and moments, and of cancelling out (at zero wing lift) the buoyancy and seal lift of the main bayonet and seal.

The lift tare due to bayonet buoyancy and seal pressure is not so simple to determine. The so-called buoyancy lift is caused by the pressure gradient along the bayonet --- the exposed part of the bayonet being in a pressure field considerably lower than atmospheric pressure (see Fig. II-12). The integrated pressure force over the entire strut system gives a net force in the lift (vertical) direction. Usually this force will be directed toward the wing. The strut-to-windshield seal also carries a pressure load which is transmitted to the strut and acts toward the wing. Results from tests show the pressure across the seal to vary from almost zero to 1-1/4 times free

stream dynamic pressure. This variation is caused by the local pressure influence from the wing as the wing is pitched and is a linear function of the local wing lift at the trunnion location. An attempt was made to determine the variation in bayonet lift with wing angle of attack, but the setup did not function properly, and the test will have to be repeated later on.* The lift curves in Fig. II-12 show the lift tare characteristics for various configurations. For image-system-in there is no tare at $C_L = 0$ but the lift curve slope is lower than the true value by about 1%**. For image system out there is a shift at $C_L = 0$ of $C_{L_t} = \pm 0.010$ and the slopes are low by about 1/2%. In calculating these values it was assumed that the bayonet buoyancy was equal to one half of the seal pressure lift. Note that the lift and drag of the tail strut seals and bayonets will cause a pitching moment tare. For wing alone tests this will be nearly constant.

It will be assumed as always at GALCIT that the dynamic pressure for normal tests without images is the averaged value determined from velocity surveys with the main windshields installed. Actually, in so far as Case I is concerned, the final δq correction determined from the tare runs is more nearly correct than the value determined from a q survey across the tunnel.

We are now ready to set up the tare determination procedure for Case I for a wing alone test:

a) Determine $q_{av} = A.F.xq^*$ from tunnel flow calibration.
   Get pressure difference setting (h) of piezometer rings from this

b) Make polar run with model inverted with given value of h

c) Make polar run with model inverted and complete image system installed, with given value of h

d) Determine strut-buoyancy and seal-pressure lift tares. May have

---

* See Appendix 1, p. II-159, for calculation of buoyancy lift.

** Error in C_{D_p} at $C_L = 0.7$ for a 1% error in C_L is 0.0004 for the steel wing.

to make extra runs to get strut buoyancy tares. Seal-pressure tares can be calculated from measurement of the windshield tip pressures during runs (b) and (c).

e) Apply strut-buoyancy and seal-pressure lift tares to lift data of runs (b) and (c). Then plot C_L (based on q_{av} of (a)) versus α_g for runs (b) and (c). Determine ration ($\mathcal{E}$) of lift curve slopes as plotted;

$$\mathcal{E} = \frac{dC_L / d\,\alpha_g \text{ for run (c)}}{dC_L / d\,\alpha_g \text{ for run (b)}}$$

Determine $\dfrac{\mathcal{E}}{\dfrac{q^*}{qxA.F.}} = \eta$ from tunnel flow data, such as Fig. II-10, and A.F. charts.

f) Reduce lift, drag, and pitching moment data to coefficient form, using as dynamic pressure,

for run (b) the value $q_{av} \dfrac{\mathcal{E}}{\dfrac{q^*}{qxA.F.}}$ or $q_{av}\,\eta$,

and for run (c) the value $q_{av} \dfrac{\mathcal{E}^2}{\dfrac{q^*}{qxA.F.}}$ or $q_{av}\,\mathcal{E}\eta$.

g) Plot results from step (f) versus α_g or C_L. The difference between the curves will be the tares as a function of α_g or C_L. Add the lift tares of step (d) to get the total lift tare.

h) There are four tare corrections resulting from steps (a) to (g) inc.: η, C_{L_τ}, C_{D_τ}, C_{m_τ}, which must be applied to all runs with model normal and no image system. The dynamic-pressure averaging correction, η, may be applied as a change in the h setting on the piezometer rings.

i) If drag and pitching moment data are to be calculated with a C_L or

a C_L^2 correction in them in step (g), be sure to use the C_L values which already have been corrected for both tares and dynamic pressure.

j) Note that the above steps are set up only for a wing alone test. It is tacitly assumed that the q corrections are applicable to the sting and tail bayonets. Although this is not strictly correct, the error should be negligible. This may not be true for a model with wing, fuselage, and tail; we will not consider the complete model tare problem at this time.

Case 2. The flow pattern for this case is illustrated in Fig. II-13. It is the case of uniform inclination (in a vertical direction only) of the streamlines with respect to the tunnel axis. Since the lift force measured by the balances is perpendicular to the tunnel axis and the drag force is measured parallel to the axis, this type of flow results in angle of attack and drag tares as is shown in the figure. The lift tare is negligible. The α tare is equal to the inclination, and the drag tare is equal to the lift forces multiplied by tan α_τ. For model-normal and downwash in the tunnel, α_τ is negative and C_{D_τ} is negative for positive lift.

The inclination angle can be determined from one half of the difference between the run with model-normal and the run with model-inverted. Because of the great sensitivity of drag to the rotation of the lift vector, it is customary to determine the inclination from the drag curves.

Case 3. The flow pattern for case 3 is the one for uniformly curved flow as shown in Fig. II-14. The effect of curvature on an airfoil is to make it act like an airfoil with camber whose curvature is just the reverse of the flow curvature. Inverting the model will change the sign of this effective camber and thus allow the determination of the lift and pitching moment tares. An

angle of attack (instead of lift) tare may be used if desired, but the lift tare is more straight-forward and will compensate for the change in $C_{L_{max}}$ due to camber.

The drag tare will be positive for both normal and inverted models and cannot be determined by the application of an image system procedure. In fact, for symmetrical airfoil wings the application of the image system tares will double the drag error due to the curvature caused by the windshield and will leave intact the drag error due to free stream curvature. This means that the final corrected drag curves for symmetrical airfoil wings will be too high by the amount of these drag errors, but normal and inverted drag curves will be identical. In general, the drag error for cambered airfoil wings will always be less than that for symmetrical airfoil wings; for positively cambered wings the final drag for model normal will be too high, while the drag for model inverted will be too low. The magnitude of these curvature errors in drag at GALCIT is unknown.

This discussion brings out the major fault of the image tare system in that it works only if the tare doubles in magnitude and retains the same sense upon installation of the image system, or if the magnitude remains the same but reverses its sense when the model is inverted. It can be shown that drag tares due to effective warping of the wing by warped flow will not be corrected for by the image system method, excepting any warpage in a horizontal plane. For the horizontal-plane warpage the image system effectively doubles the magnitude and so gives the correct drag tare.

To experimentally determine the drag tare due to flow curvature it is necessary to have an auxiliary support system which does not induce appreciable curvature in the flow, and, also, to remove all appreciable free stream curvature. Fortunately the drag tare due to curved flow is small for moderate

radii of curvature. It should be noted that the effective curvature from the windshield influence will vary with the fore and aft position of the wing and with wing chord and span.

Case 4. If one windshield induces curved flow as shown in Fig. II-14, then the addition of the image windshield will give the flow pattern shown in Fig. II-15. Estimates of the tare characteristics for this case are given by the curves in the Figure.

In Case 3 it is assumed that the radius of curvature of the flow is everywhere the same over the model. This is most likely not true if the curvature is caused by the windshield, i.e., the radius would increase with distance from the windshield tip. The flow lines of Fig. II-15 are drawn with the assumption that the curvature varies with distance from the windshield and that all of the curvature is caused by the windshields. The image system procedure will, in general, overcorrect for model normal lift and pitching moment tares, but will partially correct the curvature error in the drag tares. For model inverted tares the reverse is true.

Case 5. In this Case we will consider the proper tare procedure for the combined flow patterns of Cases 1, 2, 3, and 4, assuming also that the patterns of Cases 2, 3, and 4 vary spanwise along the wing.

a) Determine q_{av} = A.F. x q* from tunnel flow such as is shown in Fig. II-10. Calculate setting (h) of piezometer ring pressure difference for q_{av}. We shall use q_{av} as the desired operating dynamic pressure.

b) Make 3 runs: (1) model normal with image system, (2) model inverted with image system, and (3) model inverted. Use same value of h for all runs. As a check, should make a fourth run with model normal.

It is assumed that we want to determine the tares for the model-normal configuration.

c) Determine strut-buoyancy and seal-lift tares either by calculation from previous tests or by measuring them. The seal lift tare can be calculated from measurements of the windshield tip pressures during the regular tare runs. The strut buoyancy and seal lift tare combined can be experimentally determined by another run (2A) with model inverted and bayonets projecting into the trunnion wells as in run (2) but not physically touching the model. Then the difference in the lift data (at same α_g) of runs (2) and (2A) will be the lift tare.

d) Apply the strut buoyancy and seal lift tares of step (c) to the lift data of runs 2 and 3. Calculate and plot C_L (based on q_{av}) versus α_g for runs 2 and 3. Determine ratio ($\mathcal{E}$) of lift curve slopes at $\alpha_g = 0$ as plotted,

$$\mathcal{E} = \frac{dC_L / d\alpha_g \text{ for run 2}}{dC_L / d\alpha_g \text{ for run 3}}$$

Determine, $\eta = \dfrac{\mathcal{E}}{q^*/q \times \dfrac{1}{A.F.}}$

from tunnel flow calibrations (see Fig. II-10) and A.F. charts.

e) Calculate effective dynamic pressure for runs with image system,

$$q_e \text{ (with image system)} = \mathcal{E}\,\eta\, q_{av}$$

Calculate same for runs without image system,

$$q_e \text{ (no image system)} = \eta\, q_{av}$$

Now reduce all original data of runs 1, 2, and 3 to coefficient form using the proper value of the effective dynamic pressure. Be sure to calculate C_{L_g} to 4 decimals, and C_{D_g} to 5 decimals. Apply the proper strut buoyancy and seal lift tare to runs 1, 2, and 3.

f) Calculate $C_{D_p'}$ for runs 1 and 2, where $C_{D_p'} = C_{D_g} - (C_{D_i} - \Delta C_D)$ and using C_L as obtained in its corrected form in step (e). Then plot C_{m_g}, α_g, $C_{D_p'}$ vs. C_L for runs 1 and 2 and draw in the mean curve between the corresponding components, where the mean curve is the locus of the average of the values of the two runs taken at constant C_L values. These mean value curves will represent the model with image-system-in and corrected for free stream inclination lift and drag, and for free stream curvature lift and pitching moment. The drag tare due to curvature can not be accounted for (see discussion in Cases 3 and 4). Then plot C_{m_g}, α_g and $C_{D_p'}$ vs. C_L for run 3.

At constant C_L values subtract the readings of run 3 from the readings of the mean value curve for image-system-in and plot the differences against C_L. These will be the final tare values for drag, pitching moment, and angle of attack. We now have five tare corrections to apply to the runs with model normal without image system:

(1) C_{L_τ} from step (c)

(2) η, the q correction, from step (d)

(3) C_{D_τ}, C_{m_τ}, and α_τ from step (f)

All tares are to be subtracted from the uncorrected data, except that η is a multiplicative correction to dynamic pressure.

Before setting up the procedure for step (f) it was necessary to determine whether to use lift or angle of attack as the independent variable. For the flow patterns of Cases 1-4 the results will be the same with either parameter, except that when α_g is the independent variable the α_τ of step (f) is replaced by a corresponding C_{L_τ}. It is possible to give conditions under which α_g is proper, and equally possible to specify when C_L is the

proper variable. Not enough is known at present about the effect of minor modifications on the interferences between struts and model to allow for a logical decision. The use of α_g as the independent variable deserves strong consideration because its use will materially reduce the man hours required to work up a set of tares. However, for wing alone tests, and usually for complete models, the lift coefficient is certainly the most important parameter and it appears to be much better practice to correct angle of attack and thereby leave the lift unchanged and at the value obtained on the balances (except for strut and seal-pressure buoyancy effects which are not true lift). For instance, a sharp transition shift on the wing might cause a bad break in the lift curve. The use of α_g as the free variable in the tare procedure would cause this break to show up in the final corrected coefficients at a lift coefficient other than that at which the break occurred -- this would be definitely undesireable if we assume that the lift coefficient is the parameter predominantly determining the wing characteristics. By such reasoning it was decided to use C_L as the independent variable - - at least for wing alone tests.

H. Discussion of Assumptions

In the preceding sections the use of the image system for determining the interference of the struts and windshields on the wing has been rather thoroughly discussed. The more obvious inadequacies of the procedure were pointed out and the correlated assumptions were given. To summarize these considerations we will now list the basic assumptions of the tare procedure of Section G, Case 5:

1) It is assumed that the image windshields, bayonets, seals, trunnion cover plates and seals, and tunnel wall boundaries duplicate the corresponding items of the main suspension system and wall boundaries in the upper half of the tunnel to such a degree that the effects of the image system on the model are equal to the effects of the main system within the desired accuracy limits.

2) It is assumed that the strut-buoyancy and seal-pressure lift tare can be determined separately.

3) It is assumed that the interaction between the main and image support system can be eliminated by a correction to the effective dynamic pressure.

4) It is assumed that, for all runs in the tare series, the effects on model drag of flow curvature in any vertical plane parallel to the tunnel axis are negligible.

5) It is assumed that the model geometry and surface condition do not change during the tare tests.

6) It is assumed that the stagnation pressure is the same for all tare runs.

7) It is assumed that the lift coefficient C_L is the fundamental airplane parameter, not angle of attack.

8) It is assumed that the averaging procedure of step f in Case 5, Section G, eliminates the effects of nonuniformity in the free stream flow.

The validity of many of these assumptions is definitely questionable, particularly for the drag tares. Results of many tare tests (e.g. Fig. I-2, 3, 4) show α_τ and C_{m_τ} to be small and generally invariant with lift coefficient, but their relative importance is considerably increased by the indications they furnish of the interference flow patterns. For instance, nearly all GALCIT tare tests run to date have shown a shift in C_m and α_g for model normal and inverted with image-system-in, and it has been assumed that this shift was caused by curvature in the free stream - - a condition which might cause an indeterminate error in the drag tares. The results of tests, described in the next section, indicate that this C_m and α_g shift may be caused by the lift and pitching moment tare from tail-strut-buoyancy and tail-seal-pressure lift. The possibility of such an effect had been previously indicated by the fact that the orientation of the curvature as determined by the C_m shift was opposite to that determined by the α_g shift (after correction for inclination).

For routine tests the wind tunnel operator is continually faced with the difficult problem of extrapolating the tares as determined for one model configuration to use with dozens of other model configurations. This problem arises because it would at least triple the cost of a given series of runs if tares were determined for all configurations. Fortunately, most wind tunnel tests consist of a few basic runs with greatly different model configurations, and of many other runs which involve only small changes, such as elevator angle, fillets, etc. The results of dozens of GALCIT tare test series show that these small changes usually have little effect on the tares, so that it is sufficient to determine the tares only for the basic configurations and

extrapolate them for other conditions. Rules of thumb, based on this experience, are given in Part I of this paper. Even so the expense of running tare tests is frequently so prohibitive, that the test engineer is under great pressure to extrapolate the tare data too far. Thus, it is the objective of this research program, first to determine a tare procedure with the desired accuracy, and second to develop, if possible, a method for predicting the tares or at least reduce the cost of the tests.

The method of attack on these problems was divided into three parts: 1) determine experimentally the factors which cause interference, their magnitudes and characteristics; 2) survey the entire flow field in which the model is immersed to determine both direction and magnitude of the velocity at all points and under all tunnel configurations; and 3) develop a method of predicting tares without having to resort to experimental tests. Because of the great complexity of the third phase, it was decided to carry out the research phases in the order given above, with the hope that the results of the first two phases would give proper direction to the development of the third phase. The experimental results discussed in the following section are part of the work scheduled for phase one.

I. Discussion of Experimental Results

A complete listing of all runs (or tests) made to date is given in chronological order in the Run Index (page II-5). Some of the data were considered unreliable and are not presented in this report. The run numbers which are missing represent tests originally scheduled but not made because of lack of time or because results from other tests indicated that the anticipated effects would be negligible. The data of Runs 1 through 42, and 152 are tabulated in Table 3 (page II-94) in dimensionless form. Results of other runs appear in the form of plots. Definitions of nomenclature and model dimensions are given in Tables 1 and 2. Figures I-1, and II-1 through II-6 show the arrangement of the struts, windshields, and model in the tunnel throat. All results are discussed in the following Groups.

Group 1 - - Effects of Windshields and Struts on the Velocity at the Throat Center (Fig. II-16 to 20)

In Fig. II-10 are shown the dynamic pressure gradients along the tunnel axis for four conditions as determined from some old tunnel calibrations. These curves show: a) the combination of the open conning tower and the deflector increases the q along the tunnel axis by about 2%; b) the effect of the two main wing windshields at 35.42" trunnion spacing is a q increase along the tunnel axis extending from 2 ft. upstream of the yaw axis to 2 ft. downstream and reaching a magnitude of 2.4% q at the yaw axis; and c) the effect of the main tail windshield extends from 1 ft. ahead to 1.5 ft. behind the tail strut bayonet, reaching a peak value of 3.4% at the bayonet ℄ .

These effects will be compared with the data in Col. 7, Table 3, which are the readings of the pitot-static tube at the intersection of the tunnel axis and the yaw axis. It should be mentioned that $q/q^* = \frac{H - p}{(H - p)_o}$. Because of the large scatter in the data at least two readings were taken at each point, and the figures in Col. 7 are the average values.

Comparison of Runs 2 and 3 shows that the main wing windshield-to-strut seal has no effect on centerline q even though the windshield is directly above the pitot. However, the data in Fig. II-20 show an appreciable effect of the tail windshield-strut seal with the windshield 12 in. or more behind the pitot. This may possible be explained by the fact that the volume of air flowing out the wing windshield with seal open is quite small compared to the flow out the tail windshield - - the different flow rates being the result of the very small area through which the air must pass in going through the wing windshield and the comparatively large area in the tail windshield.

Comparison of the results of Runs 34 and 36 show that the opening in the floor (plus the small deflector) for the image tail windshield has a negligible effect on the q at the wing trunnion position.

In Runs 26 and 28 data were taken to show the effect on the centerline q of small vertical and lateral shifts of a wing windshield. The main wing and tail windshields were installed at the standard 35.42" spacing, and the south image wing windshield was mounted in its normal position with the 35.42" trunnion spacing (i.e., as the reflection of the south main wing windshield). The results are collected on the following page.

Run	F_I^S Position	q/q*
26	Left ½" (Looking upstream)	1.023
"	Normal	1.026
"	Right ½"	1.020
28	Up 3"	1.030
26	Normal	1.026
28	Down 3"	1.038

It is not evident to the author why both of these small lateral shifts from the normal position should decrease the centerline q (note pitot is 17 in. from windshield tip), or why both of the 3 inch vertical shifts should increase the q. Actually it had been expected that the effects would be negligible. Possibly these effects are caused by swirl in the free stream or by flow curvature induced by the windshields. Swirl or vortex flow would, of course, develop a lateral force or "lift" on the windshields.

The most important (and most disturbing) results in Group I are given in Figs. 16A and 16B, which show the change in centerline q as the main and image wing windshields are installed one by one. The image windshields cause a two to three times larger q increase than do the main windshields. Very likely this is the effect of the open conning tower (see Fig. I-1), in that the main windshields do not have the same blocking effect as do the image windshields. Also, for both main and image windshields, the north one induces a greater increase in q than does the south one - - - this could be explained by swirl in the

windstream, or by curved flow induced at the pitot by the first windshield installed and cancelled by the second windshield installed. Measurement of the shape, size, location, and attitude of the windshields did not show up any important differences except for the north image wing windshield which was 3% too small in thickness. The two image windshields increase the centerline q by 5.5% while the two main windshields increase the centerline q by only about 2%. This is a serious difference and certainly must be thoroughly investigated. An explanation of free stream swirl or windshield induced curved flow could be logically argued as the cause; but, the action of the conning tower in the tunnel ceiling is believed to be the source of the trouble.*

The results of Figs. II-17 to 20 are reasonable and require no discussion except to say that the effect of the tail strut bayonet in Fig. 20 is of doubtful validity. It should be remembered that all data shown are the averages of two or more readings and should be reliable to 0.3% of q. Comparison of the data of Table 3 (Col. 7) and Figs. II-16 to 20 with the old calibration results in Fig. II-10 shows good agreement between the tests.

Group 2 - - Effects of Windshields and Seals on Pressures inside the Windshields (Fig. II-21 to 26)

The data described in Group 1 dealt only with the disturbances in the flow at the center of the working section as measured by a Prandtl pitot-static tube. In Group 2 are presented the readings from several pressure orificies located inside the windshields. Since the possible

- - - - - - - - - -

* These conclusions are proven correct by the data given in Appendix 2, page II- 166

importance of the pressures inside the windshield has already been discussed it is sufficient to remark here that the balance readings are the resultants of all the pressure forces on the model, bayonets, seals, struts, and rigging, and that these pressure forces must be accounted for in some way. All numerical data are listed in columns 11 through 15 in Table 3, and the windshield tip pressures are plotted (and listed) in Figs. II-21 to 26. Accuracy of these data is not better than 3/4%. See also Figs. II-5 and 6.

In Fig. II-21 are shown the main wing windshield tip pressures, measured on the windstream side of the strut-windshield, rubber-diaphragm seal at the downstream side of the bayonet hole and 1-3/8" up from the windshield tip (see Fig. II-5). The pressure without a seal is 23% below the static pressure indicated by q* or $(H - p)_o$, and, when the seal is inserted, the tip pressure falls to 45% below p_o. When the bayonet is installed the tip pressure falls another 15% - - this may be a local effect caused by air flow around the elliptical bayonet. From Columns 11 and 12 of Table 3 note that on the atmospheric side of the seal there exists nearly atmospheric pressure, which means that, with bayonet in, the pressure drop across the seal is about 55% of q* or 28 lbs/ft^2 for q* = 50 lbs/ft^2. Obviously the lift load on the seal is not a negligible tare. The variation of the tip pressure with angle of yaw is interesting but not particularly important, even though the bayonet causes appreciable changes in the local pressures. Comparison of Runs 10 and 29 shows the effect of the image wing windshield, F_I^S, when mounted below the main wing windshield on the tip pressure in the

latter. The spacing is 16.3 inches and the drop in pressure is about 5%. From Fig. II-17 note that for the main wing windshield the static pressure drops only 3% at 8 inches from the pitot-static tube - - this again indicates that the image windshields have a much larger blocking effect than do the main windshields (see also Fig. II-16).

Fig. II-22 shows that the tail windshield has little effect on the main wing windshield tip pressures for tail lengths greater than 15 inches. For a 12 inch tail length there is a 1% drop in pressure. Note that the tail windshield is moving along the centerline of the throat whereas the wing windshield is offset about 16 inches from this centerline. In Fig. II-20 the tail windshield causes a rise in pressure along the centerline ahead of it which is consistent with the probable pressure distribution around the tail windshield. Data of Fig. II-23 and Col. 10 of Table 3 are in reasonable agreement with the pitot-static readings of Figs. II-16 to 20. The results of the lateral windshield shifts of Run 26 are again inconclusive as are the results of Run 28, although one could say that small shifts (less than 1 inch) of a windshield in any direction have negligible effects at points 10 inches or more from the windshield (see Col. 10, Table 3).

The effects on the main wing windshield tip pressure of the image tail windshield and its access hole in the tunnel floor (with deflector) are less than 1% of q* - - see Runs 34, 36, and 40A in Figs. II-22 to 23; but, since these data are only good to 3/4% of q* at best, it can only be concluded that the effects, if any, are small. Comparison of Runs 20 and 21, Fig. II-22, shows again that sealing the tail windshield

decreases the static pressure at the wing trunnion plane by ½% to 1% of q* for tail lengths less than 15 inches (see also Fig. II-20). Data of Col. 10, Table 3, Runs 14, 16, and 40A show no effects of the tail windshield vertical position, although Fig. II-18 does show an appreciable effect on the centerline static pressure.

Columns 11 and 12 of Table 3 show the effects of the various configurations of Runs 1 through 40A on the pressures on the atmospheric side of the wing windshield seal and on the atmospheric pressure at the working section - - all referenced to the static pressure inside the throat. Note that the tunnel is vented to atmospheric pressure at the downstream end of the working section and at the fan nacelle. Study of the data shows; 1) that the centerline static pressure rises about 4½% of q* from the clear-tunnel condition to tunnel with six windshields installed; 2) pressure inside the wing windshield is about ½% of q* below atmospheric pressure except when the seal is removed, in which case it is about 1% below atmospheric pressure (see Runs 2 and 5); and 3) use of external or atmospheric pressure as a reference for pressure levels inside the tunnel will give erroneous results.

Pressure data for the tail windshieldsare listed in Cols. 13, 14, and 15 of Table 3 and partially plotted in Figs. II-24, 25, and 26. Fig. II-6 shows sketches of the windshield, strut, bayonet and seal arrangement. Observe that the seal is located about 14 inches from the tail windshield tip as compared with 2 inches for the wing windshield, and that the tail bayonet is circular whereas the wing bayonet is elliptical. Also the tail strut seal blocks off a much larger air gap than does the wing strut seal. With this geometry in mind it is clear

why, in Fig. II-24, there is essentially no effect of angle of yaw or angle of attack on the tail windshield tip pressures, either with or without the tail bayonet. With seal-in, the tip pressure is about 63% of q* below the centerline static pressure - - this agrees with the wing windshield tip pressure of Fig. II-21. The effect of the image tail windshield is to increase the tip pressure by 3% of q*, whereas the image wing windshield decreased the tip pressures by 5% of q* - - the reason for this is not known (see Run 29 of Fig. II-21 and Run 40A of Fig. II-24).

Fig. II-25 shows the effect of the tail strut seal on the tip pressures. Because of the large air gap between the tail strut and its windshield there is considerable air flow through the windshield into the tunnel and the tip pressure rises to within 10% to 15% of atmospheric pressure. With seal out there is very little change of tip pressure as the tail windshield moves fore and aft in the tunnel; but with seal in the tip pressure decreases sharply as the windshield moves upstream. The effects of adding the tail bayonet, with and without the seal, are large, although consistent with the wing bayonet effects of Fig. II-21. Comparison of Runs 34 with Runs 15, 16, and 17 (Fig. II-25) shows the effect on the tail windshield tip pressure of adding the image wing windshield to be a pressure decrease of about 5% of q* - - this is not consistent with other results (see Fig. II-10) and places doubt on the validity of these data, although again the answer may be the much larger blocking effect of the image wing windshields. In this respect, study of the data in Fig. II-26 shows the tail windshield tip pressures are consistent for the runs listed.

Pressures on the atmospheric side of the tail strut seal are given in Col. 14 of Table 3. The values are the same as atmospheric pressure except when the windshield is not sealed, in which case the pressure is 3% below. Compare this with the results for the wing windshield value of 1% below atmospheric pressure with seal removed. Again this indicates there is a large air flow through the tail windshield when the seal is removed.

The image wing windshield was first installed in Run 25 (see Run Index) and the tip pressure was measured without a seal - - because the windshield was not vented to any pressure but the tip pressure it had previously been assumed that the image windshield tip pressure would be the same as the main windshield tip pressure. All previous tare tests at GALCIT have been run without an image windshield seal. This assumption was checked in Run 25 and found to be considerably in error, for the image windshield tip pressure (without seal) was 100% of q* lower than the main windshield tip pressure. With the seal in place the tip pressures were within 10% of the same value. Apparently the depth of the opening at the windshield tip has an important effect on the flow over the tip and the pressures inside the tip - - this is in agreement with test data reported by the British on the effect of orifice geometry on the indicated orifice pressure. In addition to obtaining the correct tip pressure in the image wing windshield a seal is required so that the lift tare on the seal (and image bayonet) may be determined, and furthermore, it is necessary to vent the image windshield to atmospheric pressure. The latter was done by drilling a 3/16" hole in

the image windshields near the base and outside of the working section (Run 30). Study of Fig. II-5 will show the image windshield is still not an exact replica of the main windshield in internal geometry, but it is believed to be close enough to give the required accuracy for tare tests.

In Run 38 (See Run Index) the same tip pressure checks were made on the main and image tail windshields. Here the tip pressure was measured at a point 14 inches from the tip (next to the seal in the main windshield, Fig. II-6); and it was found that, after sealing all leaks in the image windshield, the tip pressures were the same even though there was no seal in the image windshield. This result agrees with the conclusion implied in the preceding paragraph that the tip pressure is largely determined by conditions near and just inside the tip. An image tail windshield seal was not installed until after Run 152 of this test (GALCIT Rep. 521), which means that the tail strut lift tares were not properly determined until after that Run.

Group 3 - - Study of Air Loads on Bayonets, Struts, Seals, and Rigging without Model (Fig. II-27 to 32)

The first six columns of Table 3 contain all of the force and moment data of Runs 1 through 42 and 152. These data give the balance readings for all the runs made without a model in the tunnel, and represent the resultants of the direct air loads on the entire support system. As was expected, the readings are small but certainly not negligible. There is considerable scatter present especially in pitching and rolling moment but enough readings were taken to give quantitative results with sufficient accuracy. Later tests showed that the scatter

was caused by roughness on the knife edges and pallets of the beam balances and, when angle of yaw or pitch was varied, by deflections in the suspension system. In the following discussion each component will be considered individually. All balance data are listed in standard coefficient form based on the wing dimensions (see Table 1 or Fig. II-27) and on the nominal dynamic pressure of 50 lbs/ft^2. No corrections of any sort have been used. When studying these data one should bear in mind that this wing closely represents the average size of the models tested in this tunnel, for which the desired precision values are:

$\delta C_L \backsim 0.0020$ $\qquad$ $\delta C_m \backsim 0.0010$

$\delta C_D \backsim 0.0001$ $\qquad$ $\delta C_\ell \backsim 0.0002$

$\delta C_c \backsim 0.0010$ $\qquad$ $\delta C_n \backsim 0.0002$

Here we define a precision value as largest allowable deviation from the true reading for all normal flight attitudes of the model below $C_L = 1.0$.

(a) - - Drag

When a model is attached to the bayonets a portion of the bayonet is covered by the model and so is not exposed to the windstream. Usually the trunnion point is sunk into the model by $\frac{1}{2}$" or more. To eliminate this tip area and to prevent tip effects in yaw, 1-$\frac{1}{4}$" diameter rubber spheres (handballs) were mounted on the bayonet tips with the sphere centers on the trunnion axis for all tests except Run 152. The sphere drag (neglecting interference effects, etc) was calculated as follows:

$q = 50$ lbs/ft^2 $\qquad$ Reynolds Number = 89,000

$M = 0.185$ $\qquad$ Diam. = 1.25"

$C_{D\ \text{sphere}} = 0.45 = 0.00046$ (using wing area = 8.27 ft^2)

To obtain the drag of the exposed portion of a bayonet it is only necessary to subtract this sphere drag from the balance readings.

With strut seals in place and all bayonets removed it is to be hoped that $C_D = 0$, and actually this is true for Runs 1-3, 14-19, 34 and 36. Study of Runs 20, 21, 22, 23, and 152 shows a drag due to tail strut and seal of about 0.0003 in C_D which must be caused by circulation of air in the tip of the tail windshield below the seal. This indicates the tail strut seal should be mounted as close as possible to the tip of the tail strut windshield in a manner similar to the arrangement of the wing strut seal. The latter gave no drag readings except when the seal happened to stick during a yawing motion. However, a further check will be made to make certain that these conclusions are correct when the tail strut is attached to a model and not free to swing fore and aft as was the case in these runs. Certainly this tail strut and seal drag is much too large an error to neglect.

Inspection of Runs 4-10, 20-29, 40, 42 show quite consistently the drag of each bayonet to be, $C_D = 0.0011$ (Sphere drag has been removed). Note that this figure applies only to the flat-sided elliptical wing bayonets (MSB in GALCIT notation) and to the round, serrated, "power-off" tail bayonet which were used exclusively in these tests. It is not too surprising to find the same drag for both the wing and tail bayonets. (See Fig. II-5, 6). An approximate calculation of the drag of the tail bayonet ($R = 18{,}000$, $C_D = 1.2$, Diam. = $\frac{1}{4}$", length = 4.5") gives $C_D = 0.00113$ based on wing dimensions; this seems to be a reasonable check. These data also indicate that the vertical position

of the windshields should be kept within 1/16" of the "normal" location at all times.

Variation of wing bayonet drag with angle of yaw is shown in Fig. II-27 and 28. These are averaged results so no experimental points are plotted; however, the scatter was small. There is, of course, no drag variation with angle of attack for the wing bayonets, nor with angle of yaw for the tail bayonet.

The drag level (C_D = 0.0011) of the bayonet at zero yaw angle gives an indication of magnitude of the possible changes in drag because of the interference effects of a model. If a wing, say, produces an average increase in the windstream velocity around the wing bayonets of 10%, then the interference drag would be 0.0002. It appears that, when attempting to calculate the drag tare, one may use velocities averaged over the span of the bayonets; i.e., local variations are not important.

(b) - - Crosswind Force

Crosswind force readings were taken only during eight runs, and of these, Runs 1, 2, 3, and 152 should show zero readings. Examination of Column 6, Table 3, will indicate that the readings obtained for these four runs are considerably below the precision value desired and so may be neglected. The results of Runs 4, 6, and 9 are reasonably consistent and the averaged values are plotted in Fig. II-27. Run 5 shows up quite differently from this curve - - a result, undoubtably, of the omission of the wing strut seal for this run. In general, this same characteristic of erratic and inconsistent data occurs whenever the strut seals are omitted. The large scale for the Crosswind Force Coefficients of Fig. II-27 has been used for convenience, and not because the data are

that accurate. There is, of course, no crosswind force developed by the circular tail strut.

Close analysis of both the Drag and Crosswind Force Data in Table 3 shows the wing bayonet is not symmetrical and the force values at large positive and negative yaw angles are not identical in magnitude as they should be. However, the force tares are not important for large angles of yaw and the differences are too small to appreciably affect the moment tares; so we will neglect the lack of symmetry of the wing bayonets.

(c) - - Lift

Lift balance readings, in coefficient form, are given in Col. 1 of Table 3 for all runs without a model mounted. For Run 1 with the working section entirely clear, the lift is zero as are also all other forces and moments -- this is as it should be. Inspection of the results for all other Runs shows appreciable lift readings even though there is no model in the tunnel or any "lifting surfaces" of any sort (see Figs. II-5, 6). Clearly this must be due to one or both of two "apparent" lift tares -- pressure difference acting on the seals or the vertical component of the pressure forces on the surface of the tapered bayonets. Since both tares have the same sign it was necessary to separate them to determined the magnitude of each; and also it is possible that the spherical tips on the bayonets are inducing a lift tare because of the interference of the bayonet on the sphere pressure distribution. However, close analysis of the data indicates the following results:

Wing bayonet lift ⌣ $C_L = 0.0005$
Tail " " ⌣ $C_L = 0.0000$
Wing strut seal lift ⌣ $C_L = 0.0015$
Tail " " " ⌣ $C_L = 0.0015$

} Based on wing area = 8.27 ft^2

Rough calculations definitely show the wing and tail bayonet lift values given here are of the correct order of magnitude (calc. showed 0.0001 or less for the tail bayonet and 0.0006 or less for the wing bayonet).*

Thus the normal three-strut support system will have a lift tare (without model) of $C_L = 0.0055$, which corresponds to $\frac{1}{2}\%$ error in lift at a wing lift coefficient of one. From the pressure data of Figs. II-21 to 26 we pick out the pressure drop across the strut seals as:

Δp for wing strut seals $\doteq 45\%q$
Δp " tail " " $\doteq 57\%q$

} $q = 50$ lbs/ft^2

Then, using these figures and the seal lift tares given above, we can calculate the effective acting area of the seals as follows:

$$C_L qS = \frac{\pi r^2}{144} \Delta p, \text{ where } S = \text{wing area}, \; r = \text{effective seal radius}$$

We find:

Effective wing strut seal diameter = $2\frac{1}{4}$"
" tail " " " = 2"

Inspection of the physical dimensions of the seals (see Figs. II-5, 6) shows that the calculated effective diameter is closely equal to the actual diameter of the seals. This means that the strut seal lift tare

- - - - - - - - - -

* See Appendix 1, Page II-159

can be calculated if only the pressure drop across the seal is known. In fact, other data are presented later on which indicate that the entire lift tare with model present, can be calculated from the model geometry and attitude plus the results given above, since even 20% error in the lift tare will in most cases be within the precision limits. It should be noted that the lift tares discussed in this section are a result of the pressure differences on the model suspension system and so will vary with the "blockage" of the struts, windshields, model, etc., with the energy losses in the airstream (model drag for instance), and with the position and size of the atmospheric vents in the tunnel circuit.

The tail strut buoyancy lift will give rolling moment and pitching moment tares of appreciable magnitude. These have been calculated for a 35.42" tail length and are plotted in Fig. II-32. Because of the large scatter in the moment balance readings, no experimental moment data are shown on the plot.

The lift data for runs without the strut seals in place show the same erratic behavior which has been previously discussed.

(d) - - Pitching, Rolling, and Yawing Moment

Because of difficulties with the suspension system balances and deflections in the system there is so much scatter in the pitching and rolling moment data (Col. 3, 4 of Table 3) that only qualitative moment results were obtained, except for yawing moment. Theoretically, the relationship between the measured forces and moments are given by the following equations:

$$(1) \quad C_m = -C_{D_{sn}} \frac{x}{c} - C_{D_T} \left(\frac{z}{c} + \frac{\ell}{c} \sin \alpha_g\right) - C_{L_T} \frac{\ell}{c} \cos \psi \cos \alpha_g$$

where, x = distance above trunnion axis of wing bayonet resultant drag, $C_{D_{sn}}$

z = distance above trunnion plane of tail bayonet resultant drag, C_{D_T}

ℓ = distance from yaw axis to tail bayonet at $\alpha_g = 0^\circ$ (value is known)

c = wing chord (14")

C_{L_T} = tail bayonet and seal lift

$$(2)\quad C_\ell = C_{L_T} \frac{\ell}{b} \sin\psi \cos\alpha_g - C_{c_{sn}} \frac{y}{b}$$

where, b = wing span (85.67")

$C_{c_{sn}}$ = wing bayonet crosswind force acting at a lever arm, y

and $$(3)\quad C_n = - C_{D_T} \frac{\ell}{b} \sin\psi$$

During these tests sufficient data were taken to give many checks on the values of x, y, and z, which are the only unknown quantities in the equations above when six component readings are taken. Inspection of the bayonets (Fig. II-5, 6) would make one expect that the lever arms of the resultant drag and crosswind forces would be about 2/3 of their exposed length above the trunnion points (say x = y = 5.5", z = 3.5"). From Runs 4, 6, and 9 some 30 points were calculated which gave average values: x = 8", spread 0" to 17"; and y = 6" spread 0" to 15". With such a wide scattering, certainly the average values are no better than a rough approximation, so it was decided to use x = y = 5.5" and calculate the moment tares. For all runs without strut seals the experimental values of x and y were meaningless. No attempt has been made to determine the experimental value of z, the lever arm of the resultant force on

the tail bayonet (it will be assumed that z = 3.5"). It should be noted that eqs. 1 and 2 cannot be applied directly to the data of Runs 4, 6, and 9 since the equations have been set up assuming all three bayonets are installed, whereas in the tests only one bayonet was installed. Also it is necessary to subtract the drag of the ball tips.

From the drag and crosswind results of Runs 6 and 9 the yawing moment for each point was calculated and compared with the measured C_n values; excellent agreement was obtained. For this comparison the drag of the ball tip is not deducted.

In Figs. II-29, 30 and 31 are curves showing moment tares calculated by use of equations 1, 2, and 3 and the drag and crosswind force values of Figs. II-27 and 28. Moment tares due to lift are shown in Fig. II-32. Again all experimental points have been omitted because of the excessive scatter.

(e) - - Discussion

To sum up the results described in Group 3, we can certainly say that all of the forces and moments of any importance, on the normal suspension system (without model) arrangement have been adequately accounted for, both as to their origin and to their magnitude. On Fig. II-33 are plotted the complete tares for all six components, with the scales adjusted to make 5mm equal to the desired precision values.

Group 4 - - Variation of Wing strut Seal Lift with Model Attitude

(Fig. II-34 to 35)

To the seal lift tares (without model) discussed in section (c) of Group 3 must be added the influence of the model on the windshield tip pressures. The variation of the seal lift with wing lift has been

calculated (Appendix 3, Page II-168) using a 12% thick Joukowski airfoil shape rather than the actual shape which is an 0012 airfoil. To a first approximation, the relation between the local wing lift and the seal pressure is given by

$$\frac{d\left(\Delta p/q\right)}{d\, C_\ell} = -0.395,$$

where $\frac{\Delta p}{q}$ = pressure ratio at seal on pressure side of wing

C_ℓ = local wing lift coefficient

The spanwise lift distribution for the GALCIT steel calibration wing is shown on Fig. II-34 with the two trunnion locations indicated.

In Runs 44, 45, 49, 51, and 55 the seal pressures were measured for the full angle of attack range from negative to positive stall. These data are plotted in Fig. II-35 as Seal Pressure Coefficient, C_{sp}, against wing lift coefficient C_L. The former is defined as:

$$C_{sp} = \frac{\Delta p}{q}\left(\frac{C_L}{C_\ell}\right),$$

where $\frac{C_L}{C_\ell}$ = ratio of wing lift coefficient to local lift coefficient

Then by substitution we have,

$$\frac{d\left(\Delta p/q\right)}{d\, C_\ell} = \frac{d\, C_{sp}}{d\, C_L} = -0.395 \text{ (pressure side)}$$

$$= +0.395 \text{ (suction side)}$$

The measured slopes of the experimental curves are:

$$\left.\begin{array}{l} -0.405 \\ -0.386 \\ -0.420 \\ +0.405 \end{array}\right\} \quad 35.42\text{" trunnion spacing } \frac{C_\ell}{C_L} = 1.12$$

$$\left.\begin{array}{l} -0.394 \\ -0.392 \\ +0.386 \end{array}\right\} \quad 58\text{" trunnion spacing } \frac{C_\ell}{C_L} = 1.00$$

Thus the agreement between theory and experiment is satisfactory.

Using the effective seal area previously derived, the seal lift tare is

$$\frac{\delta C_L}{C_L} = + 0.0107 \frac{C_{\ell}}{C_L}$$

for two seals on the pressure side of the wing. Of course this applies only to the wing used in these tests; the numerical value will vary with wing planform and chord, the fore and aft position of the trunnions in the wing, and with the wing thickness.

Measurement of the interference of the model on the wing bayonet forces and moments was attempted but the technique used was inadequate and no results were obtained. Calculation of this should not be too difficult when time permits.

Group 5 - - Effects of Several Modifications to the Wing and Windshields (Fig. II-36 to II-45)

For tare investigations the importance of maintaining exactly the same surface conditions, of filling the trunnion wells flush with the wing surface, of not inducing transition by putting the trunnions too far forward, of keeping the strut seals in good condition, etc., has been pointed out many times, and examples have been given to show what pitfalls await the unwary wind tunnel operator. Also, it is well to remember that some airfoils are more sensitive than others, that the interference effects on high aspect ratio wings will differ from those on low aspect ratio wings, that procedures which are succesful at one Reynolds Number (or Mach Number, or turbulence level) are not necessarily

successful at another. Thus the operator is in a continual squeeze on one side from the insistent demands to keep the cost down and on the other side from the possibility that an unwarranted simplification in the tare procedure will cause errors of sufficient magnitude to nullify the value of the results. The problem of interferences between a model and its support system has many ramifications; but little experimental work and practically no theoretical work has been done to find a solution.

To further our understanding of these interference effects a series of modifications were made to the wing surface and to the windshields, the results of which are presented in this Group. No attempt is made to analyze these data.

In Figs. II-36 to 38 are shown the results of several modifications to the normally sealed trunnion wells. The effects are surprisingly small, except for one case. In Fig. II-36 the trunnion wells at the 58" spacing on the lower side of the wing (bayonets are on upper side) are opened up completely but only drag is noticeably changed and that by only 0.0006. Opening up the upper trunnion wells at the 58" spacing shows the same results (Fig. II-37), and even having an open air passage (0.13 sq. in.) through the wing is not important. With both upper and lower trunnion wells open (58" spacing; air passage of 0.13 sq. in.) in Fig. II-38, only drag is changed - - by about 0.0018. For Run 114 the trunnion wells at the 35.42" spacing are opened up causing large changes in drag and pitching moment and a 4½% decrease in the slope of the lift curve. Apparently this is the result of the larger open air passage (0.79 sq. in.) through the wing. These results should be compared with the data of Figs. II-7, 8, 9. Clearly this steel calibration wing is

not critical to roughness or large deformations between the 20% and 30% chord lines, whereas the Davis Wing was extremely critical to much smaller roughness and deformation.

In Figs. II-39 to 42 are presented the interferences of the image windshields on the wing. No image bayonets are installed, nor are any corrections made for the blocking of the image windshields. Fig. II-39 shows the effects of vertical position of one image windshield when mounted in the center of the tunnel. Note that C_m and α_g at $C_L = 0$ increase as the windshield approaches the wing, slope of the lift curve remains essentially constant, $\frac{dC_{m_g}}{dC_L}$ increases, and the drag curve rotates clockwise - - all of which can be explained by a combination of the flows described in Figs. II-13, 14, 15; i.e., the windshield has curved flow over the top of it with upwash at the wing leading edge. The same characteristics are clearly evident in Fig. II-40 - - note that F_I^s and F_I^n do not show the same results as they should. In Fig. II-41 again we see that F_I^s and F_I^n do not give the same results. Also the lift curve slope and rotation of the drag curve decrease as the windshield moves outboard while pitching moment and α_g ($C_L = 0$) do not change. Fig. II-42 gives a better picture of the effects of lateral position of one image windshield - - no change in C_m, little change in C_L vs. α_g, and a definite decrease in effective inclination as the windshield moves outboard. One should also remember that these windshield effects may be considerably influenced by the presence of the main wing windshields and by whatever swirl is present in the windstream. An estimate of the importance of swirl can be obtained from a study of the data of Fig. II-43; a 2° rotation of one image windshield about a vertical axis causes no

change in pitching moment, a small increase in slope of the lift curve, and a small counterclockwise rotation of the drag curve. It should also be pointed out that a change in the effective air speed (caused by windshield blocking say) will, if not corrected for, cause a small rotation of the C_{D_p} curves because of the resulting error in the C_L^2 correction to drag. Thus an increase in the blocking will increase the slope of the lift curve and cause the C_{D_p} curve to rotate clockwise (the C_D curve would rotate counterclockwise).

In Fig. II - 44 is shown the effects caused by removing the wing strut seals. The increase in drag at positive lifts (here lift is positive upward) is quite large. The data of Fig. II - 45 show the repeatability of the test results when the test is run carefully and the model is not stalled.

At this point it might be well to outline several events which took place during the tests and which modify the interpretation of the results:

(a) After Run 33 the two image wing windshields were sealed at 1-3/4" below the tip and the section below this seal was vented to atmospheric pressure. This arrangement has now been incorporated in the standard tare procedure at GALCIT. Sometime after these tests were finished a seal was installed in the image tail windshield.

(b) The balances and suspension system were overhauled before the test started, after Run 101, and finally after Run 137. Previous to Run 137 all efforts to get repeatable force and moment data were no good if the model was allowed "bounce and jump" such as happens in the stall and large zero shifts were frequently obtained. After Run 137 the balances were completely dismanteled, the knife edges and pallets sharpened, and all critical parts carefully ex-

amined and reworked where necessary. The suspension system was realigned and the balances recalibrated - - the calibration equipment also had to be reworked. After all this the entire system functioned satisfactorily.

(c) Measurement of the effects of the image windshields during Runs 115 to 129 showed definite discrepancies between the two image wing windshields and a check of the dimensions verified this - - the north windshield (F_I^N) was too thin by over 1/4 inch. This was corrected during the $2\frac{1}{2}$ week shutdown after Run 137 for balance repairs. Thus the runs before and after Run 137 with image system installed can not be compared directly. Similarity of all six windshields is still not too good, but is probably adequate if the model surface is not too close to them.

(d) During the windshield tests it was noticed that there was a constant rolling moment developed by the wing at zero yaw angle, indicating some sort of swirl or non symmetrical flow pattern. This was adjusted in Run 130 by deflecting the turning vane trailing edges in the corner upstream of the throat until the wing rolling moment was negligible. By approximate calculations it is estimated that the swirl was of the order of 0.2°. The next day in Run 136 the rolling moment reappeared but with opposite sign - - evidently the vane trailing edges had warped to a new position during the five preceding runs. In Run 137 the vane trailing edges were again tweaked until the wing rolling moment was negligible. Of course this procedure does not necessarily eliminate swirl, just averages the inclination across the wing, and certainly one can't assume rolling moment would be negligible for a wing of different span or planform; this procedure for adjusting the flow pattern in the throat leaves much to be desired. Unfortunately all 12 of the yaw runs were made before it was

realized that the rolling moment at zero yaw was so large (C_ℓ = -0.0032) that it equalled nearly half of the largest rolling moment tares. Because of these difficulties, one cannot put much faith in the rolling moments measured with the wing installed. After consideration of these results and of the "yaw-tare" data presented in the next Group, the author recommends a more complete survey be made of swirl and inclination in the throat and that the corner vanes be adjusted until these conditions are satisfactory and stable at all operating speeds and temperatures. It is suspected that the vane trailing edges might now be warping with changes in speed and, particularly, in temperature.

(e) In connection with this suspected temperature effect on rolling moment, it was noticed that the wing drag would increase as the tunnel temperature increased by as much as 0.0006 in drag coefficient. At first this was attributed to balance errors, but after the complete overhaul of the balance system (between runs 138 and 139) the drift of the drag level was still present. Thereupon a test (Run 145) was made to determine if the drift was caused by the changing temperature in the model itself, or possibly by the difference in temperature between the model and the windstream. The model was set at $\alpha_g = -5^\circ$ and not moved again until the temperature tests were finished. Lift, drag, and pitching moment were read for the standard speed (50 lb/ft^2) over period of twenty minutes for: (1) Tunnel and wing initially at room temperature, 70°F; (2) tunnel at 70°F and wing at 160°F; (3) tunnel at 70°F and wing at 200°F; and (4) tunnel at 70° F and wing at 30°F. It took about 45 sec. to bring the tunnel up to speed after heating the wing, so that it is possible the steel wing temperature equalized so rapidly during this starting period that the looked for effects would not be apparent after

the first reading. Wing temperature was not measured during the run. In any case, no positive effect of temperature could be found; the spread of the readings was:

$$\delta C_L = 0.003$$

$$\delta C_D = 0.00015$$

$$\delta C_m = 0.0007$$

This amount of scatter in the data is much larger than one would like for such conditions. One reason for so much scatter was traced to the variations in the tunnel speed setting, which were caused by pressure fluctuations at the piezometer rings and the poor accuracy inherent in setting the dynamic pressure by a pressure reading which is only 1/3 the magnitude. During the past year these difficulties have been worked on and considerable improvement is now possible. Techniques for damping the fluctuations have been developed. A "Bell-Smith Piezometer Bump" has been built for the tunnel, which will make the piezometer ring pressure difference equal to the dynamic pressure in the throat.

In conclusion it should be pointed out that these errors and scatter effects are not necessarily present in the experimental data included in this report. Any data which were definitely questionable have been omitted. A great many points were repeated several times. The scatter increments listed on page II - 76 are probably a good indication of the reliability of the lift, drag, and pitching moment data; and, for the other three components it is estimated that:

$$\delta C_\ell = 0.0010 \text{ (Level may be off by } 0.0030)$$

$$\delta C_n = 0.0002$$

$$\delta C_c = 0.0005$$

Group 6 - - Image System and Sting Tare Effects (Figs. II-46 to II-63)

We now come to the discussion of such regular tare determinations as were made during these experiments. Because of the difficulties described in Group 5 and elsewhere, it was not possible to put together enough complete and accurate data to determine the tares exactly as outlined in Section G. Therefore, the data of this Group have not been corrected for strut-seal and bayonet lift and moments, nor for the variation of average velocity with yaw of the windshields (windshield blocking decreases with angle of yaw). These corrections probably do not total more than 3% of the forces on the model for any condition tested. Examination of the rolling and pitching moments (especially for $\psi \neq 0$) shows generally that the tares for these components make no sense at all. All components are referenced to stability axes (wind axes rotated with yaw angle). In all cases the subscript "g" on a coefficient symbol indicates that no corrections have been applied to the balance data, the subscript "u" indicates tare corrections have been made but not wall corrections, and the subscript "s" indicates the coefficient value is referenced to stability axes (note that ψ, α_g, C_{L_g}, and C_{n_g} are not changed by rotation of the reference system about the yaw axis). Also one must keep in mind that, unless otherwised noted, all data are calculated for wing W_A, i.e., the suction surface faces down in tunnel. When the wing is inverted, W_A^i, the suction surface is up in the tunnel and the signs of the balance readings and angles are reversed (except for drag and rolling moment). Note that the conning tower is "open" for all runs included in this Group.

In Figs. II-46 and 47 are shown the six component data for polar runs from negative to positive stall angles of attack at 0°, 19°, and 27° yaw angle with no corrections applied - - subtraction of the $C_{L_g}^2$ term from the drag

coefficient was used to "flatten" the drag curves. In Figs. II-48 and 49 are presented similar results for 0°, $\pm 19^\circ$, and $\pm 27^\circ$ yaw angle. The data of the first two figures were taken before and that of Figs. II-48 and 49 were taken after the windstream swirl was adjusted - - the primary difference appears to be an upward shift of the effective windstream inclination. The correlation of results for positive and negative yaw angles is reasonably good.

In Fig. II-50 are shown data of the four runs which make up a standard GALCIT tare investigation at zero yaw angle. The results are normal and reasonably consistent. The drag tare at $C_{L_g} = 0$ is 0.0039, which compares with the value for drag tare without model of 0.0033 (See Fig. II-28). Pitching moment tare at zero lift is -0.0015, which compares favorably with the value of -0.0012 from Fig. II-29. The difference of 0.0006 in drag seems much too large to be model interference effect on the bayonet drag, and so must be explained by bayonet interference on the model or (more likely) by poor balance data for the model tests. It is believed that the windshield interference on the model drag at zero lift is negligible although conclusive evidence is lacking.

For tares at various angles of yaw there was not sufficient time to make a complete 4 - run series, so only two runs (model inverted, image system in and out) were made, and it was assumed that tares were the same for model normal or inverted and for positive and negative yaw angles of the same magnitude. Close inspection of the data in Figs. II-48, 49, and 50 showed these assumptions to be adequate for the accuracy limits of the balances. The standard GALCIT tare procedure was used even though the wing was yawed; and the lift coefficient was taken as the independent parameter as usual. Because only two of the customary four runs were made, it was not possible to correct for irregularities in the clear tunnel flow, with the result that tares for pitch-

ing moment (and presumably rolling moment) could not be determined even if the windstream swirl had not been present.

Tare runs for $\psi = 19^{\circ}$ and wing trunnion spacing of 58" are plotted on Figs. II-51 and 52. Pitching moment, lift, and drag curves are quite similar to those for zero yaw angle. The drag tare (in stability axes) at $C_{L_g} = 0$ is 0.0030, which compares favorably with the value of 0.0029 calculated from the data of Figs. II-27 and 28. The side-force tare $C_{c_{\tau_s}}$ at zero lift is 0.0095 as compared with 0.0082 predicted by Figs. II-27 and 28. Yawing moment tare is essentially zero (Fig. II-52) as predicted by Fig. II-30. In all six components the effect of the image windshields is to change the apparent inclination - - see particularly the drag curves of Fig. II-51.

On Figs. II-53 and 54 are plotted the tare runs for $\psi = 19^{\circ}$ and wing trunnion spacing of 35.42" (90 cm). The results are quite similar to those for the 58" spacing which were discussed in the preceding paragraph. Drag tare at $C_{L_g} = 0$ is 0.0029, side-force tare is 0.0089, and yawing moment tare is -0.005; the corresponding values from Figs. II-27, 28, 30, are 0.0029, 0.0082, and -0.001, respectively. However, there is a large difference in effective windstream inclination for the two trunnion spacings - - 0.33° downwash for the 58" spacing and 0.18° for the other - - which may be an indication of the reason for large differences in the rolling moment data. On the other hand the data of Fig. II-42 show a shift of one image windshield from 35.42" to 58" spacing rotates the drag curve by an amount equivalent to 0.04° increase in downwash - - thus two windshields might cause an inclination change of 0.08°, which still is only half of the shift measured in the tare runs at $\psi = 19^{\circ}$. It is plausible to expect that the effective upwash produced by the image windshields will decrease as they are moved toward

the wing tips.. Another comparison, provided by the data of Fig. II-55, shows no change in inclination at $\psi = 0^\circ$ for the two trunnion spacings without image windshields present - - note that these runs were made after the corner vanes had been adjusted to remove the swirl as interpreted by the wing rolling moment at $\psi = 0^\circ$. Also, at $\psi = 0^\circ$ and 58" spacing the measured inclination was 0.21° downwash. Clearly these phenomena must be further explored, particularly with regard to the effect of the conning tower.

The tare runs for $\psi = 27^\circ$ and wing trunnion spacing of 35.42" are plotted on Figs. II-56 and 57, and show characteristics quite similar to those for 0° and 19° yaw angle. Drag tare at $C_{L_g} = 0$ is 0.0038, side-force tare is 0.0110, and yawing moment tare is -0.0007; the corresponding values from Figs. II-27, 28, and 30 are 0.0032, 0.0095, and -0.0002, respectively. The effective inclination, as measured by the drag curves is 0.28° downwash.

In Table 4 are collected the numerical values which have already been discussed as well as some others of interest. The displacement of the α_g vs. C_{L_g} curve from the origin is taken as the angle of attack tare, α_τ, and is approximately equal to the inclination measured from the rotation of the drag curves (with images installed) from a position symmetrical about the C_{L_g} axis. The blockage correction factor to q caused by the image windshields is $\frac{1}{2}$ to 3/4% lower at 19° and 27° yaw angle than at 0° yaw angle, which is to be expected.

Table 4

	$\psi = 0^\circ$ $t_M^{SN} = 58"$	$\psi = 19^\circ$ $t_M^{SN} = 58"$	$\psi = 19^\circ$ $t_M^{SN} = 35.42"$	$\psi = 27^\circ$ $t_M^{SN} = 35.42"$
$C_{D_{\tau_s}}$ ($C_{L_g} = 0$); from tare runs	0.0039	0.0030	0.0029	0.0038
" ; from Figs. II-27, 28	0.0033	0.0029	0.0029	0.0032
$C_{M_{\tau_s}}$ ($C_{L_g} = 0$); from tare runs	-0.0015	—	—	—
" ; from Fig. II-29	-0.0012	—	—	—
$C_{c_{\tau_s}}$ ($C_{L_g} = 0$); from tare runs	0	0.0095	0.0089	0.0110
" ; from Figs. II-27, 28	0	0.0082	0.0082	0.0095
C_{N_τ} ($C_{L_g} = 0$); from tare runs	0	0	-0.0005	-0.0007
" ; from Fig. II-30	0	-0.0001	-0.0001	-0.0002
Windstream downwash; from drag curves	0.21°	0.33°	0.18°	0.28°
" " ; from α_g curves	0.21°	0.30°	0.20°	0.30°
Image windshield blockage correction to q	0.969	0.976	0.975	0.973

The image system tare procedure was devised to give the force and moment interferences on the model by the three suspension struts and their windshields as they are represented by the image system. For a wing such as was used in this research it is desirable to put the tail strut far aft and connect it to the wing with a slender steel bar or sting. Thus the sting really becomes part of the wing and, in any case, the tares which have been determined are applicable only to the wing and sting combination. Therefore the effects of the sting must be determined and added to the image system tares to get the total tare values. It is customary, at GALCIT, to mount a dummy sting (duplicate of main sting in size and shape) along side of the main sting and

assume the resulting increments are equal to the sting tare. For wings of only moderate sweepback or for quite small angles of yaw this procedure probably is quite reliable. In Fig. II-58 are shown the effects of the dummy sting at $\psi = 0^{\circ}$: no appreciable effect on α_g and pitching moment, and a nearly constant increase in drag coefficient of about 0.0008. At all positive C_{L_g} values the α_g curve is shifted to the right by 0.15° for no apparent reason (since it is not believed that this is a true sting effect). It was assumed that this α_g shift was in reality an error in C_{L_g} and the drag data for Run 97A were corrected accordingly before the sting drag was determined. These corrections are not shown on the plot.

When the wing is yawed one sting will approach and at a large enough yaw angle enter the wake of the other sting, thereby producing an interaction between the two so the effects of both stings together will not equal twice the effects of one sting. Thus the true sting tare cannot be determined by this procedure unless the spacing is sufficiently large to preclude such interactions. On the other hand the dummy sting should be as close as possible to the main sting position in order to be immersed in the same flow conditions. For these experiments the dummy sting was spaced 8" from the main sting. It is believed that the interactions for $\psi = 19^{\circ}$ were negligible, but not for $\psi = 27^{\circ}$. In Figs. II-59 and 60 are presented the results for model with and without the dummy sting at $\psi = \pm 19^{\circ}$. As usual the pitching and rolling moment data are questionable and will not be considered. The most important effect is the increase in $\frac{dC_{L_g}}{d\alpha_g}$ by 2.6%. No such effect was found at zero yaw angle (See Fig. II-58). Also the dummy sting drag becomes negative at large C_{L_g} magnitudes - - if this "lift" of the dummy sting is taken out of the data the sting drag turns out to be positive and nearly constant as expected. The lift

increase is the same percentage for $\psi = 27^{\circ}$ (See Fig. II-61) so it does not appear to be caused by interaction between the stings, since the effect should be more pronounced at the larger yaw angle. The "lifting area" of the sting is about 2% of the wing area, but with such an extremely low aspect ratio it is difficult to believe the sting could develop so much lift, and, furthermore, the sting lift should be the same at $\psi = 0^{\circ}$ which was not the case at all. The author believes that the stings are acting as double flaps of small chord or small stall plates which build up the pressure on the pressure side more than on the suction side and thereby produce an effective lift - - even in this case it seems that the effect should increase with angle of yaw. In any case, it was decided that this lift increase of 2.6% was a true sting tare. Therefore the sting drag tare for $\psi = \pm 19^{\circ}$ was assumed to be 0.0006 for all angles of attack. Side force and yawing moment sting tares look normal. The tare values for positive and negative yaw angles are in good agreement.

In Figs. II-61 and 62 are shown the effects of the dummy sting at $\psi = 27^{\circ}$. The results are quite similar to those obtained for the previous case. A lift tare of 2.6% was measured and the drag tare is assumed to be constant at 0.0006 for all angles of attack.

The sum of the image system and sting tares are collected in Fig. II-63 for the three yaw angles, 0°, 19°, and 27°. The total drag-tare for $\psi = 19^{\circ}$ and trunnion spacing of 35.42" is given in Fig. II-53 - - it is closely the same as the curve for the 58" spacing. Note that the slope of the total drag-tare curves increases with yaw angle. It was assumed that the sting tares were not effected by the wing trunnion spacing. These tares are to be applied to data with model normal (W_A) at $\psi = 0^{\circ}$, 19°, and 27°. Actually no suitable runs were made concurrently with the image tare tests at the proper yaw angles, so it was assumed that the tares were applicable (with the proper sign changes)

to tests with model normal at $\psi = 0^\circ$, -19°, and -27°. The final wing characteristics are plotted on Fig. II-64. As usual, pitching and rolling moment data are not given, except that pitching moment tares for $\psi = 0^\circ$ are given on Fig. II-50.

Group 7 - - Discussion of Corrected Wing Characteristics (Fig. II-64)

Before analyzing the final results of Fig. II-64 the problem of the variation of wall interference corrections with angle of yaw must be considered. Of course the wall corrections are zero at zero wing lift so that the problem does not arise for this important point. Swanson (Ref. 42) shows that α and C_D wall corrections increase by roughly 8% for $\psi = 19^\circ$ and 15% for 27° for a tunnel of rectangular cross section. For the circular GALCIT tunnel the percentage variation should be about the same. Therefore the accuracy of these final results will not be much disturbed if the variations of the wall effects with yaw angle are neglected. Wall corrections for side force and yawing moment are quite small and may also be neglected.

Parasite drag at $C_L = 0$ and $\psi = 0^\circ$ is 0.0070. This is somewhat below the values given by others. For example, Heaslet and Nitzberg (Ref. 47) give 0.0071 for a Reynolds Number of 2.7×10^6 and lower turbulance levels. However the true drag level is probably within the accuracy limit of 3% which has been estimated for these tests - - it must be remembered that several corrections have been omitted in getting these final results. The drag curve for $\psi = 0^\circ$ is not symmetrical about the zero lift point as it should be for a symmetrical airfoil - - presumably this is caused both by the incompleteness of the tare procedure and by the lack of symmetry of the wing at the leading edge. The experimental airfoil efficiency factor for $\psi = 0^\circ$ is 90%, which agrees with the result reported by Jacobs and Abbott (Ref. 35). There is no reliable information available which gives the variation of C_{D_P} with C_L

for the conditions of these tests. Actually the drag curve corresponds closely to the equation: $C_{D_p} = 0.0070 + 0.0100\ C_L^2$ or, for total drag, $C_D = 0.0070 + 0.0644\ C_L^2$, which corresponds to an effective aspect ratio of 5.2 or 84.5% of the geometrical value. The average slope of the C_L vs. C_m curve gives an aerodynamic center for the wing of 23.3% of the chord aft of the leading edge - - this is 1% less than the value given by Jacobs and Abbott (Ref. 35). Furthermore the application of the wall correction for pitching moment would reduce this experimental value to 23.1%. It is quite possible that the application of the corrections for bayonet and strut seal lift would account for these differences in the aerodynamic center position.

There seems to be little useful experimental data on yawed wings which have been corrected for suspension system tares or wall interferences. Hoerner (Ref. 36) gives as the results of his theoretical calculations that:

$$C_L(\psi) = C_{L_{(\psi = 0)}} \cos^2 \psi$$

$$C_{D_S}(\psi) = C_{D_{(\psi = 0)}} \cos^2 \psi$$

$$C_{C_S}(\psi) = \text{Function of } \sin \psi$$

$$C_n(\psi) = \text{Function of } \psi$$

These functions can be checked against our experimental values.

Table 5

	$\psi = 0^\circ$	$\psi = -19^\circ$	$\psi = -27^\circ$
$dC_L/d\alpha_u$	0.0784	0.0679	0.0605
$dC_L/d\alpha_u \times \frac{1}{\cos^2\psi}$	0.0784	0.0760	0.0762
$dC_L/d\alpha \times \frac{1}{\cos^2\psi}$	0.0732	0.0707	0.0709
$dC_L/d\alpha_u \times \frac{1}{\cos^2\psi}$ (Not corrected for sting lift tare)	0.0784	0.0780	0.0782
$dC_L/d\alpha \times \frac{1}{\cos^2\psi}$ (Not corrected for sting lift tare)	0.0732	0.0725	0.0724

Table 6

	$\psi = 0^\circ$	$\psi = -19^\circ$	$\psi = -27^\circ$
C_{D_S} $(C_L = 0)$	0.0071	0.0066	0.0056
C_{D_S} $(C_L = 0) \times \frac{1}{\cos^2\psi}$	0.0071	0.0074	0.0071
B, with drag and lift multiplied by $\frac{1}{\cos^2\psi}$	0.0100	0.0120	0.0130

Table 7

	$\psi = 0^\circ$	$\psi = -19^\circ$	$\psi = -27^\circ$
C_{C_S} $(C_L = 0)$	0	-0.0030	-0.0058
C_{C_S} $(C_L = 0) \times \frac{100}{\sin\psi}$	—	0.92	1.28
C_{C_S} $(C_L = 0) \times \frac{100}{\sin^2\psi}$	—	2.84	2.81
C_n $(C_L = 0)$	0	0.0012	0.0017
C_n $(C_L = 0) \times \frac{10,000}{\psi}$	—	0.635	0.630

In Table 5 the lift vs. α_u curve slope is given for $\psi = 0^\circ$, -19°, and -27° for five conditions: a) $\frac{dC_L}{d\alpha_u}$ is the slope of the curve as plotted on Fig. II-64, the variation with yaw angle is 13% for 19° and 23% for 27°; b) dividing the lift by $\cos^2 \psi$ brings the values to within 3% of each other; c) correcting for wall interference has little effect; d) leaving out the sting lift tare brings the slopes to within 1% of the $\cos^2 \psi$ relationship. This shows that the $\cos^2 \psi$ law for lift is as good as the accuracy of the experimental results. Certainly the validity of the sting lift tare is now questionable.

In Table 6 it is shown that the $\cos^2 \psi$ relationship works quite well for drag at zero lift coefficient. To check the effect of yaw angle on drag with lift different from zero, the lift and drag were corrected by the $\cos^2 \psi$ law and parabolas were matched to the corrected curves. The term, B, as defined by the equation $C_{D_S} = A + B\, C_L^2 + 0.04051\, C_L^2$, is given for the three yaw angles -- the correlation is satisfactory.

In Table 7 it is seen that side force, C_{C_S}, at zero lift appears to be a function of $\sin^2 \psi$ rather than the $\sin \psi$ relationship which Hoerner gives. However it should be noted that C_{C_S} does reverse sign according to the sign of the yaw angle. The yawing moment does agree with the theory in that it is a linear function of the angle of yaw.

It appears that the theory agrees with the experimental results within the accuracy of the measurements. Such good agreement can also be used to claim that the image system tare procedure is satisfactory for wings at yaw.

Conclusion - Part II

A good start has been made in the study of the details of the aerodynamic interactions between wind tunnel models and their support systems, but much remains to be done.

The air loads on the bayonets and strut seals have been measured, the results being consistent with each other and showing good agreement with theory and other experiments. Comparison of the tare values without wing present and with wing at zero lift indicates that the interferences of the wing on the support system are small, as might be expected, and when expressed in terms of the wing dimensions, do not vary over 10%. The important effect of the lift tare from the bayonets and strut-to-windshield seals, is demonstrated, and methods are developed for either measuring or predicting the actual tare.

It is clear that the dominant factor in the interference effects on the wing is the change in both magnitude and direction in free stream velocity produced by the windshields. The effects are large and vary rapidly with distance from the windshield surfaces. The change in direction is apparently the more important, with flow curvature being the most troublesome feature. It is shown how the image system procedure can not determine the drag tares due to curved flow except in isolated and limited cases. More experimental work should be done to determine the magnitude of these curvature effects, particularly with regard to spanwise variations. This should be compared with theoretical calculations wherever possible, especially the effects on aspect ratio and wall corrections.

The sharply increased throat area, caused by having the "conning tower" open, is shown to result in decreasing the blocking of the upper windshield to less than one half that of the lower windshields - - a circumstance which definitely violates the basic assumptions of the image system method. It

is recommended that the next experiments be directed toward complete tare measurements on the wing with and without the throat ceiling fairings in place. It is well to note that this effect probably does not appear in the tare data at zero wing lift, except possibly in the pitching moment as a curvature correction.

For the first time, image system tares have been measured for a yawed wing. The results indicate that the standard procedures will probably be adequate for angle of attack variations at a fixed yaw angle. The procedure for tare determinations at a fixed angle of attack and yaw angle variable can be developed when necessary. At least for straight wings, the tare characteristics at angles of yaw up to 27° are quite similar to those for $\psi = 0^{\circ}$, provided all forces and moments are referenced to stability axes.

Some means must be developed to stabilize the flow pattern in the clear tunnel at the condition of negligible swirl and inclination. If the calibration wing is used for this, the settings should be made with the complete image system installed and ceiling fairings in. The procedure, sometimes used, of adjusting the clear tunnel inclination to counteract the effects of one set of windshields and of having the conning tower open is definitely improper.

It must be remembered that the results and conclusions of this report apply to the GALCIT tunnel and to the simple wing and windshield system used in the tests. Tare determination techniques for swept wings, wings with fuselages, nacelles, tails, etc., and models with non-lifting surfaces, such as missiles, have not been considered.

References and Bibliography

1. Bairstow, L., Hyde, J. H., and Booth, H., "The New Four-Foot Wind Channel; with a Description of the Weighing Mechanism Employed in the Determination of Forces and Moments", R & M 68, March, 1913.

2. "Experiments on Small-Scale Models of Large Aerofoils Tested at the Aerotechnical Institute of the University of Paris", R & M 72 part VI, March, 1913.

3. Bairstow, L., Pannell, J. R., and Lavender, T., "Experiments on the Variation of the Forces and Moments on an Aerofoil as the Speed Changes". R & M 148, March, 1915.

4. Bryant, L. W. and Irving, H. B., "Description of Improved Moment Measuring Apparatus for Tests on Models in the Wind Channel, with an Appendix on the Determination of Corrections Due to Interference of Apparatus on Model", R & M 192, June, 1915.

5. Relf, E. F., Bryant, L. W., and Irving, H. B., "Experiments on Models of Complete Aeroplanes", R & M 198, July, 1915.

6. Pannell, J. R. and Campbell, N. R., "Methods of Support for Models During the Measurement of Their Aerodynamic Resistance", R & M 244, July, 1916.

7. Pannell, J. R., "The Wind Channel: Its Design and Use", Jour. Roy. Aero. Soc., Vol. 22, p. 211, July, 1918.

8. Davidson, W. E. and Bacon, D. L., "The Determination of the Effective Resistance of a Spindle Supporting a Model Aerofoil", TN 37, Jan., 1921.

9. Wieselsberger, C., "Effect of Method of Suspending Models in Airstream on Resulting Measurements", T.M. 169, Nov., 1922.

10. Eiffel, G., "Method Rendering It Possible, in Testing Airplane Wing Models at the Eiffel Laboratory, to Obtain Comparable Polars, Whether the Supports are Attached to the Upper or Lower Side of Model", T.M. 156, Nov., 1922.

11. Zahm, A. F., "The Six-Component Wind Balance", NACA T. R. No. 146, 1922.

12. Bacon, D. L., "Model Supports and Their Effect on the Results of Wind Tunnel Tests", T. N. 130, Feb., 1923.

13. Glauert, H., "A Generalized Type of Joukowoski Airfoil", R & M 911, Jan., 1924

14. Robert, Lieut. Col., "Methods of Experimentation with Models and Utilization of Results", T. M. 247, Feb., 1924.

References and Bibliography (Cont'd)

15. Reid, Elliott G., "Standardization Tests of NACA No. 1 Wind Tunnel", NACA T.R. No. 195, 1924

16. Kerneis, Jean, "Wire Suspensions in Wind Tunnel Experiments", TM 342, Dec. 1925

17. Lapresle, A., "French Wind Tunnel Methods", Jour. Roy. Aero. Soc., Vol. 33 p. 838, Oct. 1929 (Abstract)

18. Ward, Kenneth E., "Interference Effects and Drag of Struts on a Monoplane Wing", NACA T.N. No. 365, Feb. 1931

19. Jacobs, Eastman N., "Tests of Six Symmetrical Airfoils in the Variable Density Wind Tunnel", NACA T.N. No. 385, July 1931

20. Ward, K.E., "The Interference Effects on an Airfoil of a Flat Plate at Mid-Span Position", T.N. 403, Dec. 1931

21. Harris, T. A., "The 7 by 10 Foot Wind Tunnel of the National Advisory Committee for Aeronautics". T.R. No. 412, 1932

22. Jacobs, E.N. and Abbott, I.H., "The NACA Variable Density Wind Tunnel", T.R. No. 416, 1932.

23. Jacobs, Eastman N., "Airfoil Section Characteristics as Affected by Protuberances", NACA T.R. 446, 1932

24. Jacobs, E.N., Ward, K.E., and Pinkerton, R.M., "The Characteristics of 78 Related Airfoil Sections from Tests in the Variable-Density Wind Tunnel", T.R. No. 460, 1933

25. Jacobs, E.N. and Sherman, Albert, "Wing Characteristics as Affected by Protuberances of Short Span", NACA T.R. 449, 1933

26. Theodorsen, T. and Silverstein, A., "Experimental Verification of the Theory of Wind Tunnel Boundary Interference", NACA T.R. 478, 1934

27. Silverstein, Abe, "Scale Effect on Clark Y Airfoil Characteristics from NACA Full-Scale Wind Tunnel Tests", NACA T.R. 502, 1934

28. Jacobs, E.N. and Clay, W.C., "Characteristics of the NACA 23012 Airfoil from Tests in the Full-Scale and Variable-Density Tunnels", NACA T.R. 530, 1935

29. Jacobs, E.N. and Sherman, A., "Airfoil Section Characteristics as Affected by Variations of the Reynolds Number", T.R. No. 586, 1937

30. Doetsch, H., "Profilwiderstandsmessungen im grossen Windkanal der DVL", Luftfahrtforschung, Vol. 14, No. 4/5, 20, p. 173-178, April 1937 and DVL Jahrbuch, 1937

References and Bibliography (Cont'd)

31. Disprose, K.V., "Drag Tests on a Fabric Covered, and a Polished Plywood, Wing in the 24 ft. Tunnel", R & M 1813, March 25, 1937

32. Doetsch, H. and Kramer, M., "Systematic Airfoil Tests in the Large Wind Tunnel of the DVL", TM 852, March 1938

33. Goett, H.J. and Bullivant, W.K., "Tests of NACA 0009, 0012, and 0018 Airfoils in the Full-Scale Tunnel", NACA T.R. 647, 1938

34. Goett, H.J., "Experimental Investigation of the Momentum Method for Determining Profile Drag", T.R. 660, 1939

35. Jacobs, E.N. and Abbott, I.H., "Airfoil Section Data Obtained in the NACA Variable-Density Tunnel as Affected by Support Interferences and Other Corrections", NACA T.R. 669, 1939

36. Hoerner, Sighard, "Forces and Moments on a Yawed Airfoil". T.M. 906, Aug. 1939

37. Rumph, L.B., Jr. and Schairer, Robert, "Boundary Layer and Wake Survey Measurements in Flight and in the Wind Tunnel". J. Ae. Sc., Vol. 7, No. 10, p. 425, Aug. 1940

38. Bullivant, W.K., "Tests of the NACA 0025 and 0035 Airfoils in the Full-Scale Wind Tunnel", T.R. No. 708, 1941

39. Klein, A.L., Serrell, P.V.H., and Millikan, C.B., "A New Two-Parameter Model Suspension System for the GALCIT 10-Ft. Wind Tunnel", J. Ae. Sc. Vol. 9, No. 8, p. 302, June 1942

40. Keune, F., "Two-Dimensional Potential Flow Past an Ordinary Thick Wing Profile", Jahrbuch 1938 der Deutschen Luftfahrtforschung (TM 1023, July 1942)

41. Eaton, A.R. Jr., "Report on Wind Tunnel Tests on Strut Fittings and Windshield Tips for the GALCIT Two-Parameter Rigging System", GALCIT Rep. 327, Nov. 5, 1942 (Not published)

42. Swanson, Robert S., "Jet-Boundary Corrections to a Yawed Model in a Closed Rectangular Wind Tunnel". NACA Wartime Report L-603, Feb. 1943

43. Smith, J.E., "Report on Wind Tunnel Tests of the Curtiss-Wright (Buffalo) 0015 Rectangular Calibration Wing", GALCIT Rep. 402, May 11, 1944 (Not published)

44. Smith, J.E., "Report on the GALCIT Method for Determining the Aerodynamic Interference Effects of the Model Suspension System", GALCIT Rep. 402 Appendix, July 20, 1944 (Not published)

45. Swanson, Robert S. and Gillis, Clarence L., "Wind-Tunnel Calibration and Correction Procedures for Three-Dimensional Models", NACA Wartime Report No. L-1, Oct. 1944

References and Bibliography (Cont'd)

46. Hensel, R. W., "Proposed Calibration and Correction Procedures for Wright Field 10-Foot Wind Tunnel", Preliminary Report for Air Technical Service Command, March 23, 1945 (Not published)

47. Heaslet & Nitzberg, "The Calculation of Drag for Airfoil Sections and Bodies of Revolution at Subcritical Speeds". NACA Research Memorandum RM No. A7B06, April 23, 1947

48. Millikan, C.B., Smith, J.E., and Bell, R.W., "High-Speed Testing in the Southern California Cooperative Wind Tunnel", J. Ae. Sc. Vol. 15, No. 2, p. 69, Feb. 1948

TABLE 3

	1	2	3	4	5	6	7	8	9	10	11	12	13	14	15	16
RUN NO.	C_L	C_D	C_m	C_ℓ	C_n	C_c	$\frac{H-P}{(H-p)_0}$	$\alpha_{g\,SEL.}$ DEGREES	$\psi_{SEL.}$ DEGREES	$\frac{H-T_M}{(H-p)_0}$	$\frac{H-A}{(H-p)_0}$	$\frac{H-G_M}{(H-p)_0}$	$\frac{H-T_\ell^M}{(H-p)_0}$	$\frac{H-G_L}{(H-p)_0}$	$\frac{H-T_\ell^I}{(H-p)_0}$	SPECIAL SETTINGS
1	0.0000	0.0000	0.0000	0.0000	0.0000	0.0000	0.984	—	—	—	1.001	—	—	—	—	—
2	0.0011	0.0000	-0.0003	0.0000	0.0000	0.0001	1.008	—	0	1.228	1.009	1.017	—	—	—	—
↓	"	"	-0.0006	"	"	-0.0001	"	—	5	1.232	"	"	—	—	—	—
	"	"	-0.0008	"	-0.0001	0.0002	1.009	—	15	"	"	"	—	—	—	—
	"	"	-0.001C	-0.0001	0.0000	0.0001	"	—	25	1.236	"	"	—	—	—	—
	"	"	-0.0002	0.0000	"	"	—	—	0	—	—	—	—	—	—	—
3	0.0014	0.0001	-0.0003	0.0000	0.0000	0.0003	1.009	—	0	1.434	1.007	1.009	—	—	—	—
↓	"	0.0000	"	-0.0001	"	0.0002	—	—	15	1.443	"	"	—	—	—	—
	"	"	-0.0004	0.0000	"	0.0004	—	—	25	1.447	"	"	—	—	—	—
4	0.0019	0.0015	-0.0005	0.0000	0.0000	0.0000	—	—	0	1.585	1.006	1.009	—	—	—	—
↓	"	0.0016	-0.0009	-0.0001	"	0.0014	—	—	5	—	—	—	—	—	—	—
	"	0.0018	"	"	"	0.0020	—	—	10	—	—	—	—	—	—	—
	"	0.0021	-0.0011	-0.0002	"	0.0025	—	—	15	1.528	1.006	1.009	—	—	—	—
	"	0.0026	-0.0012	-0.0003	"	0.0026	—	—	20	—	—	—	—	—	—	—
	"	0.0033	-0.0015	-0.0002	"	0.0027	—	—	25	1.492	1.006	1.009	—	—	—	—
	"	0.0035	-0.0016	-0.0003	"	0.0033	—	—	27	—	—	—	—	—	—	—
↓	"	0.0015	-0.0007	0.0000	"	0.0001	—	—	0	—	—	—	—	—	—	—
5	0.0017	0.0015	-0.0003	0.0000	0.0000	0.0011	—	—	0	1.212	1.001	1.009	—	—	—	—
↓	"	0.0016	-0.0007	-0.0001	"	0.0001	—	—	5	1.224	"	"	—	—	—	—
	0.0019	0.0018	"	"	"	0.0012	—	—	10	1.232	"	"	—	—	—	—
	"	0.0021	-0.0011	-0.0002	"	"	—	—	15	1.228	"	"	—	—	—	—
	"	0.0026	-0.0010	-0.0003	"	0.0020	—	—	20	1.232	"	"	—	—	—	—
	0.0017	0.0033	-0.0015	"	-0.0001	0.0026	—	—	25	1.195	"	"	—	—	—	—
↓	"	0.0035	-0.0014	-0.0004	"	0.0025	—	—	27	1.187	"	"	—	—	—	—

TABLE 3 CONT

1	2	3	4	5	6	7	8	9	10	11	12	13	14	15	16
RUN NO.	C_L	C_D	C_m	C_ℓ	C_n	C_c	$\frac{H-p}{(H-p)_o}$	$\alpha_{g\,SEL.}$ DEGREES	$\psi_{SEL.}$ DEGREES	$\frac{H-T_M}{(H-p)_o}$	$\frac{H-A}{(H-p)_o}$	$\frac{H-G_M}{(H-p)_o}$	$\frac{H-T_E^M}{(H-p)_o}$	$\frac{H-G_L}{(H-p)_o}$	$\frac{H-T_E^L}{(H-p)_o}$	SPECIAL SETTINGS
6	0.0017	0.0038	-0.0019	0.0005	-0.0003	-0.0036	0.986	—	-27	1.365	0.997	1.001	—	—	—	—
↓	"	0.0036	-0.0018	"	"	-0.0035	0.989	—	-25	1.394	1.009	1.013	—	—	—	—
	0.0019	0.0031	-0.0013	"	"	-0.0041	0.985	—	-20	1.487	"	"	—	—	—	—
	"	0.0024	-0.0007	0.0004	"	-0.0032	0.997	—	-15	1.568	"	"	—	—	—	—
	"	0.0022	-0.0005	"	-0.0004	-0.0023	0.991	—	-10	1.552	"	"	—	—	—	—
	"	0.0018	-0.0008	0.0003	-0.0003	-0.0013	0.989	—	-5	1.573	"	"	—	—	—	—
	0.0021	0.0016	-0.0009	"	"	-0.0003	0.992	—	0	1.605	"	"	—	—	—	—
	"	0.0016	-0.0001	0.0002	-0.0002	-0.0005	0.994	—	"	"	"	"	—	—	—	—
	"	0.0017	-0.0003	"	-0.0003	-0.0008	0.990	—	5	1.572	"	"	—	—	—	—
	"	0.0019	"	0.0001	"	-0.0021	0.997	—	10	1.556	"	"	—	—	—	—
	"	0.0022	-0.0000	"	"	"	"	—	15	1.530	"	"	—	—	—	—
	"	0.0026	-0.0001	0.0002	"	-0.0027	0.998	—	20	1.549	"	"	—	—	—	—
	"	0.0035	-0.0004	0.0000	"	-0.0029	"	—	25	1.499	"	"	—	—	—	—
	"	0.0036	"	"	"	-0.0031	0.997	—	27	1.475	"	"	—	—	—	—
9	0.0015	0.0038	-0.0026	0.0007	-0.0005	-0.0037	0.982	—	-27	1.362	0.997	0.997	—	—	—	—
↑	"	0.0035	-0.0030	0.0003	-0.0006	"	0.977	—	-25	"	1.003	1.003	—	—	—	—
	"	0.0028	-0.0026	0.0005	"	-0.0035	0.988	—	-20	1.495	"	"	—	—	—	—
	"	0.0023	-0.0015	"	-0.0005	-0.0033	0.992	—	-15	1.532	"	"	—	—	—	—
	0.0013	"	-0.0019	0.0007	"	-0.0022	0.966	—	-10	"	"	"	—	—	—	—
	0.0015	0.0018	-0.0016	0.0005	-0.0006	-0.0011	0.982	—	-5	1.568	"	"	—	—	—	—
	0.0017	0.0016	-0.0014	0.0003	"	-0.0000	0.984	—	0	1.560	"	"	—	—	—	—
	0.0015	"	-0.0008	"	"	-0.0011	0.991	—	5	1.564	1.005	1.009	—	—	—	—
	"	0.0019	-0.0012	0.0002	"	-0.0020	0.986	—	10	1.560	"	"	—	—	—	—
	0.0019	0.0021	-0.0006	0.0003	-0.0005	-0.0022	0.996	—	15	1.540	"	"	—	—	—	—
	0.0023	0.0026	-0.0008	"	-0.0006	-0.0027	0.993	—	20	1.535	"	"	—	—	—	—
	0.0019	0.0032	-0.0010	"	"	"	0.986	—	25	1.487	1.009	1.017	—	—	—	—
	"	0.0034	"	0.0002	"	-0.0034	0.996	—	27	1.491	"	"	—	—	—	—

TABLE 3 CONT.

	1	2	3	4	5	6	7	8	9	10	11	12	13	14	15	16
RUN NO.	C_L	C_D	C_m	C_ℓ	C_n	C_c	$\frac{H-p}{(H-p)_o}$	$\alpha_{g\,SEL.}$ DEGREES	$\psi_{SEL.}$ DEGREES	$\frac{H-T_M}{(H-p)_o}$	$\frac{H-A}{(H-p)_o}$	$\frac{H-G_M}{(H-p)_o}$	$\frac{H-T_E^M}{(H-p)_o}$	$\frac{H-G_\ell}{(H-p)_o}$	$\frac{H-T_\ell'}{(H-p)_o}$	SPECIAL SETTINGS
10	0.0038	0.0040	—	—	—	—	1.004	—	-27	1.362	1.008	1.012	—	—	—	—
	"	0.0038	—	—	—	—	1.006	—	-25	1.394	"	"	—	—	—	—
	"	0.0031	—	—	—	—	1.005	—	-20	1.516	"	"	—	—	—	—
	"	0.0025	—	—	—	—	1.006	—	-15	1.560	"	"	—	—	—	—
	0.0036	0.0022	—	—	—	—	1.008	—	-10	1.556	"	"	—	—	—	—
	0.0034	0.0018	—	—	—	—	1.005	—	-5	1.580	"	"	—	—	—	—
	"	0.0016	—	—	—	—	1.008	—	0	1.613	"	"	—	—	—	—
	"	"	—	—	—	—	—	—	5	—	—	—	—	—	—	—
	"	0.0017	—	—	—	—	—	—	10	—	—	—	—	—	—	—
	"	0.0021	—	—	—	—	—	—	15	—	—	—	—	—	—	—
	"	0.0025	—	—	—	—	1.008	—	20	1.540	1.008	1.012	—	—	—	—
	"	0.0032	—	—	—	—	—	—	25	—	—	—	—	—	—	—
	"	0.0034	—	—	—	—	—	—	27	—	—	—	—	—	—	—
14	0.0028	0.0000	—	—	—	—	1.003	-20	0	1.447	1.009	1.013	—	—	—	—
	"	"	—	—	—	—	1.006	-10	"	"	"	"	—	—	—	—
	"	"	—	—	—	—	1.005	0	"	"	"	"	—	—	—	—
	"	"	—	—	—	—	1.008	0	"	"	"	"	—	—	—	—
	"	"	—	—	—	—	1.011	10	"	"	"	"	—	—	—	—
	"	"	—	—	—	—	1.009	20	"	1.451	"	"	—	—	—	—
15	0.0034	0.0000	—	—	—	—	—	0	0	—	—	—	1.600	1.013	—	—
16	0.0021	0.0000	—	—	—	—	0.995	20	0	1.451	1.009	1.015	1.617	1.009	—	—
	"	"	—	—	—	—	1.000	10	"	"	"	"	1.621	"	—	—
	"	"	—	—	—	—	1.005	0	"	1.447	"	"	"	"	—	—
	0.0027	"	—	—	—	—	1.002	0	"	1.451	"	"	"	"	—	—
	0.0021	"	—	—	—	—	1.007	10	"	"	"	"	1.624	"	—	—
	"	"	—	—	—	—	1.009	20	"	1.455	"	"	1.633	"	—	—

TABLE 3 CONT.

	1	2	3	4	5	6	7	8	9	10	11	12	13	14	15	16
	RUN NO.	C_L	C_D	C_m	C_l	C_n	C_c	$\frac{H-p}{(H-p)_0}$	$\alpha_{g\,SEL}$ DEGREES	ψ_{SEL} DEGREES	$\frac{H-T_M}{(H-p)_0}$	$\frac{H-A}{(H-p)_0}$	$\frac{H-G_M}{(H-p)_0}$	$\frac{H-T_E^M}{(H-p)_0}$	$\frac{H-G_E}{(H-p)_0}$	$\frac{H-T_t^I}{(H-p)_0}$	SPECIAL SETTINGS
	17	0.0032	0.0000	—	—	—	—	1.005	0	-27	1.455	1.013	1.017	1.633	1.013	—	—
	↓	"	"	—	—	—	—	"	"	-20	1.458	"	"	1.637	"	—	—
		"	"	—	—	—	—	1.002	"	-10	1.455	"	"	1.629	"	—	—
		"	"	—	—	—	—	1.003	"	0	"	"	"	1.637	"	—	—
		"	"	—	—	—	—	1.001	"	10	1.477	"	"	1.633	"	—	—
		"	"	—	—	—	—	1.003	"	20	1.443	"	"	"	"	—	—
	↓	"	"	—	—	—	—	1.005	"	27	"	"	"	1.641	"	—	—
	18	0.0032	0.0000	—	—	—	—	1.006	0	0	1.446	1.013	1.017	—	1.013	—	—
	19	0.0034	0.0000	—	—	—	—	1.008	0	0	1.446	1.013	1.017	1.143	1.043	—	ℓ_M = 40"
	↓	"	"	—	—	—	—	1.003	"	"	1.442	"	"	"	"	—	20"
		"	"	—	—	—	—	0.999	"	"	1.450	"	"	1.147	"	—	15"
	↓	"	"	—	—	—	—	1.000	"	"	1.455	"	"	1.155	"	—	11.75"
	20	0.0036	0.0032	—	—	—	—	1.005	0	0	1.612	1.013	1.017	1.126	1.045	—	ℓ_M = 40"
	↓	0.0023	0.0033	—	—	—	—	1.003	"	"	"	"	"	"	"	—	20"
		0.0037	0.0031	—	—	—	—	0.996	"	"	"	"	"	1.130	"	—	5"
	↓	0.0043	0.0033	—	—	—	—	0.997	"	"	"	"	"	1.134	"	—	11.75"
	21	0.0047	0.0031	—	—	—	—	—	0	0	1.613	1.013	1.017	1.441	1.013	—	ℓ_M 40"
	↓	0.0049	0.0033	—	—	—	—	—	"	"	"	"	"	1.511	"	—	20"
		0.0045	0.0032	—	—	—	—	—	"	"	1.616	"	"	1.426	"	—	15"
	↓	0.0051	0.0033	—	—	—	—	—	"	"	1.620	"	"	1.483	"	—	11.15"
	22	0.0049	0.0017	—	—	—	—	—	0	0	1.604	1.009	1.013	1.532	1.009	—	ℓ_M = 40"
	↓	"	"	—	—	—	—	—	"	"	"	"	"	1.564	"	—	20"
		0.0051	0.0018	—	—	—	—	—	"	"	1.608	"	"	1.568	"	—	15"
	↓	0.0053	"	—	—	—	—	—	"	"	1.616	"	"	1.584	"	—	11.75"
	23	0.0032	0.0015	—	—	—	—	1.001	0	0	1.592	1.005	1.009	1.597	1.005	—	—

TABLE 3 CONT.

	1	2	3	4	5	6	7	8	9	10	11	12	13	14	15	16
	RUN NO.	C_L	C_D	C_m	C_l	C_n	C_c	$\frac{H-p}{(H-p)_0}$	$\alpha_{g_{SEL.}}$ DEGREES	$\alpha_{SEL.}$ DEGREES	$\frac{H-T_M}{(H-p)_0}$	$\frac{H-A}{(H-p)_0}$	$\frac{H-G_M}{(H-p)_0}$	$\frac{H-T_t^M}{(H-p)_0}$	$\frac{H-G_t}{(H-p)_0}$	$\frac{H-T_t^I}{(H-p)_0}$	SPECIAL SETTINGS
	26	0.0030	0.0016	—	—	—	—	1.023	0	0	1.649	1.013	1.017	1.609	1.013	—	$t_I^S = 34.42"$
	↓	"	"	—	—	—	—	1.026	"	"	"	"	"	"	"	—	35.42"
		0.0032	0.0015	—	—	—	—	1.020	"	"	1.635	1.009	1.013	"	1.009	—	36.42"
	28	0.0032	0.0016	—	—	—	—	1.030	0	0	1.665	1.017	1.021	1.620	1.017	—	F_I^S UP 3"
	↓	"	0.0015	—	—	—	—	1.038	"	"	1.685	"	"	1.616	"	—	F_I^S DWN 3"
	29	0.0032	0.0020	—	—	—	—	—	0	−10	1.584	1.013	1.017	1.616	1.013	—	—
		"	0.0016	—	—	—	—	—	"	−3	1.629	"	"	"	"	—	—
		"	0.0015	—	—	—	—	—	"	0	1.653	"	"	"	"	—	—
		"	"	—	—	—	—	—	"	3	1.657	"	"	"	"	—	—
	↓	"	0.0018	—	—	—	—	—	"	10	1.584	"	"	"	"	—	—
	30	0.0030	0.0025	—	—	—	—	—	0	0	1649	1.017	1.017	—	1.017	—	BRASS BLOCK IN F_I^S:
		"	0.0026	—	—	—	—	—	"	"	"	"	"	—	"	—	1¾" BELOW TIP
		"	0.0027	—	—	—	—	—	"	"	"	"	"	—	"	—	1¼" " "
		"	0.0026	—	—	—	—	—	"	"	"	"	"	—	"	—	2¼" " "
		"	0.0028	—	—	—	—	—	"	"	"	"	"	—	"	—	2¾" " "
		"	0.0027	—	—	—	—	—	"	"	"	"	"	—	"	—	3¾" " "
		"	0.0026	—	—	—	—	—	"	"	"	"	"	—	"	—	BRASS BLOCK OUT
		0.0028	0.0025	—	—	—	—	—	"	"	"	"	"	—	"	—	BRASS BLOCK 1¾" BELOW TIP AND F_I^S UP ¼"
		"	0.0026	—	—	—	—	—	"	"	"	"	"	—	"	—	" ½"
	↓	"	0.0029	—	—	—	—	—	"	"	"	"	"	—	"	—	DWN ¼"
																	" ½"
	34	0.0026	0.0000	—	—	—	—	1.055	0	0	1487	1.027	1.030	1.628	1.027	—	$l_M = 40"$
	↓	"	"	—	—	—	—	1.048	"	"	1.490	"	"	1.665	"	—	20"
		0.0028	"	—	—	—	—	1.045	"	"	1.487	"	"	1.685	"	—	15°
	36	0.0023	0.0000	—	—	—	—	1.055	0	0	1.495	1.045	1.049	1.640	1.045	—	$l_E = 40"$
	↓	"	"	—	—	—	—	1.052	"	"	"	"	"	1.637	"	—	29"
	40	0.0041	0.0021	—	—	—	—	—	0	0	—	—	—	—	—	—	F_I SET AT $\alpha_g = 0°$
	↓	0.0036	"	—	—	—	—	—	2	"	—	—	—	—	—	—	"

TABLE 3 CONT

	1	2	3	4	5	6	7	8	9	10	11	12	13	14	15	16
RUN NO.	C_L	C_D	C_m	C_ℓ	C_n	C_c	$\frac{H-p}{(H-p)_0}$	$\alpha_{g\,SEL.}$ DEGREES	$\psi_{SEL.}$ DEGREES	$\frac{H-T_M}{(H-p)_0}$	$\frac{H-A}{(H-p)_0}$	$\frac{H-G_M}{(H-p)_0}$	$\frac{H-T_\ell^M}{(H-p)_0}$	$\frac{H-G_\ell}{(H-p)_0}$	$\frac{H-T_\ell^I}{(H-p)_0}$	SPECIAL SETTINGS
40A	—	—	—	—	—	—	—	-6	0	1.498	1.045	1.049	1.608	1.045	1.608	E_2 SET AT C_2-0°
	—	—	—	—	—	—	—	-4	"	"	"	"	1.600	"	1.596	"
	—	—	—	—	—	—	—	-2	"	"	"	"	"	"	1.588	"
	—	—	—	—	—	—	—	0	"	"	"	"	1.596	"	"	"
	—	—	—	—	—	—	—	2	"	"	"	"	1.588	"	1.580	"
	—	—	—	—	—	—	—	4	"	"	"	"	"	"	1.576	"
↓	—	—	—	—	—	—	—	6	"	"	"	"	1.592	"	"	"
42	0.0034	0.0031	—	—	—	—	—	0	0	—	—	—	—	—	—	—
152	0.0031	0.0000	-0.0008	0.0005	0.0000	0.0003	—	0	-27	—	—	—	—	—	—	NO BAYONETS OR TAIL STRUT SEAL
	0.0027	"	-0.0004	0.0001	"	"	—	"	-19	—	—	—	—	—	—	
	0.0017	0.0003	0.0010	0.0001	"	0.0002	—	"	0	—	—	—	—	—	—	F_M^{SN} SEALS IN
	0.0015	0.0002	0.0013	0	0.0001	0.0001	—	"	19	—	—	—	—	—	—	GIVES PRESS. EFFECT
	0.0017	0.0003	-0.0001	-0.0001	"	0.0000	—	"	27	—	—	—	—	—	—	ON MAIN STRUTS & SEALS
	0.0032	0.0022	0.0015	0.0001	"	-0.0001	—	"	0	—	—	—	—	—	—	SAME AS ABOVE + B_M^{SN}
	0.0019	0.0004	0.0035	0.0002	0.0000	0.0004	—	"	0	—	—	—	—	—	—	NO BAYONETS. F_M^{SN} SEALED OFF AT TIPS. TAIL STRUT & SEAL IN. GIVES PRESS. EFFECT ON TAIL STRUT ONLY
↓	0.0025	0.0003	"	-0.0004	"	0.0001	—	"	27	—	—	—	—	—	—	

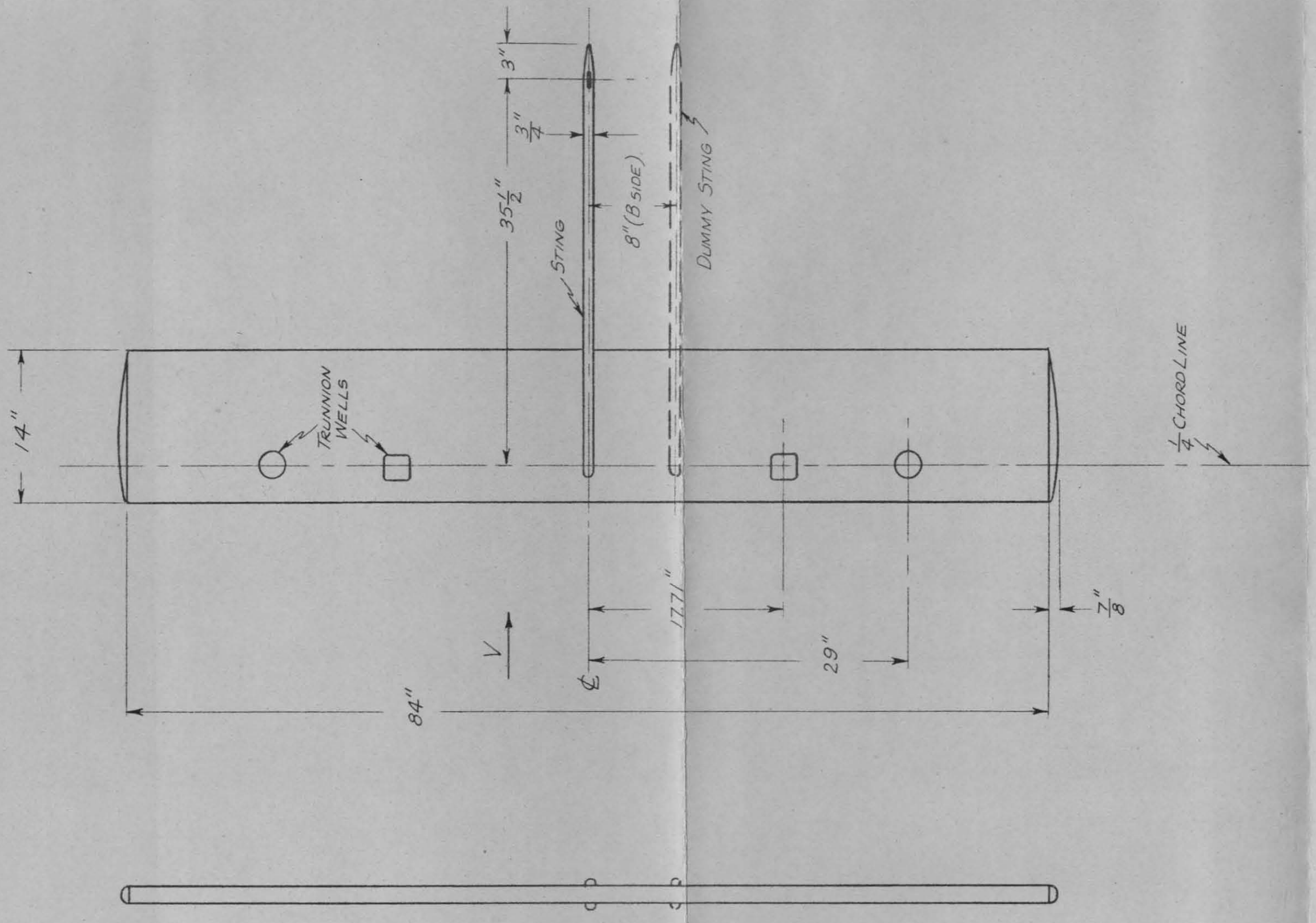

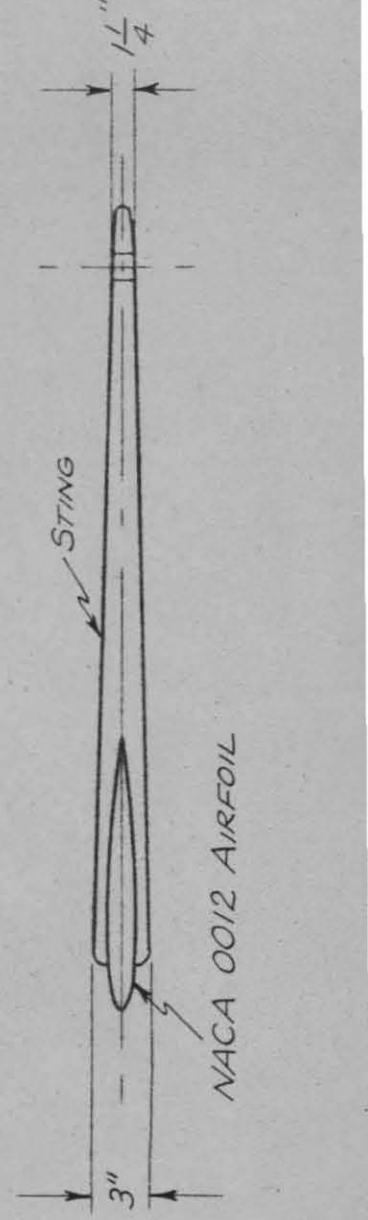

THREE VIEW SKETCH OF GALCIT
STEEL CALIBRATION WING AND STING

VERTICAL SECTION THROUGH 10 FT. WIND TUNNEL
2 PARAMETER 6 COMPONENT SUSPENSION SYSTEM
GUGGENHEIM AERONAUTICS LABORATORY
CALIFORNIA INSTITUTE OF TECHNOLOGY

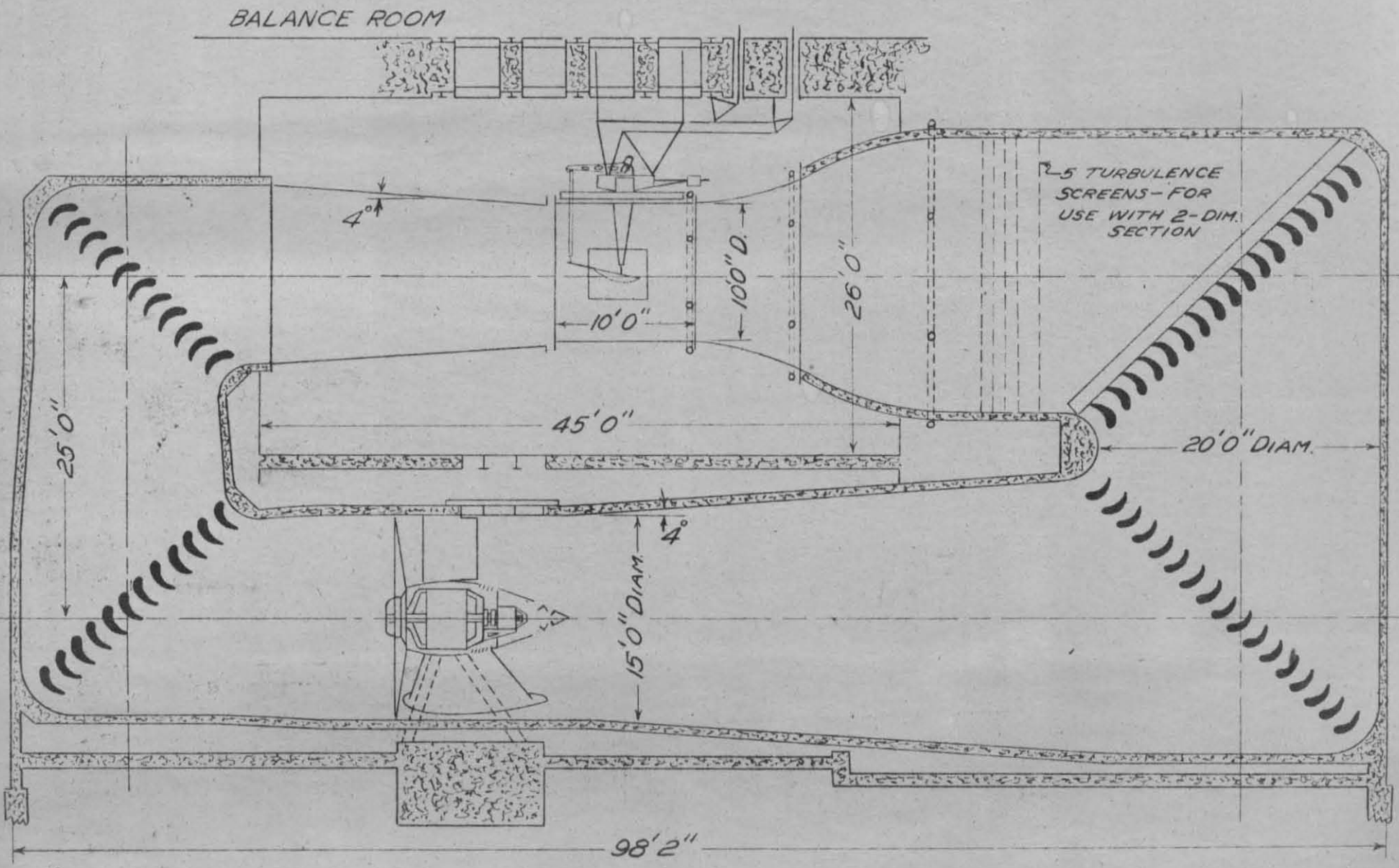

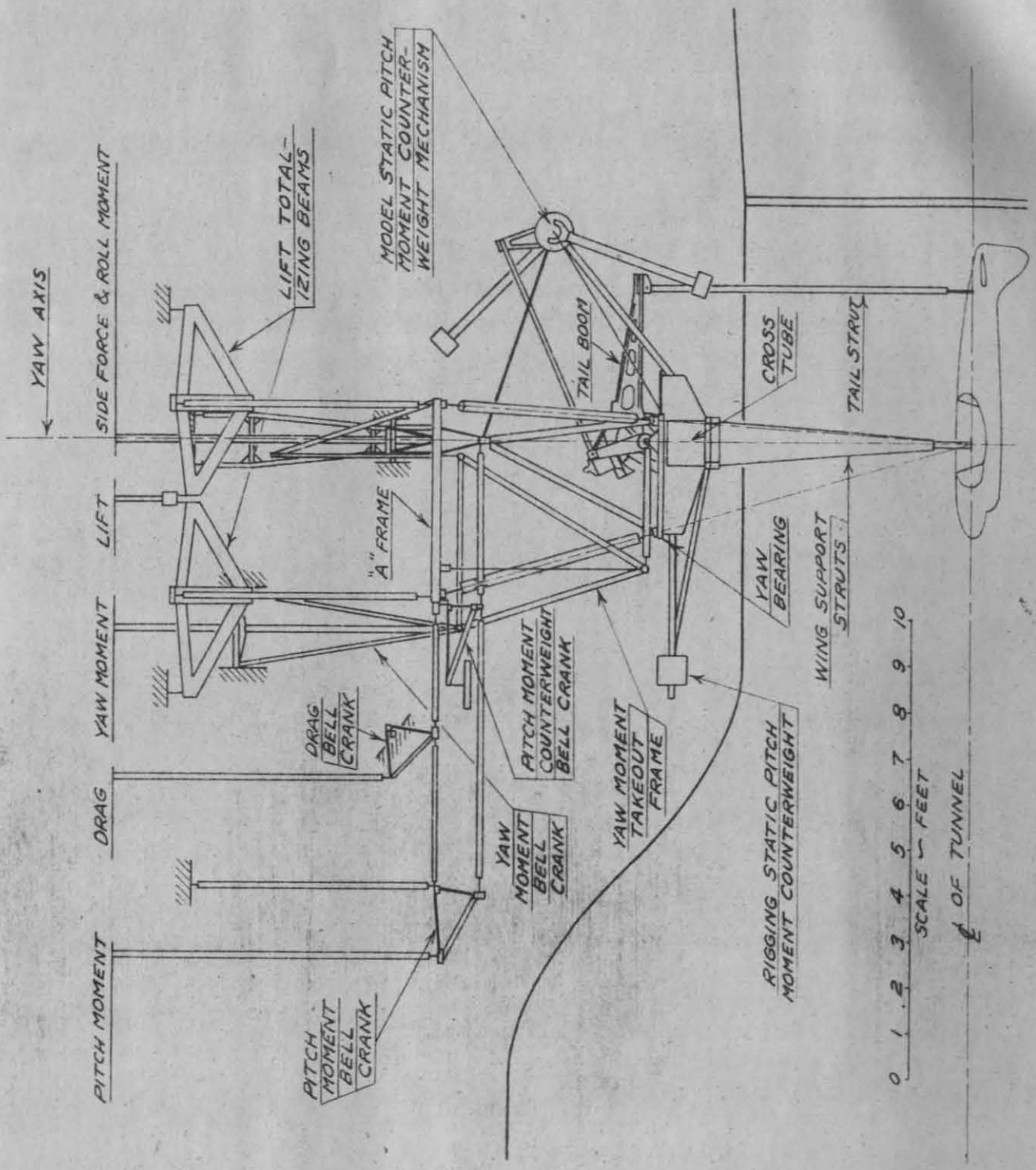

SKETCH OF GALCIT 2 PARAMETER
6 COMPONENT MODEL SUSPENSION SYSTEM
GALCIT 10 FOOT TUNNEL

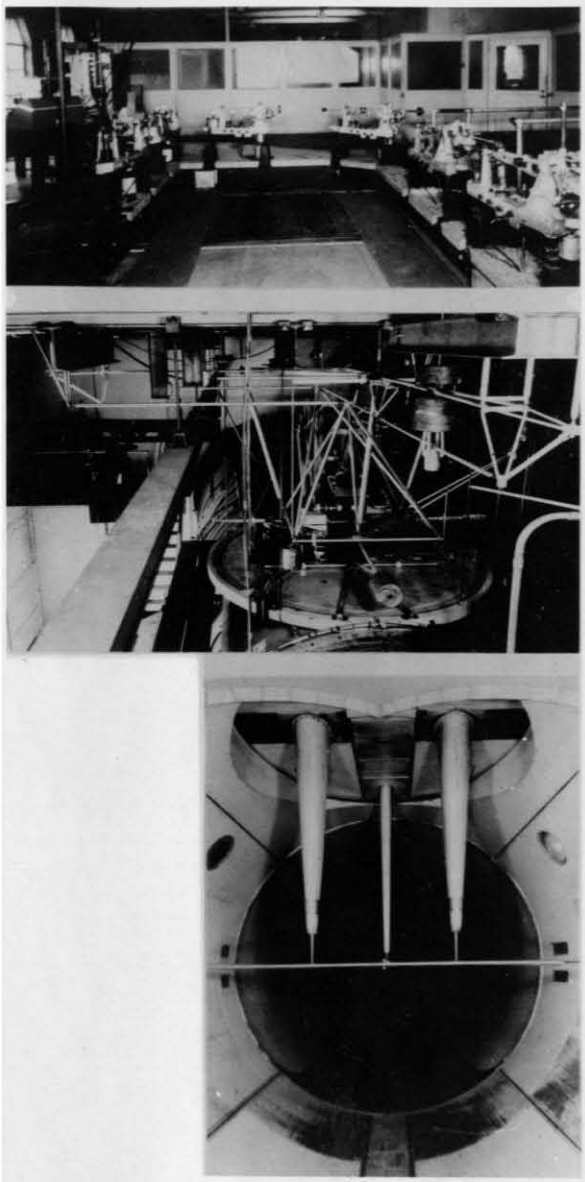

Composite View of Balance Room, Suspension System, and Throat of GALCIT Ten Foot Wind Tunnel

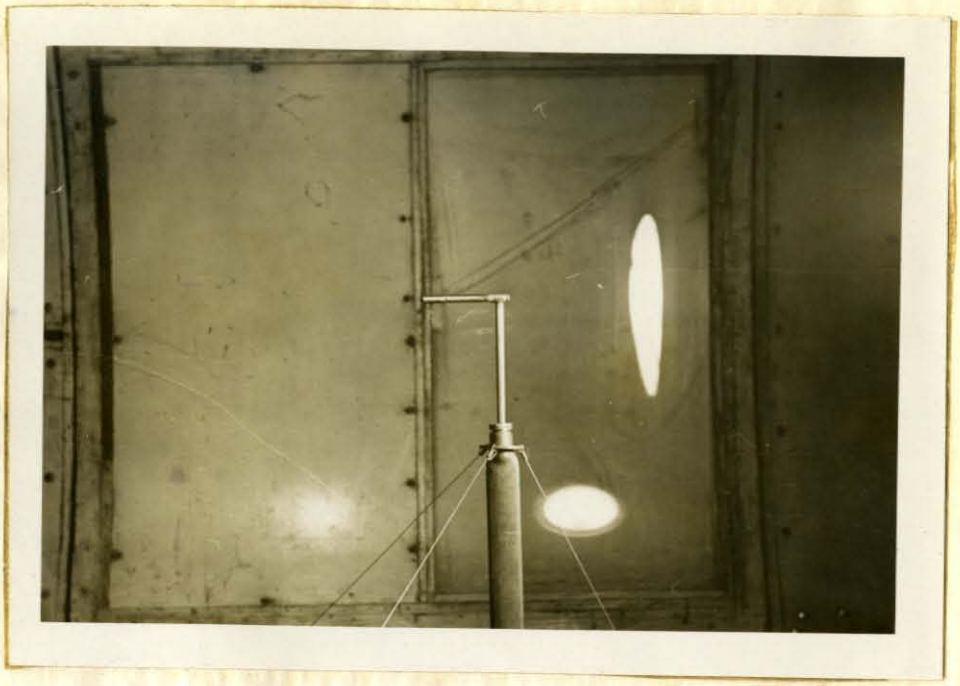

Photo No. 1. Pitot-static tube mounted at centerline of throat. View looking across tunnel.

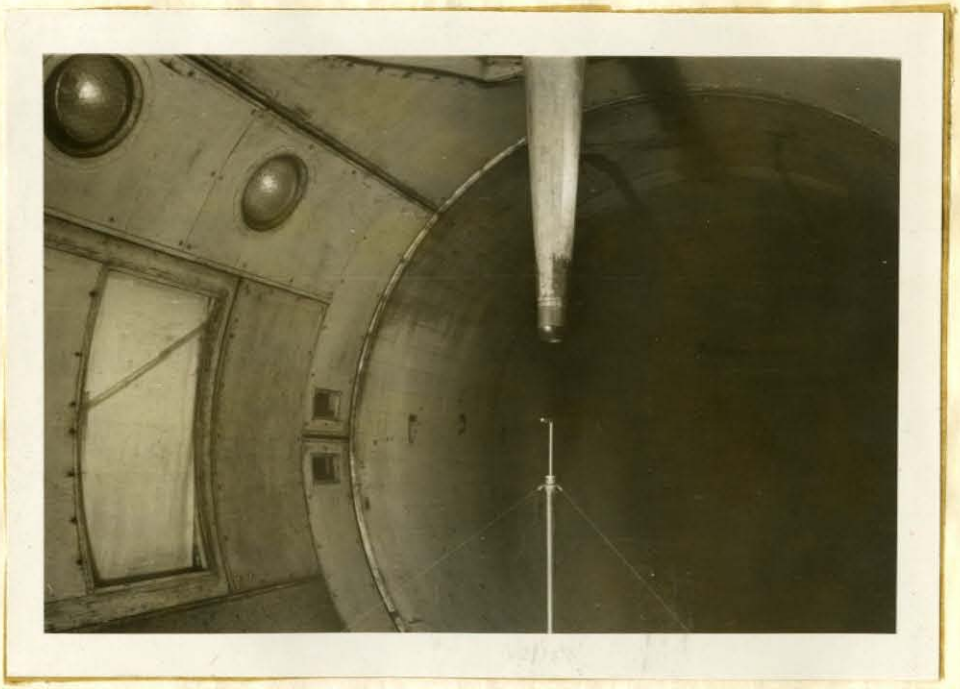

Photo No. 2. Main wing windshield mounted on yaw axis above pitot-static tube. View looking downstream.

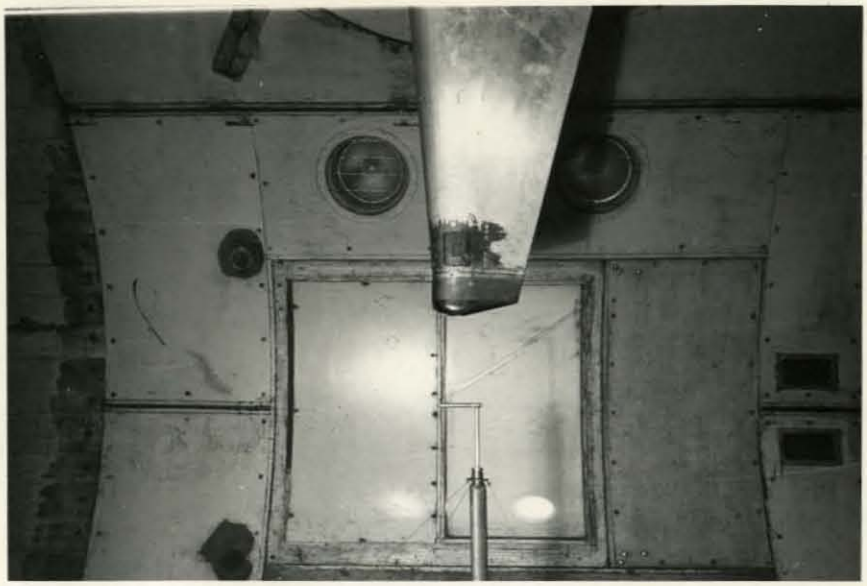

Photo No. 3. Main wing windshield mounted on yaw axis above pitot-static tube, View looking across tunnel.

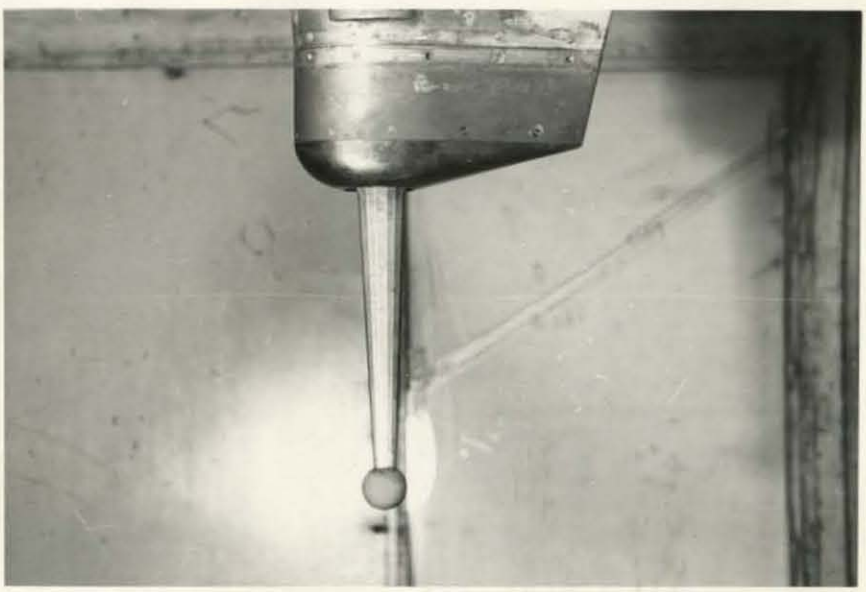

Photo No. 4. View looking across tunnel showing main wing windshield and bayonet with ball tip.

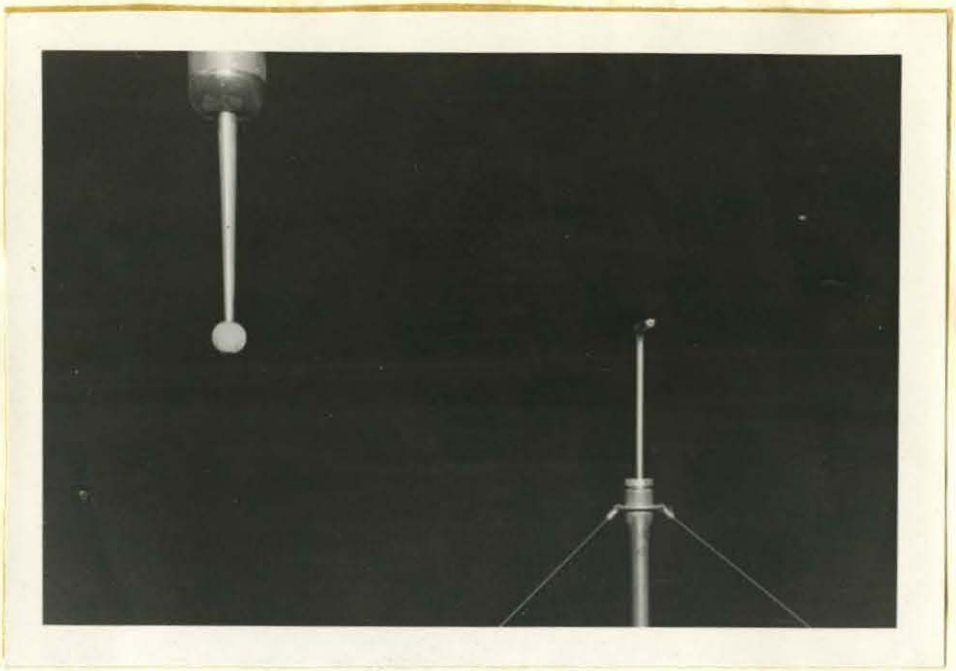

Photo No. 5. View looking downstream at pitot-static tube on tunnel centerline and main wing windshield and strut at the 35.42" trunnion spacing.

Photo No. 6. Downstream view of all three main windshields and south image wing windshield with bayonets.

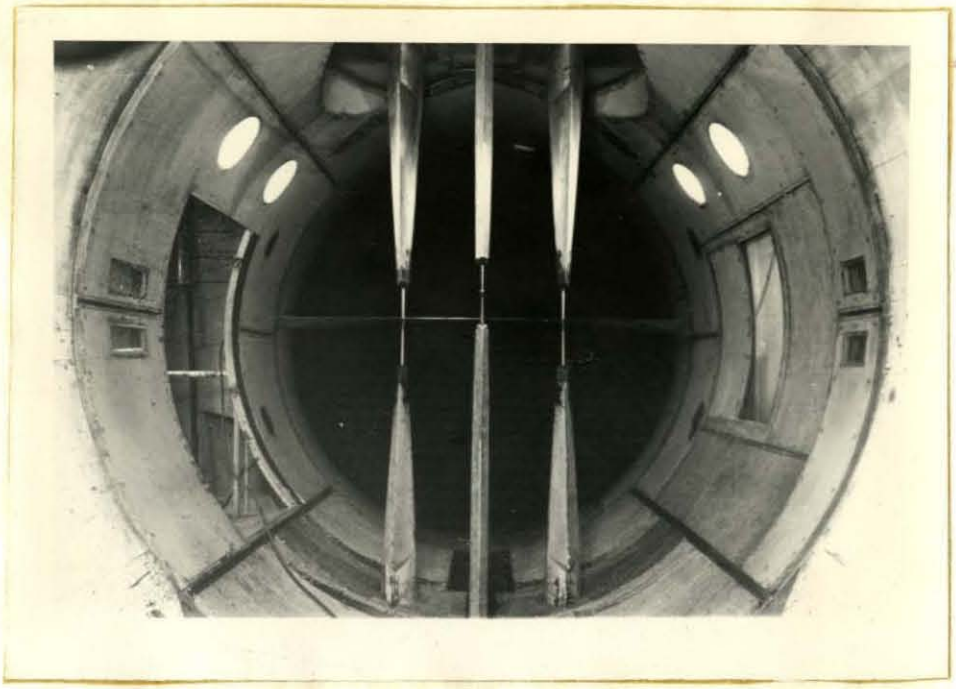

Photo No. 7. Upstream view of steel wing mounted on suspension system and image system in place.

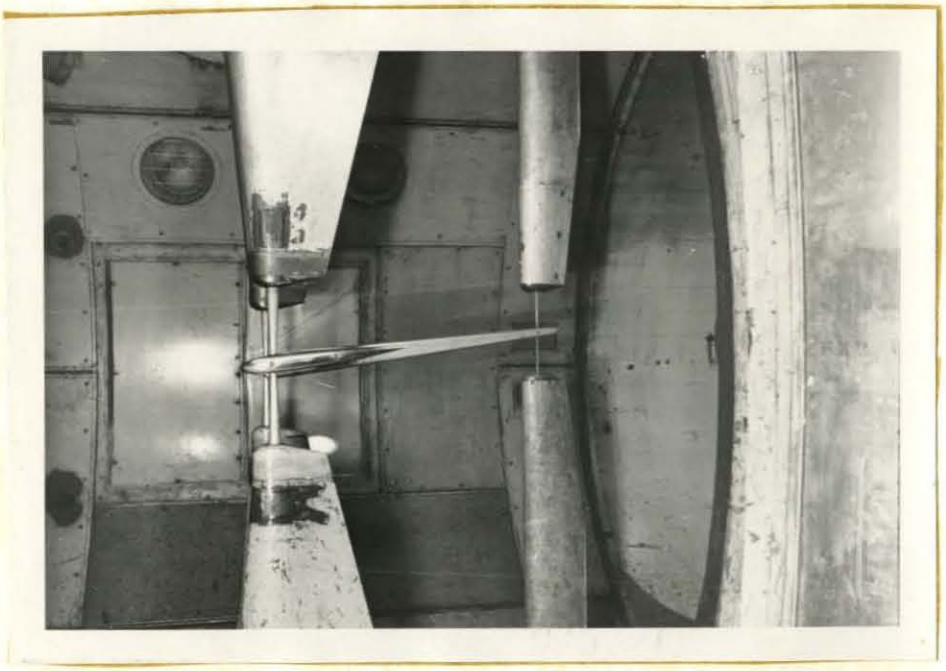

Photo No. 8. Side-view showing wing and all six windshields and bayonets.

Photo No. 9. View looking upstream showing wing tare setup $\psi = 27^{\circ}$.

Photo No. 10. Side view showing wing tare setup at $\psi = 27^{\circ}$.

Photo No. 11. Closeup view showing junction of main wing bayonet and wing.

Photo No. 12. Closeup view showing sting attached to wing.

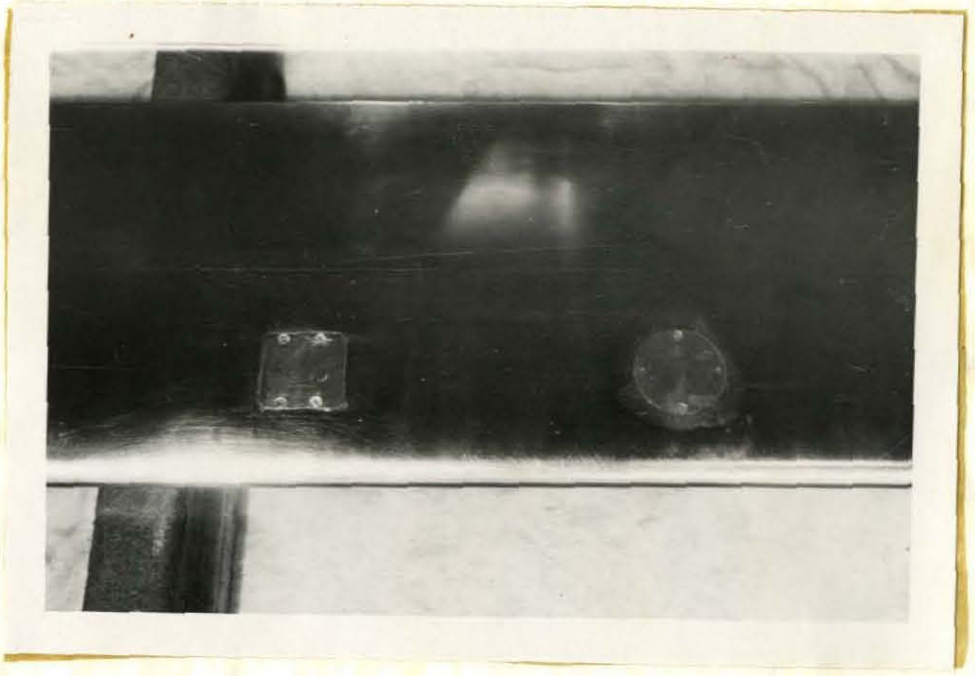

Photo No. 13. Closeup view showing cover plates for both trunnion spacings.

Appendix No. 1

Buoyancy Lift on Struts and Bayonets

When a strut (or bayonet) is exposed to the action of the windstream or the pressures developed by the windstream inside of the windshields the resulting pressure forces are measured by the balances as an aerodynamic load, and so cause an aerodynamic interference or tare. The magnitude of this tare depends on the size and shape of the supports, and on the pressure distribution as a function of the general pressure level inside (and outside) of the throat, and of the velocity field produced by the model. For the GALCIT system this "buoyancy" force on the bayonets results in a lift tare.

. This tare can be estimated if the average pressure on the bayonets is known. In the following pages the average pressure on the surface of a cylinder and a 12% Joukowski airfoil are calculated.

(a) Circular Cylinder

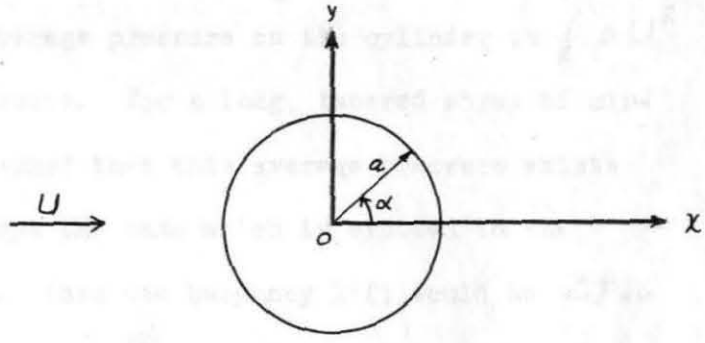

Let U = freestream velocity

p_o = " static pressure

$q = 2U \sin\theta$

= local velocity on cylinder surface, assuming two-dimensional, potential flow (incompressible)

p = local pressure on cylinder

Appendix No. 1 (Cont'd)

Assume the pressure outside of the tunnel is equal to the free-stream static pressure.

Then the "buoyancy pressure" on the cylinder (or strut) is given by the integration of $(p-p_o)$ over the surface.

The buoyancy force, F, per unit length of the cylinder is

$$F = \int_0^{2\pi} a(p-p_o)\,d\theta = \frac{1}{2}\rho a \int_0^{2\pi} (U^2 - q^2)\,d\theta$$

$$= \frac{1}{2}\rho U^2 a \int_0^{2\pi} (1 - 4\sin^2\theta)\,d\theta$$

$$= -\pi \rho a U^2$$

The average pressure is $\frac{F}{2\pi a}$

or, $\Delta p_{\text{average}} =$

$$= -\frac{1}{2}\rho U^2$$

Thus, with potential flow, the average pressure on the cylinder is $\frac{1}{2}\rho U^2$ below the free stream static pressure. For a long, tapered strut of circular cross section it may be assumed that this average pressure exists over every part of the strut except the base which is exposed to the pressure p_o outside the tunnel. Then the buoyancy lift would be $\Delta p_{av.}$ multiplied by the base area.

Obviously the lift tare will be smallest when the strut seal is at the tip of the windshield.

Appendix No. 1 (Cont'd)

(b) Joukowski Airfoil

Assume two-dimensional flow of an incompressible ideal fluid and use the Joukowski Transformation from a cylinder to symmetrical airfoil. (Ref. Durand, "Aerodynamic Theory", Vol. II, Div. E, p. 65.) Calculate the average pressure per unit length of the airfoil.

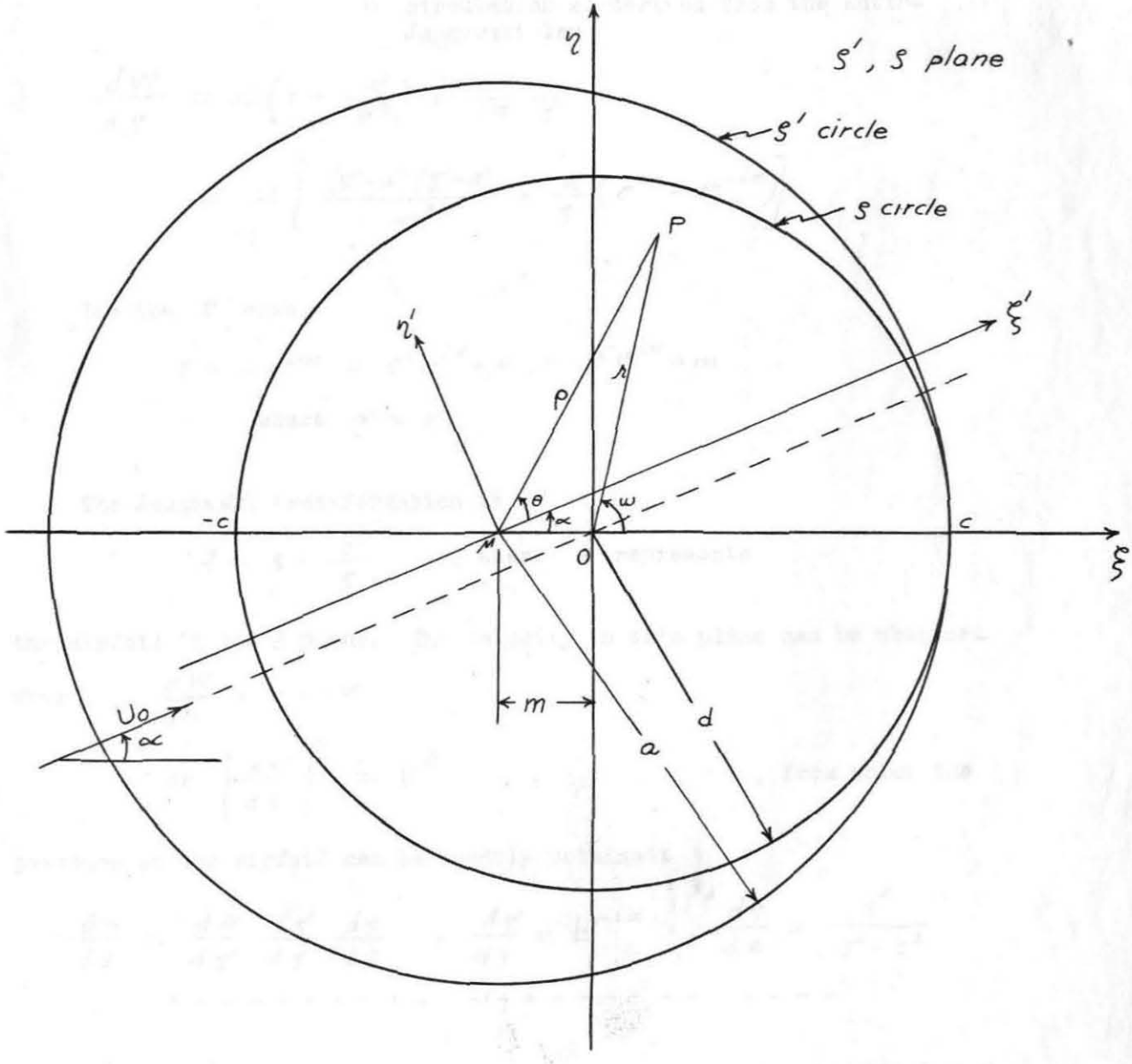

Appendix No. 1 (Cont'd)

The complex potential function for the cylinder in the ζ' plane is

$$W(\zeta') = U_o\left(\zeta' + \frac{a^2}{\zeta'}\right) + \frac{i\Gamma}{2\pi} \ln \frac{\zeta'}{a}$$

where $\zeta' = \rho e^{i\theta}$

U_o = free stream velocity

$\Gamma = 4\pi a U \sin\alpha$

= circulation as derived from the Kutta-Joukowski law

$$\frac{dW}{d\zeta'} = U_o\left(1 - \frac{a^2}{\zeta'^2}\right) + \frac{i\Gamma}{2\pi}\frac{1}{\zeta'}$$

$$= U_o\left[\frac{(\zeta'+a)(\zeta'-a)}{\zeta'^2} + \frac{a}{\zeta'}\left(e^{i\alpha} - e^{-i\alpha}\right)\right]$$

For the ζ axes,

$$\zeta = \rho e^{i\omega} = \zeta' e^{i\alpha} + \mu = \zeta' e^{i\alpha} - m$$

where $m = \varepsilon c$

The Joukowski transformation is

$$Z = \zeta + \frac{c^2}{\zeta}$$, where Z represents

the airfoil in the Z plane. The velocity in this plane can be obtained from $\frac{dW}{dZ} = u - iv$

or $\left|\frac{dW}{dZ}\right|^2 = V^2$, from which the

pressure on the airfoil can be readily obtained.

$$\frac{dW}{dZ} = \frac{dW}{d\zeta'}\frac{d\zeta'}{d\zeta}\frac{d\zeta}{dZ} \quad , \quad \frac{d\zeta'}{d\zeta} = e^{-i\alpha} \quad , \quad \frac{d\zeta}{dZ} = \frac{\zeta^2}{\zeta^2 - c^2}$$

- -

To get the average pressure it is necessary to determine the length of the periphery of the airfoil. For this let $\alpha = 0$, $\rho = a$,

Appendix No. 1 (Cont'd)

and S = periphery.

Then $$S = \oint |dz| = \oint \left| d\varsigma' \frac{d\varsigma}{d\varsigma'} \frac{dz}{d\varsigma} \right|,$$

$$|d\varsigma'| = |\rho i e^{i\theta} d\theta| = a\, d\theta,$$

$$\left|\frac{d\varsigma}{d\varsigma'}\right| = 1 \quad , \quad \left|\frac{dz}{d\varsigma}\right| = \left| 1 - \frac{c^2}{\varsigma^2} \right|$$

Then $$S = \oint a \left| 1 - \frac{c^2}{\varsigma^2} \right| d\theta \qquad , \text{ where } \quad \varsigma = \varsigma' - \varepsilon c$$

Neglect all terms of order ε^3 or higher and calculate $\left|\frac{d\varsigma}{dz}\right|^2$

$$\frac{d\varsigma}{dz} = \frac{(\varsigma' - \varepsilon c)^2}{(\varsigma' - \varepsilon c)^2 - c^2} = \frac{a^2 e^{2i\theta} - 2a\varepsilon c\, e^{i\theta} + \varepsilon^2 c^2}{a^2 e^{2i\theta} - 2a\varepsilon c\, e^{i\theta} + \varepsilon^2 c^2 - c^2}$$

$$\left|\frac{d\varsigma}{dz}\right|^2 = \frac{\left[1 + 2\varepsilon(1+\varepsilon)(1 - \cos\theta)\right]^2}{8\varepsilon^2(1 - \cos\theta) + 4(1+2\varepsilon)\sin^2\theta}$$

Then, $$S = a \oint \frac{\sqrt{8\varepsilon^2(1 - \cos\theta) + 4(1+2\varepsilon)\sin^2\theta}}{1 + 2\varepsilon(1+\varepsilon)(1 - \cos\theta)}\, d\theta$$

$$\doteq a \oint \sqrt{8\varepsilon^2(1 - \cos\theta) + 4(1+2\varepsilon)\sin^2\theta} \left(1 - 2\varepsilon + 2\varepsilon^2 + 2\varepsilon\cos\theta - 6\varepsilon^2\cos\theta + 4\varepsilon^2\cos^2\theta\right) d\theta$$

Now let $t^2 = 1 + \cos\theta$

Substitution gives

$$S = -4a\sqrt{1+2\varepsilon} \oint \sqrt{\frac{2\varepsilon^2}{1+2\varepsilon} + t^2} \left[(1 - 4\varepsilon + 12\varepsilon^2) + (2\varepsilon - 14\varepsilon^2)t^2 + 4\varepsilon^2 t^4 \right] dt$$

Integrating around the periphery and removing terms of higher order gives

$$S = \frac{8c}{3}\left[\frac{3\varepsilon^2}{\sqrt{1+2\varepsilon}} \ln\left(\frac{\sqrt{1+2\varepsilon}}{\varepsilon} + \frac{1+\varepsilon}{\varepsilon} \right) + 3 + \varepsilon^2 \right]$$

Expand and simplify to get answer

$$S = 8c\left(1 + 1.0264\,\varepsilon^2 - \varepsilon^2 \ln\varepsilon\right)$$

Appendix No. 1 (Cont'd)

For 12% thickness, $\varepsilon = 0.0924$

or $S = 8c(1.0291)$

It is interesting to note that if the same calculation is performed by neglecting all terms of ε^2 or higher the answer is $S = 8c(1+2\varepsilon)$, which is a difference of 15%.

The average pressure on the airfoil is,

$$P_{av} = \frac{1}{S}\oint \Delta p\, dS$$

where $\Delta p = p - p_0 = \frac{1}{2}\rho U_0^2\left(1 - \frac{V^2}{U_0^2}\right) = \frac{\rho}{2}U_0^2\left[1 - \frac{1}{U_0^2}\left|\frac{dW}{dz}\right|^2\right]$

Then $$P_{av} = \frac{1}{S}\oint \frac{\rho}{2}U_0^2\left\{1 - \frac{1}{U_0^2}\cdot\left|\frac{dW}{d\zeta'}\,\frac{d\zeta'}{d\zeta}\,\frac{d\zeta}{dz}\right|^2\right\}\cdot\left|d\zeta'\right|\cdot\left|\frac{dz}{d\zeta}\right|$$

$$= \frac{\rho}{2S}\oint\left\{a U_0^2\left|\frac{dz}{d\zeta}\right|\right\}d\theta - \frac{\rho a}{2S}\oint\left|\frac{dW}{d\zeta'}\right|^2\cdot\left|\frac{d\zeta}{dz}\right|d\theta$$

$$= \frac{\rho}{2}U_0^2 - \frac{\rho a}{2S}\oint 4U_0^2\sin^2\theta\left|\frac{d\zeta}{dz}\right|d\theta$$

since $$\frac{1}{S}\oint a\left|\frac{dz}{d\zeta}\right|d\theta = 1$$

and $$\left|\frac{dW}{d\zeta'}\right|^2 = U_0^2\left|1 - e^{-2i\theta}\right|^2 = 4U_0^2\sin^2\theta$$

Let $t^2 = 1 + \cos\theta$

Then

$$\sin^2\theta\left|\frac{d\zeta}{dz}\right|d\theta = \frac{\left\{-t^2\left[1 + 4\varepsilon(1+\varepsilon)\right] + 2t^4\varepsilon(1+\varepsilon)\right\}dt}{\sqrt{1+2\varepsilon}\,\sqrt{\frac{2\varepsilon^2}{1+2\varepsilon} + t^2}}$$

Appendix No. 1 (Cont'd)

Substitute this into the equation for P_{av} and get

$$P_{av} = \frac{\rho U_0^2}{2}\left[1 - \frac{1+2\varepsilon+2.3069\varepsilon^2+\varepsilon^2\ln\varepsilon}{1+1.0264\varepsilon^2-\varepsilon^2\ln\varepsilon}\right]$$

Then $$P_{av} = -\frac{\rho U_0^2}{2}\left(2\varepsilon + 1.2805\varepsilon^2 + 2\varepsilon^2\ln\varepsilon\right)$$

For a 12% Joukowski airfoil we get

$$P_{av} = -0.151\,\frac{\rho U_0^2}{2}$$

Appendix No. 2

Effect of Conning Tower on Windshield Blocking

Some time after the completion of the tests described in Part II, Section I, Group 1, an opportunity arose to determine the blocking of the different windshields with the conning tower closed (throat ceiling fairings in and deflector out). From the data of Runs 153 through 157 (see Run Index) and from the data in Fig. II - 16B the following tabulation has been prepared:

$\Delta\, q/q^*$ per windshield

	F_M^S	F_M^N	F_I^S	F_I^N
Conning tower open	0.006	0.011	0.023	0.030
Conning tower closed	0.022	-----	0.020	0.022

Unfortunately there was not time to determine the incremental effect of F_M^N, but these data are sufficient to substantiate the belief that having the conning tower open results in the image windshields not duplicating the blocking effect of the main windshields.

Because the measured image-system blocking correction is applied to the tare runs in the calculation procedure, and because the operating q for normal tests is determined by actual surveys with a pitot-static tube, it is not likely that this differential blocking directly influences the magnitude of the tares or of the final model characteristics. If there are errors, it is probable they will be caused by the image system not duplicating the flow curvature and inclination patterns induced by the main windshields. It should be pointed out that the q correction factor, η, (see Sec. G, cases 1 and 5) can not be used unless the blocking of the two

Appendix 2 (Cont'd)

windshield systems is the same; i.e., do not use the γ correction if the conning tower is open. It is believed that these discrepancies had only a small effect on the steel wing characteristics, but that important errors may occur in tests on complete models.

Appendix No. 3

Variation of Wing-Strut-Seal Pressure with Wing Lift

To determine the variation with wing lift of the pressure at the tip of the wing windshield, we will add the velocity increment due to the wing to that at the tip without the wing present and then calculate the pressure.

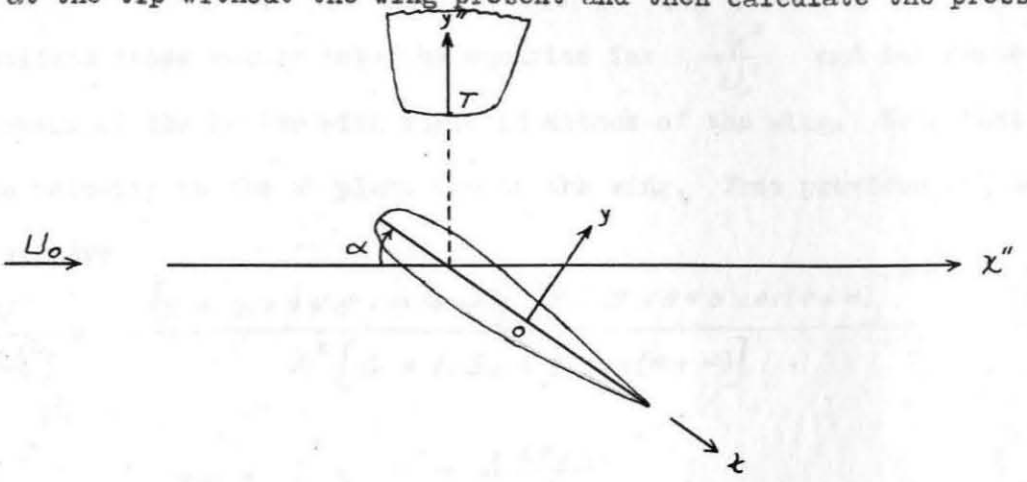

First calculate the position of the windshield tip in terms of θ and λ, where θ is angular position of the point P in the ζ' plane and $\lambda = \frac{\rho}{c}$, (see sketch in App. 1 b). This will be done for $\alpha = 0^\circ$, and it will be assumed that θ and λ do not change appreciably with small changes in α. Also assume the airfoil chord is $4c$.

The Joukowski transformation from the ζ' plane to the z plane gives the ordinates (x,y) in the z plane as, (neglecting ε^2 terms),

$$\frac{x}{c} = \frac{1}{\lambda^2}\left[2\varepsilon\cos^2\theta + (\lambda^3+\lambda)\cos\theta - \lambda^2\varepsilon - \varepsilon\right]$$

$$\frac{y}{c} = \frac{1}{\lambda^2}\left[\lambda^3 - \lambda - 2\varepsilon\cos\theta\right]\sin\theta$$

Transferring these to the wind tunnel axes x'', y'' (see sketch) gives

$$\frac{x''}{c} = 1 + \lambda\cos\theta - \varepsilon + \frac{1}{\lambda}\cos\theta + \frac{\varepsilon}{\lambda^2}\cos 2\theta \doteq 1 - \varepsilon + \cos\theta\left(\lambda + \frac{1}{\lambda}\right)$$

$$\frac{y''}{c} = \lambda\sin\theta - \frac{1}{\lambda}\sin\theta - \frac{\varepsilon}{\lambda^2}\sin 2\theta \doteq \sin\theta\left(\lambda - \frac{1}{\lambda}\right)$$

Appendix No. 3 (Cont'd)

Now $c = 3.5''$, $\varepsilon = 0.0924$, $\frac{y''}{c} = 2.33$

Then $\sin\theta = 2.33\,\frac{\lambda}{\lambda^2-1}$, $\cos\theta = (\varepsilon-1)\,\frac{\lambda}{\lambda^2+1}$

and $\theta = 106^\circ 44'$, $\lambda = 2.79$

Now substitute these values into the equation for $\frac{V^2}{U_o^2}$ and determine the variation of the latter with angle of attack of the wing. Note that V is the velocity in the z plane due to the wing. From previous calculations we have

$$\frac{V^2}{U_o^2} = \frac{\left[E + 2.1848\cos(\theta-\alpha)\right]\left[F - 0.1848\cos(\theta+\alpha)\right]^2}{\lambda^2\left[G + 1.8152\cos(\theta+\alpha)\right]}$$

where $E = \lambda + \frac{1.1933}{\lambda}$

$F = \lambda + \frac{0.0085}{\lambda}$

$G = \lambda + \frac{0.8237}{\lambda}$

and the value of ε for a 12% thick wing has been substituted.

Then calculate $\frac{d\left(\frac{V^2}{U_o^2}\right)}{d\alpha}$ and substitute the values of θ and λ given above.

The result for $\alpha = 0^\circ$ is,

$$\left[\frac{d\left(\frac{V^2}{U_o^2}\right)}{d\alpha}\right]_{\alpha=0} = 1.696$$

Let $\frac{d\alpha}{dC_L} = \frac{1}{a}$

Then $$\left[\frac{d\left(\frac{V^2}{U_o^2}\right)}{dC_L}\right]_{C_L=0} = \frac{1.696}{a}$$

Appendix No. 3 (Cont'd)

Also the velocity for $\alpha = 0^\circ$ due to the wing at the windshield tip was calculated to be

$$\left[\frac{V^2}{U_o^2}\right]_{\alpha=0} = 1.051 = \frac{(U_o + \Delta V_2)^2}{U_o^2}$$

We will assume the velocities due to the windshield, wing at $\alpha = 0^\circ$, and wing circulation can be added algebraically to the free stream velocity, U_o, to obtain the total velocity at the windshield tip. Thus,

$$U = U_o + \Delta V_1 + \Delta V_2 + \Delta V_3$$

where ΔV_1 = velocity increment due to windshield

ΔV_2 = " " " " wing at $\alpha = 0^\circ$

ΔV_3 = " " " " " circulation

From the experiments reported in Part II (Fig. II-21) we know the pressure at the windshield tip without a wing present is given by,

$$\frac{(U_o + \Delta V_1)^2}{U_o^2} = 1.60, \text{ or } \frac{\Delta V_1}{U_o} \doteq 0.264$$

The effect of the wing at $\alpha = 0^\circ$ was given as

$$\frac{(U_o + \Delta V_2)^2}{U_o^2} = 1.051, \text{ or } \frac{\Delta V_2}{U_o} \doteq 0.025$$

From the equation for change of pressure with wing lift we can write

$$\delta\left(\frac{V^2}{U_o^2}\right) = \frac{1.696}{a}\delta C_L = \frac{1}{U_o^2}\left[(\Delta V_3 + \Delta V_2 + U_o)^2 - (\Delta V_2 + U_o)^2\right]$$

$$= \frac{\Delta V_3^2}{U_o^2} + 2.05\,\frac{\Delta V_3}{U_o}$$

NOTE: for ∞ AR 4 0012 airfoil $a = 5.40$

Solving for ΔV_3 gives $\frac{\Delta V_3}{U_o} \doteq 0.153\, C_L$

We can now calculate Δp, the tip pressure

$$\frac{\Delta p}{\frac{1}{2}\rho U_o^2} = 1 - \frac{1}{U_o^2}\left[U_o + \Delta V_1 + \Delta V_2 + \Delta V_3\right]^2$$

or $$\left[\frac{d\left(\Delta p/\frac{1}{2}\rho U_o^2\right)}{d\,C_L}\right]_{C_L=0} = -0.395$$